AN INVESTIGATION OF TEMPERATURE FLUCTUATIONS ON BLUFF BODIES

Thesis by

Jacek Piotr Gorecki

In Partial Fulfillment of the Requirements

For the Degree of

Doctor of Philosophy

California Institute of Technology

Pasadena, California

1960

ACKNOWLEDGEMENTS

The author takes pleasure in thanking Dr. Hans Wolfgang Liepmann for his encouragement and advice on this research. Helpful discussions with members of the GALCIT Fluid Mechanics Group, particularly Dr. Anatol Roshko, are gratefully acknowledged.

The experimental program was supported by private funds provided by the Guggenheim Aeronautical Laboratory, California Institute of Technology. Special thanks are due Dr. Clark B. Millikan, Director of the GALCIT, for making these funds available.

The models and experimental apparatus were constructed in the GALCIT shops. Their help was much appreciated, particularly Mr. Marvin E. Jessey's assistance with the design of the electronic equipment.

It is a pleasure to acknowledge the contributions of Mrs. Dorothy Diamond and of Mrs. Geraldine Krentler in the preparation of the drawings and of the typescript.

Finally the author would like to thank the Instituto Tecnológico de Aeronautica, São José dos Campos, São Paulo, Brazil for granting him a prolonged leave of absence; and the Brazilian Research Council (Conselho Nacional de Pesquisas) and California Institute of Technology for financial assistance without which his studies here would have been impossible.

ABSTRACT

Temperature fluctuations and recovery temperatures on the surface of a circular cylinder (with axis normal to a subsonic compressible flow) and the field of flow about the cylinder, particularly the wake area, are investigated experimentally in range between $M = 0.35$, $Re = 117,000$ and $M = 0.70$, $Re = 201,000$.

Spectral analysis of fluctuations on body surface and other evidence indicate that formation of discrete vortex cores from the separated shear layers is initially an impulsive random process (of the generalized "shot effect" type), although the wake farther downstream from the model has a definitely periodic structure.

Impulsive formation of vortex cores can be enhanced by wind tunnel resonance or by a high turbulence level in the free stream and is accompanied by abnormal cooling of the model surface in the separated area - the mechanism of these effects is also investigated.

TABLE OF CONTENTS

LIST OF TABLES

LIST OF FIGURES

NOTATION

A	constant defined by equation (19)
a	speed of sound
B	constant defined by equation (19)
b	model span
$b_{1,2,3}$	film gauge dimensions (Fig. 5)
$C_{1,2}$	intensity of a "sharp" peak defined by equation (21)
C_{Dp}	pressure drag coefficient $= \dfrac{D_p}{\frac{1}{2}\rho_1 U_1^2 bd}$
C_p	pressure coefficient $= \dfrac{p - p_1}{\frac{1}{2}\rho_1 U_1^2}$
C_{ps}	pressure coefficient, sonic
$c_{1,2,3}$	film gauge dimensions (Fig. 5)
c_p	specific heat at constant pressure
$\widetilde{D}_{1,2}$	intensity of a "diffuse" peak defined by equation (22)
D_p	pressure drag (time-average)
d	model diameter
f	power spectral density of temperature fluctuations
G	voltage gain of amplifier
g	gap
H	tunnel height (Fig. 13)
h	distance between vortex rows (Fig. 1)
I	current
k	thermal conductivity

ℓ	longitudinal spacing in vortex street (Fig. 1)
M	Mach number = U/a
n	frequency
p	pressure
$\vec{q}$	heat flux
R_T	gauge (transducer) resistance
Re	Reynolds' number = Ud/ν
r	polar coordinate = $\sqrt{x^2 + y^2}$
r	temperature recovery factor = $\frac{T_t - \overline{T_w}}{T_t - T_l}$
St	Strouhal number = nd/U
T	temperature
t	time
$t_{b,f}$	thickness, base or film
U	stream velocity
u	x - component of velocity
u_d	increment in x - velocity on tunnel centerline (doublet term)
u_s	increment in x - velocity on tunnel centerline (source term)
Δu	increment in x - velocity on tunnel centerline due to wall interference
$\vec{w}$	velocity vector
x, y	Cartesian coordinates defined in figures 1 and 3
α	temperature coefficient of resistivity
β	temperature penetration factor = $\sqrt{k \rho c_p}$
Γ	circulation
γ	ratio of specific heats (1.4 for air)

$\delta_{T'}$	characteristic thickness or depth of penetration for temperature fluctuations
θ	polar coordinate defined in figure 13
κ	thermal diffusivity $= \frac{k}{\rho c_p}$
$\lambda_{T'}$	characteristic length of temperature fluctuations
μ	viscosity
ν	kinematic viscosity $= \mu/\rho$
ρ	density
τ	time constant
τ_c	(auto) correlation time
ϕ	velocity potential
ψ	(auto) correlation function
ω	circular frequency $= 2\pi n$

Subscripts and superscripts

Flow and temperature

$(\;)$	local free stream
$(\;)_\infty$	free stream in absence of walls
$(\;)_l$	tunnel free stream
$(\;)^*$	sonic conditions
$(\;)_t$	total (reservoir condition)
$(\;)_w$	at wall (interface)
$(\;)'$	fluctuating component
$\overline{(\;)}$	time-average

Material properties

$(\;)_0$	at standard temperature and pressure (0°C, 1 atm)
$(\;)_{25}$	at room temperature and standard pressure (25°C, 1 atm)

Gauge

$(\;)_a$	air (in gauge neighborhood)
$(\;)_b$	base (i.e. pyrex glass base of gauge)
$(\;)_f$	film (i.e. Pt film gauge proper)
$(\;)_m$	model (in gauge neighborhood)

I. INTRODUCTION

1. Aerodynamics of bluff bodies - some problems and difficulties

The flow about bluff bodies, one of the oldest problems in fluid mechanics, is still associated with many theoretical difficulties. These difficulties are especially apparent in the range of intermediate and high Reynolds' numbers at which flow separation occurs, followed by complex time-dependent wake patterns. This makes it a particularly difficult problem to set up mathematically. Large changes in streamline curvature, even at moderate, subsonic Mach numbers, make linearization in the physical plane difficult. At higher subsonic speeds the large extent of transonic regimes both on the body and in the wake area adds further complications.

Figure 1 shows qualitatively a typical bluff body in subsonic flow at intermediate Reynolds' number. The upper half of the drawing shows, in a time-average sense, the (laminar) boundary layer in the attached flow on the front part of the body, a separation point S where the boundary layer becomes a free shear layer, the growth of the shear layer up to and beyond transition point T. A "dead-air" zone, or recirculation zone, is also outlined, R denoting a reattachment point. At a distance x_D (one or two diameters from the body) most of the vorticity has been transferred from the shear layer to the moving system of discrete alternating vortices (in the two-dimensional case, at least). They are denoted by Γ in their (instantaneous) position.

The lower half of figure 1 shows, in a time-average sense, a qualitative distribution of lines of equal density around the body and

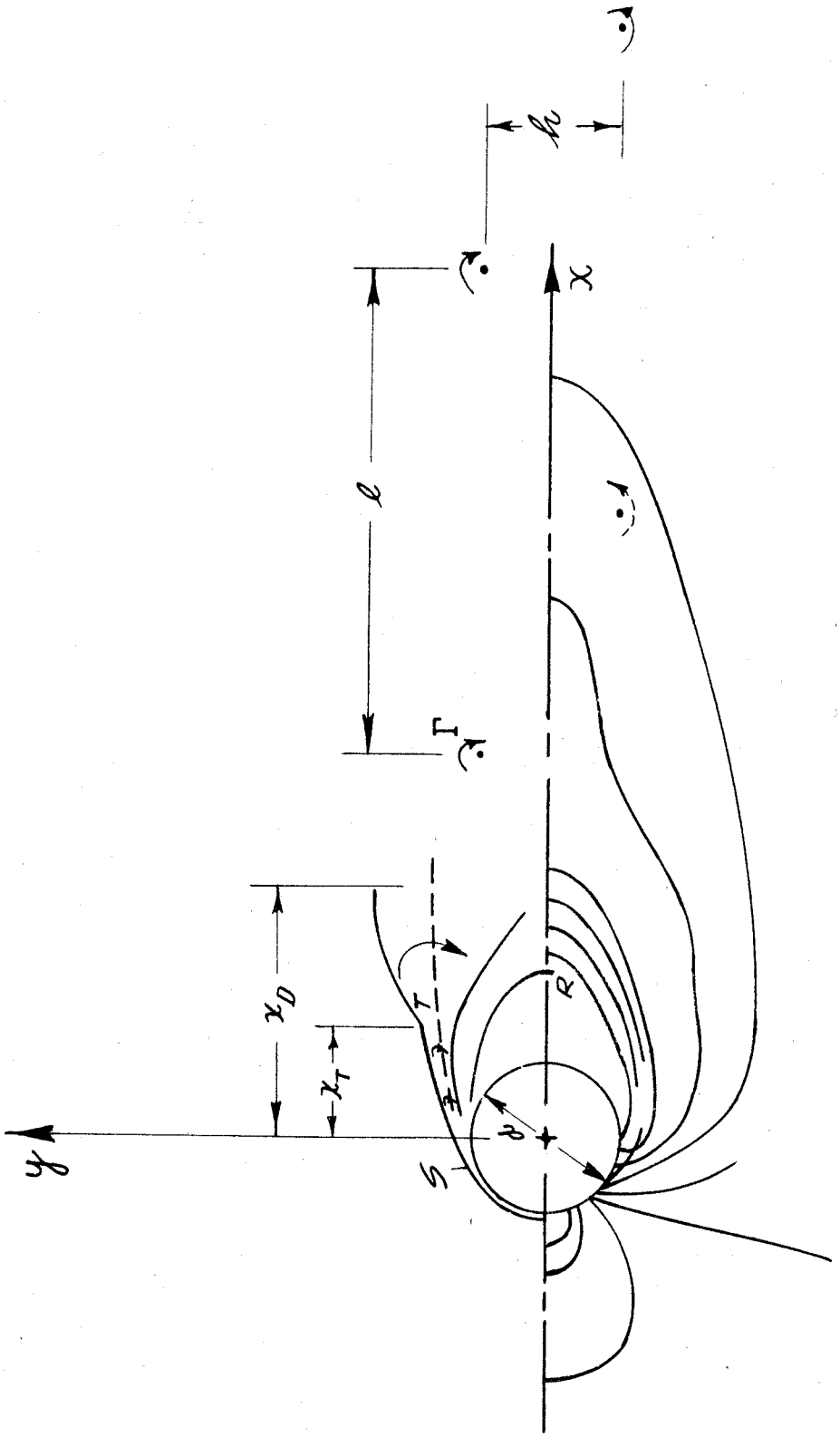

Fig. 1 - Field of flow about a bluff body

in the wake area. Note that the density gradients in the "dead-air" zone are of comparable magnitude with those in the attached flow area.

Even this average picture is fairly complex. And any inspection of actual time-dependent flows, e.g. the flash schlieren photographs of figures 25 to 32, shows how crude this average representation may be.

Since no exact solutions of the Navier - Stokes equations are available in the range of intermediate Reynolds' numbers, even in the incompressible case, the flow about bluff bodies and their wakes is usually described by approximate models or by restricted phenomenological theories, based on some experimentally determined parameters.

The attached flow is usually described by a combination of potential and boundary layer methods, extended to predict separation (Ref. 9 and others).

Reference 1 summarizes some of the phenomenological theories applied to the separated flow and wake areas. Two of the best known are the free-streamline theory (Refs. 2 and 3), more recently extended in reference 4, and Kármán's theory of the vortex street (Ref. 6). The two provide a reasonable picture of the initial separated flow pattern and of the fully developed vortex street in incompressible flow at intermediate Reynolds' numbers; they neglect, however, all viscous or turbulent exchange mechanisms.

Vortex streets and vortex wakes have been studied quite extensively, at very low Mach numbers, in references 7 and 8.

Many interesting problems arise in the intermediate stages of separated flow behind bluff bodies - in the recirculation zone between the initial free shear layer and the fully developed vortex street - particularly at the higher subsonic and transonic speeds.

Attempts have been made to apply quasi-stationary mixing theories (e.g. Refs.10 and 11) to the recirculation zone; some measure of success has been achieved in restricted cases with a single free shear layer, e.g. behind a step. Transition in the free shear layer (as shown in Ref. 12) is one of the important factors in such computations. The mixing theories attempt essentially to apply to the recirculation zone problem the same kind of approach used in boundary layer theory, i.e. that of weak interaction between potential and dissipative flows and quasi-equilibrium in the thermodynamic sense.

At the higher Reynolds' numbers, particularly in compressible flow, non-stationary phenomena seem however to dominate in the recirculation zone and are expected to have a large effect both on the body (fluctuating pressures, lift and drag) and on the wake (through the influence on exchange mechanisms). This may lead to strong interactions, and possibly interactions between fairly distant parts of the flow process.

One interesting problem related largely to the recirculation zone is that of abnormal surface cooling which is observed in the separated flow area on the surface of bluff bodies in subsonic flow at intermediate and high Reynolds' numbers. Temperature recovery factors as low as $r = 0$ or $r = -0.25$ have been observed by

Eckert and Weise (Ref. 13) and by Ryan (Ref. 14) on the rear surface of circular cylinders at high subsonic speeds; even more negative recovery factors have been observed on other bluff bodies. Ryan noted also that particularly intense cooling accompanied the strong sound effects (whistling) which occurred at certain tunnel conditions ("resonance").

Ackeret (Ref. 25) and Schultz-Grunow (Ref. 26) suggested two different mechanisms to explain these abnormal cooling effects.

Ackeret considers the non-stationary term in the (compressible) Bernoulli equation

$$c_p T + \frac{|\vec{w}|^2}{2} + \frac{\partial \phi}{\partial t} = c_p T_\infty + \frac{U_\infty^2}{2} \quad ; \qquad (1)$$

this non-stationary term is assumed to be due to the potential field of vortices streaming by. The vortices are assumed to be formed gradually close to the body (at $r = 1.3\,\frac{d}{2}$, $\theta = 110^\circ$) and periodically shed at the frequency of the fully developed vortex street.

Schultz-Grunow considers the turbulent exchange in a stratified fluid. In the case of the wake behind a bluff body he assumes the stratification to be due to the centrifugal field associated with the large streamline curvature in some of the separated flow areas.

The assumptions underlying any of these two mechanisms are more fundamental than the problem of surface temperatures. They postulate in fact certain basic exchange mechanisms between different parts of the flow process. It thus appears advisable not

only to gather more information on abnormal cooling in separated flow areas, but also - and this is even more important - to check the fundamental assumptions as to the kind of mechanism involved.

2. Choice of models and methods

The investigation of non-stationary flows requires detailed information on the flow field around the body (in space and time) and on the conditions at the surface of the body, also in space and time. Such information should be obtained with sufficiently high resolution and the least possible disturbance of the flow field.

Techniques of generalized harmonic analysis appear particularly suitable since flow involves both periodic phenomena and random processes with some degree of statistical regularity. Reference 15 summarizes some of these techniques.

Optical methods and some hot-wire measurements were decided upon to survey the flow field; a two-dimensional configuration is of course most favorable in optical work. The simplest possible geometry in two-dimensional flow is that of the circular cylinder. This was chosen not only because of its simplicity but also because of the large amount of conventional aerodynamic data accumulated on this geometry (e.g. Refs.13, 14, 16, 17, 18).

It was felt that a supersonic flow with its shock wave patterns restricts some of the interactions which are believed to be an essential feature of recirculation zone flows - an investigation in the subsonic (and locally transonic) range was therefore preferred.

Some interferometric measurements (Ref. 18) were available in that range; they were completed by a thorough survey with flash

and time-exposure schlieren pictures.

The problem of obtaining data on conditions at the surface of the body required a very small transducer with sufficiently high frequency resolution. The possibility suggested itself of using thin metal film resistance gauges (Refs.19, 20 and 21), which could be used directly as thermometers for the measurement of average and fluctuating temperatures, as time-average heat transfer gauges, and indirectly to measure pressure fluctuations just outside the model surface.

In spite of the fact that the interpretation of temperature fluctuations measured with thin resistance films is not as simple as that of pressure fluctuations measured with piezoelectric devices, resistance film gauges have some experimental advantages. Their main feature as transducers is their low electrical impedance which makes feasible the use of some form of transmission line between transducer and preamplifier. This facilitates the construction of small size models instrumented with several transducers. Simultaneous observation of conditions at several stations close together thus becomes possible; space, time or space-time correlation work becomes feasible in a relatively small model area.

Main disadvantage of resistance gauges on model surface is that only a very small fraction of free stream temperature fluctuations appears as wall temperature fluctuations.

Most of the experimental program reported hereafter is based on the spectral analysis of the signal obtained with platinum film resistance gauges at the surface of a circular cylinder model in conjunction with optical and hot-wire surveys of the flow field, in the subsonic (and partially transonic) range $M = 0.35$ to $M = 0.70$.

II. APPARATUS AND METHODS

1. Wind tunnel and schlieren system

All the measurements were made in the GALCIT 4 x 10 inch Transonic Wind Tunnel. This continuous type closed circuit wind tunnel and its schlieren system were originally described in reference 22; the modified test section, flexible nozzle and traversing gear are described in reference 23.

Figures 2 and 3 show the tunnel and test section configuration used in most tests.

In the subsonic range tunnel Mach number can be varied continuously between 0.3 and choking; reservoir conditions are always nearly atmospheric.

Free stream turbulence level, at low subsonic speeds, is estimated at

$$\frac{\sqrt{\overline{u'^2}}}{U} = 0.04\ ^{o}/o.$$

The schlieren system is provided both with a continuous light source and shutter for time exposures, and a spark source for 3-4 μ sec flash exposures.

Reservoir and static pressures are measured with mercury manometers; a shielded thermistor probe, with a calibrated bridge circuit, indicates reservoir temperature.

In this particular test series special precautions had to be taken to prevent erosion of platinum films and of hot wires by dust particles in the airstream. Besides the regular cyclone and oil bath

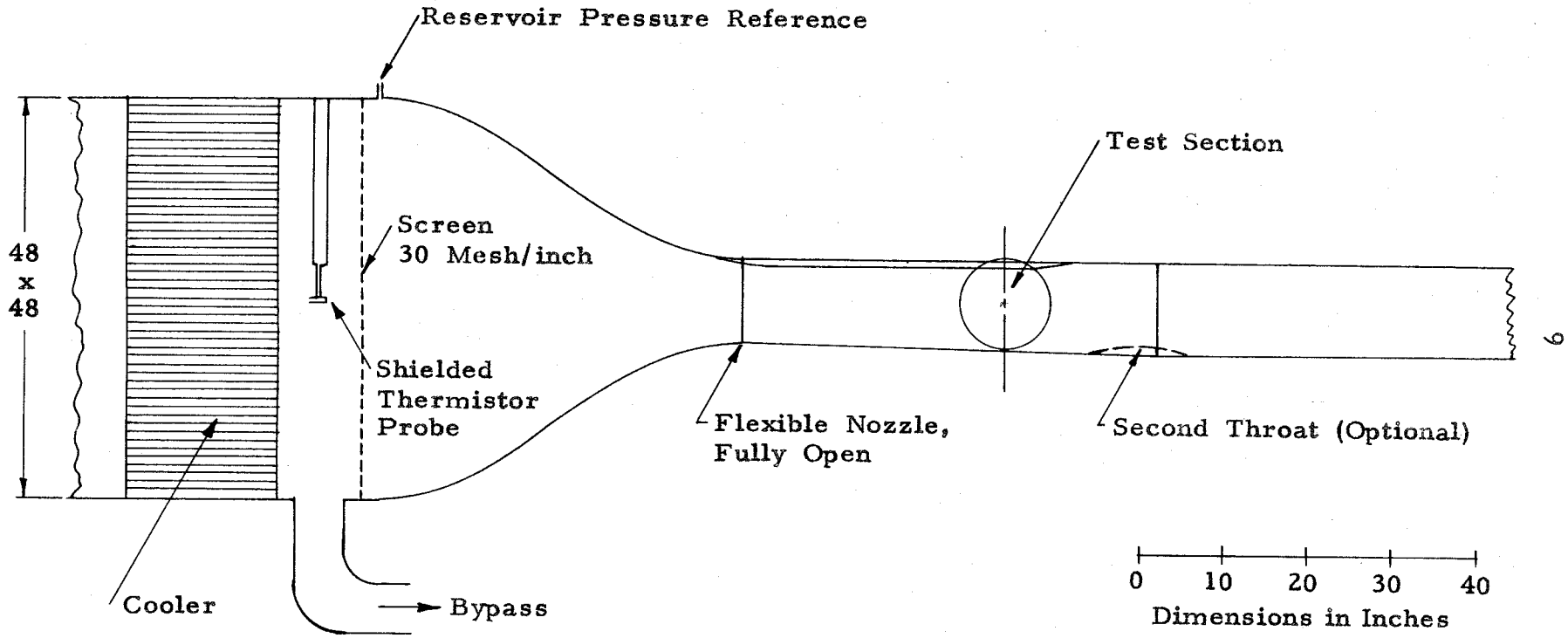

Fig. 2 - Wind tunnel

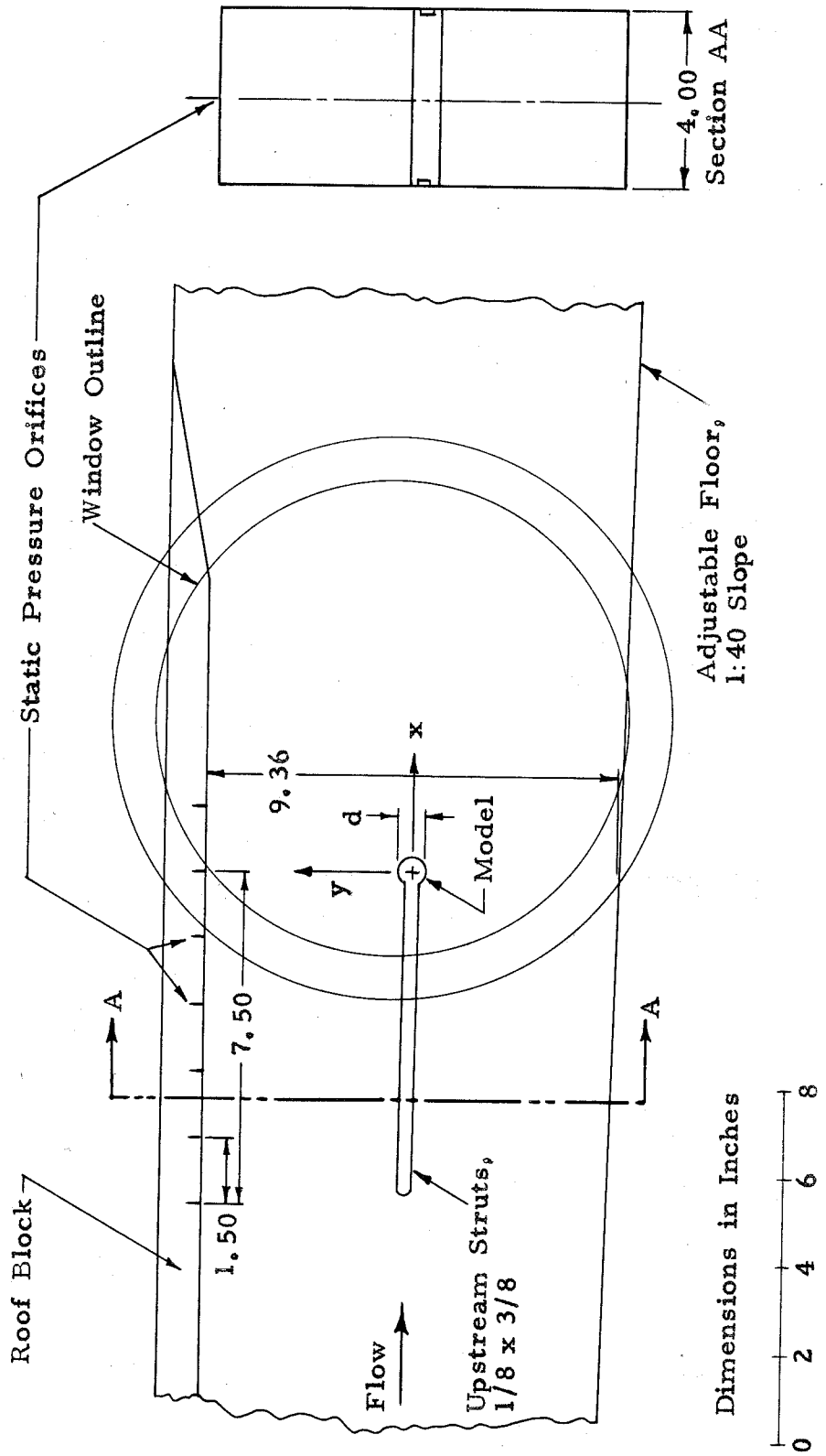

Fig. 3 - Test section - model installation and coordinate system

type filter installed in the dryer circuit a special filter was installed in the main wind tunnel circuit on the upstream side of the cooler. The special filter consists of 2 layers of fine mesh nylon marquisette material soaked in oil. This type of filter arrangement proved satisfactory - hot-wires lasted for several hours in the air-stream and no erosion of the models and platinum films could be detected.

2. Models

All the models used were circular cylinders spanning the tunnel test section. They ranged in diameter from 0.375 inch ($\frac{d}{H} = 0.0400$, $\frac{b}{d} = 10.67$) to 0.624 inch ($\frac{d}{H} = 0.0666$, $\frac{b}{d} = 6.41$).

Figure 3 shows schematically a model installed in the test section and the reference coordinate system attached to it. Up-stream struts 0.125 inch x 0.375 inch cross section (with beveled corners on the side exposed to the airstream) run along the walls and provide model support. Models are further restrained by friction against test section windows.

The 0.375 inch diameter plain model (solid brass rod) is used only for optical observation and wake surveys.

The pressure-distribution and temperature-fluctuation models are both 0.624 inch diameter. The first is constructed of stainless steel tube and provided with six 0.020 inch diameter pressure holes evenly spaced around the circumference at mid-span. The second is constructed of pyrex glass tube cemented to brass end pieces (Fig. 4). It is instrumented with platinum film resistance gauges, discussed

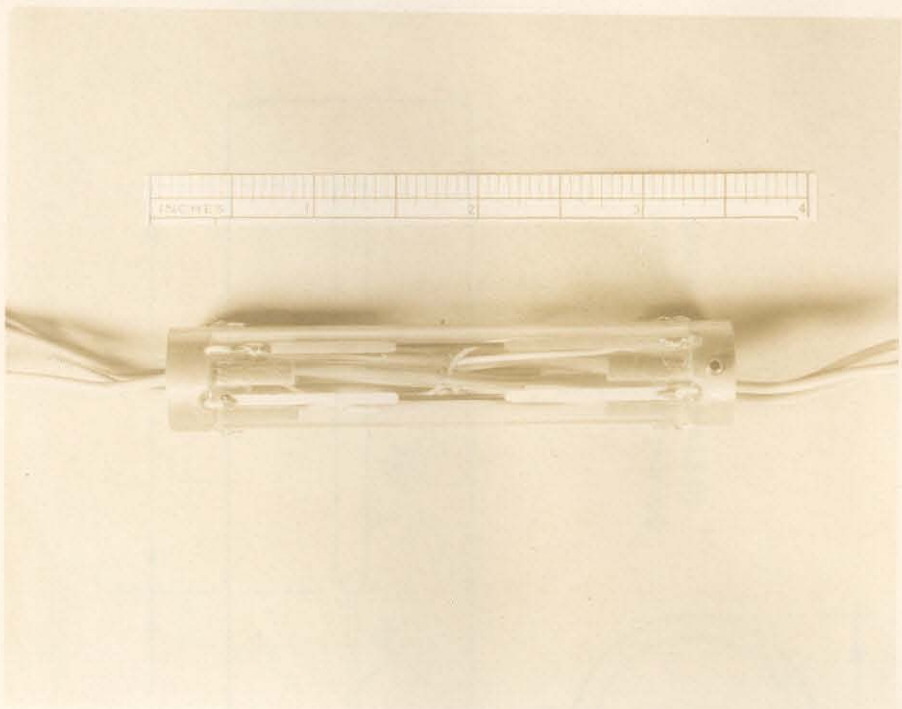

Fig. 4 - Model instrumented with platinum film transducers

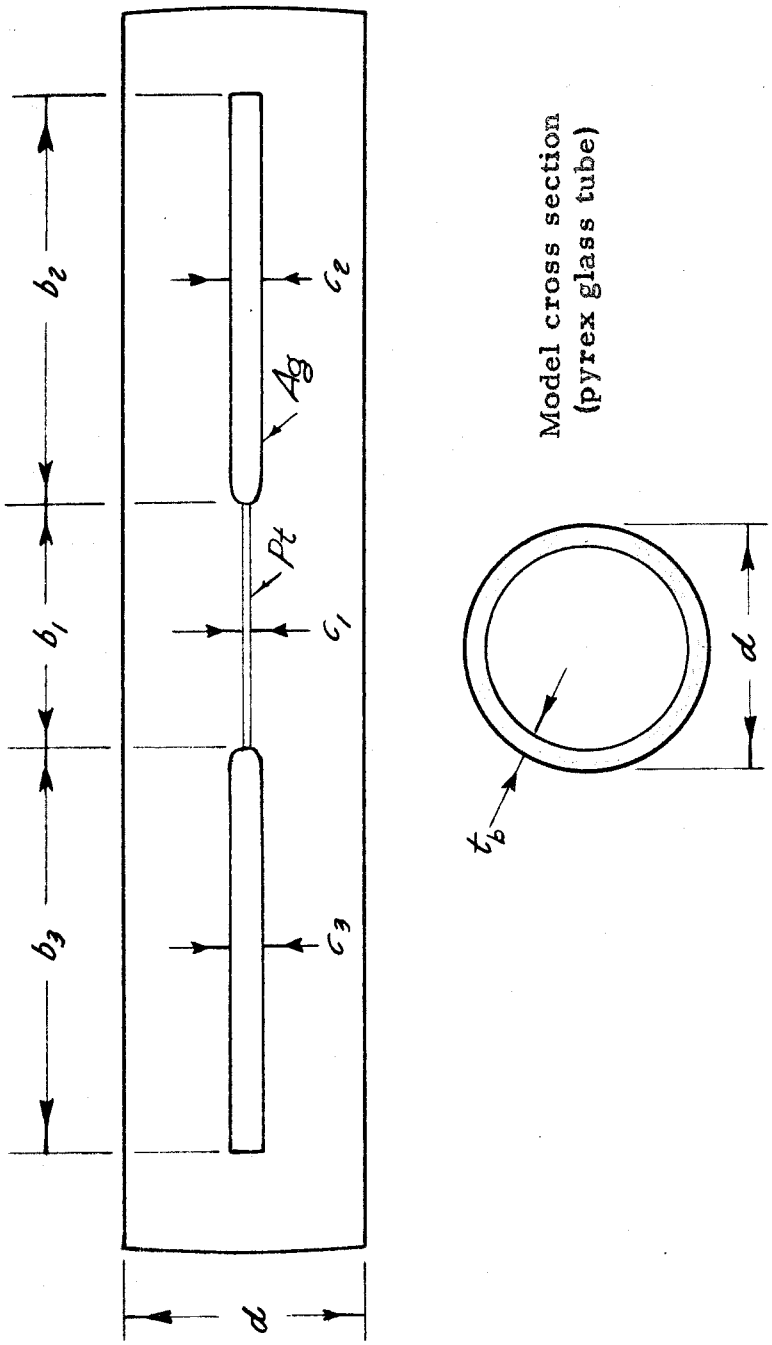

Fig. 5 - Transducer Dimensions

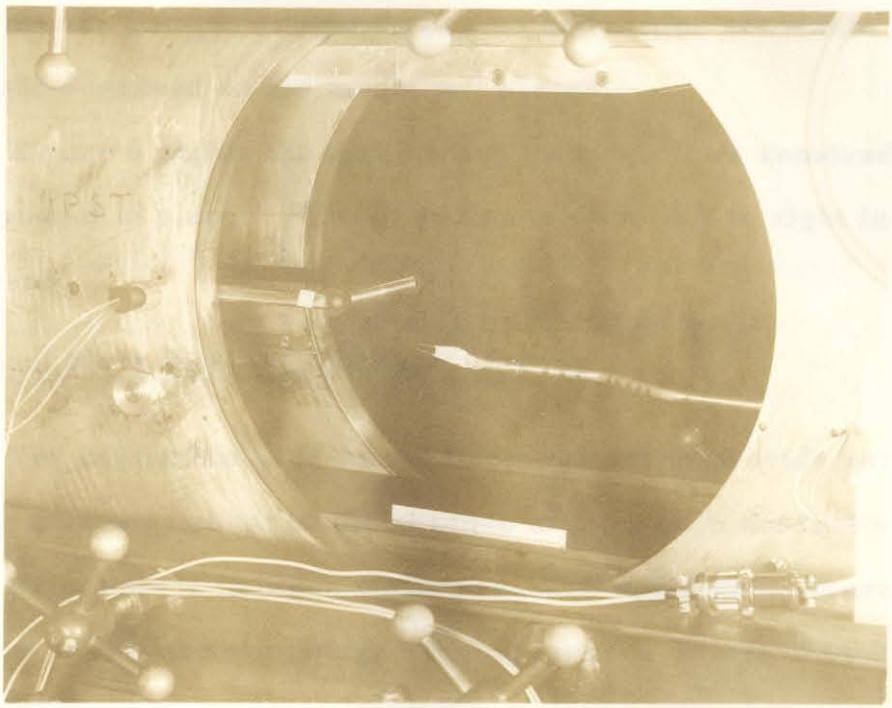

Fig. 6 - Model installed in wind tunnel

in Section II-4. Relevant dimensions of the platinum film gauges are defined in figure 5.

Both the pressure-distribution and temperature-fluctuation models can be rotated around their axis and angles set within $\pm 0.5^{o}$ on a scale engraved on the model end pieces.

Figure 6 shows the test section (with windows removed) and a typical model in place. Flow direction is from left to right in this photograph.

3. Tunnel Mach number; blockage; choking

The adjustable wind tunnel floor was set to provide zero static pressure gradient in the absence of models in the test section.

With models in place static pressure could be measured at 7 stations in the tunnel ceiling, ranging from $x = -7.50$ inch to $x = +1.50$ inch.

The station $x = -7.50$ inch was selected as providing reference static pressure p_1; tunnel Mach number M_1 was determined from the standard isentropic formula

$$\frac{p_1}{p_t} = \left(1 + \frac{\gamma - 1}{2} M_1^2\right)^{-\frac{\gamma}{\gamma - 1}} \qquad (2)$$

All the results are presented in terms of tunnel Mach number M_1.

Blockage corrections can be estimated from the wall pressure distributions measured during most runs - see appendix 1.

With 0.624 inch diameter cylindrical models spanning the test section, i.e. $\frac{d}{H} = 0.0666$, choking occurred at $M_1 = 0.73$,

almost exactly the value predicted by the inviscid one-dimensional analysis. Tests were restricted to Mach number range 0.35 to 0.70; the lower value was determined largely by the sensitivity of available schlieren system and manometers, while the higher one was close to the choking limit.

4. Model instrumentation

The temperature-fluctuation and heat transfer model was instrumented with 6 platinum film resistance gauges, of the type originally described in references 19, 20 and 21 for use in shock tubes. The use of a similar device as a skin-friction meter was discussed in reference 24.

Figure 4 shows the cylinder model, constructed of pyrex glass tube, and instrumented with Pt film resistance gauges. The 6 gauges are equally spaced around the circumference of the cylinder; dimensions of the supporting pyrex glass tube, gauges and silver film connecting strips (see Fig. 5) are:

$d = 0.624$ in.	$t = 0.052$ in.
$b_1 = 0.625$ in.	$c_1 = 0.040$ in.
$b_2 = b_3 = 1.050$ in.	$c_2 = c_3 = 0.080$ in.

Thickness of Pt films is of the order of 0.2μ ; thickness of silver film connecting strips is of the order of 10μ .

With these dimensions resolution of gauges is: in space - chordwise, 0.06 d; spanwise, 1.0 d; in time (see Section II-6) - a few microseconds for temperature fluctuation work.

Platinum films were deposited by sputtering, shaped to

precise outlines by scraping off excess material and permanently bonded to the glass by baking at 620° C. Silver film connecting strips were painted on and bonded by baking at 480° C. Wire leads were soldered directly to the silver strips with Sn - Pb - Ag solder.

Calibration, static and dynamic characteristics of the Pt film gauges are discussed in Section II-6.

5. Electronic equipment

Figure 7 shows a block diagram of the electronic equipment used for most tests.

The 5-channel bridge and 3-channel amplifier, supplied entirely by batteries, were specially designed and constructed to provide low electrical noise levels in spite of intense environmental acoustic noise levels and of stray electromagnetic fields from wind tunnel machinery.

Figures 8 and 9 show a typical bridge channel and its calibration curve, obtained with standard resistors in place of transducer R_T.

The low-noise 5-channel bridge was used to supply the platinum film gauges in a constant current circuit. It also supplied hot-wires used in wake surveys.

Each amplifier channel, designed for a voltage gain of 1000 or 4000, and flat response in the audio frequency range, consists of 2 pentode connected 5840 subminiature tubes in a conventional amplifier circuit, followed by a triode connected 5840 cathode follower.

Figure 10 shows typical amplifier gain calibration curves, both

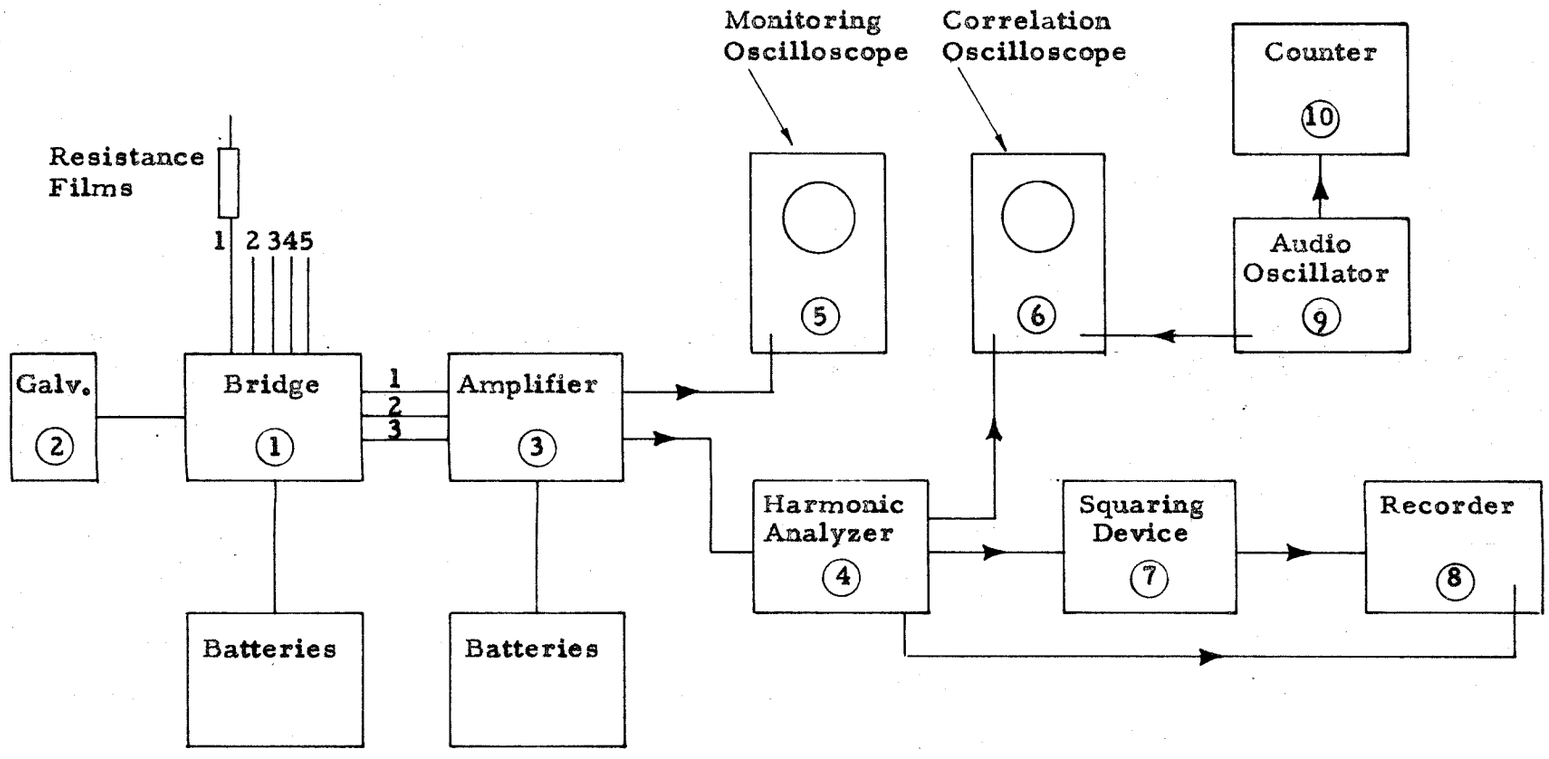

Fig. 7 - Electronic equipment - block diagram

1. Bridge, 5-channel, special
2. Galvanometer (Leeds and Northrup Type 2420-B)
3. Amplifier, 3-channel, special
4. Harmonic Analyzer (Technical Products TP 626 Oscillator and TP 627 Analyzer with 2 cps, 20 cps, and 50 cps filters)
5. Oscilloscope (DuMont Type 324)
6. Oscilloscope (DuMont Type 340)
7. Squaring and Integrating Device (Ballantine Labs. Model 320 True Root Mean Square Meter with external capacity to modify time constant)
8. Two-Axis Recorder (Moseley Autograf Model 5)
9. Oscillator (Hewlett Packard Model 200 CD)
10. Electronic Counter and Timer (Beckman Berkeley 7360)

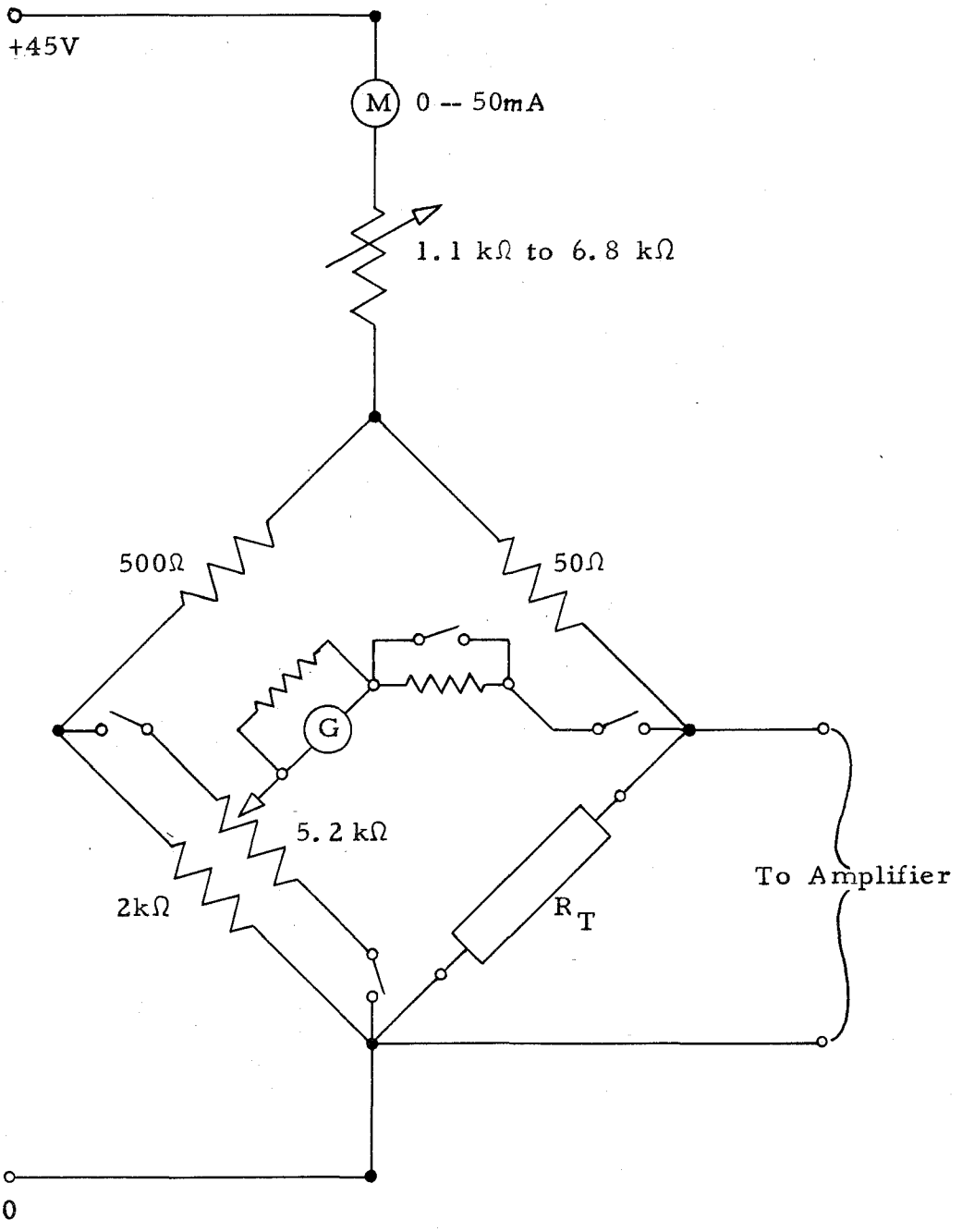

Fig. 8 - Bridge channel - schematic

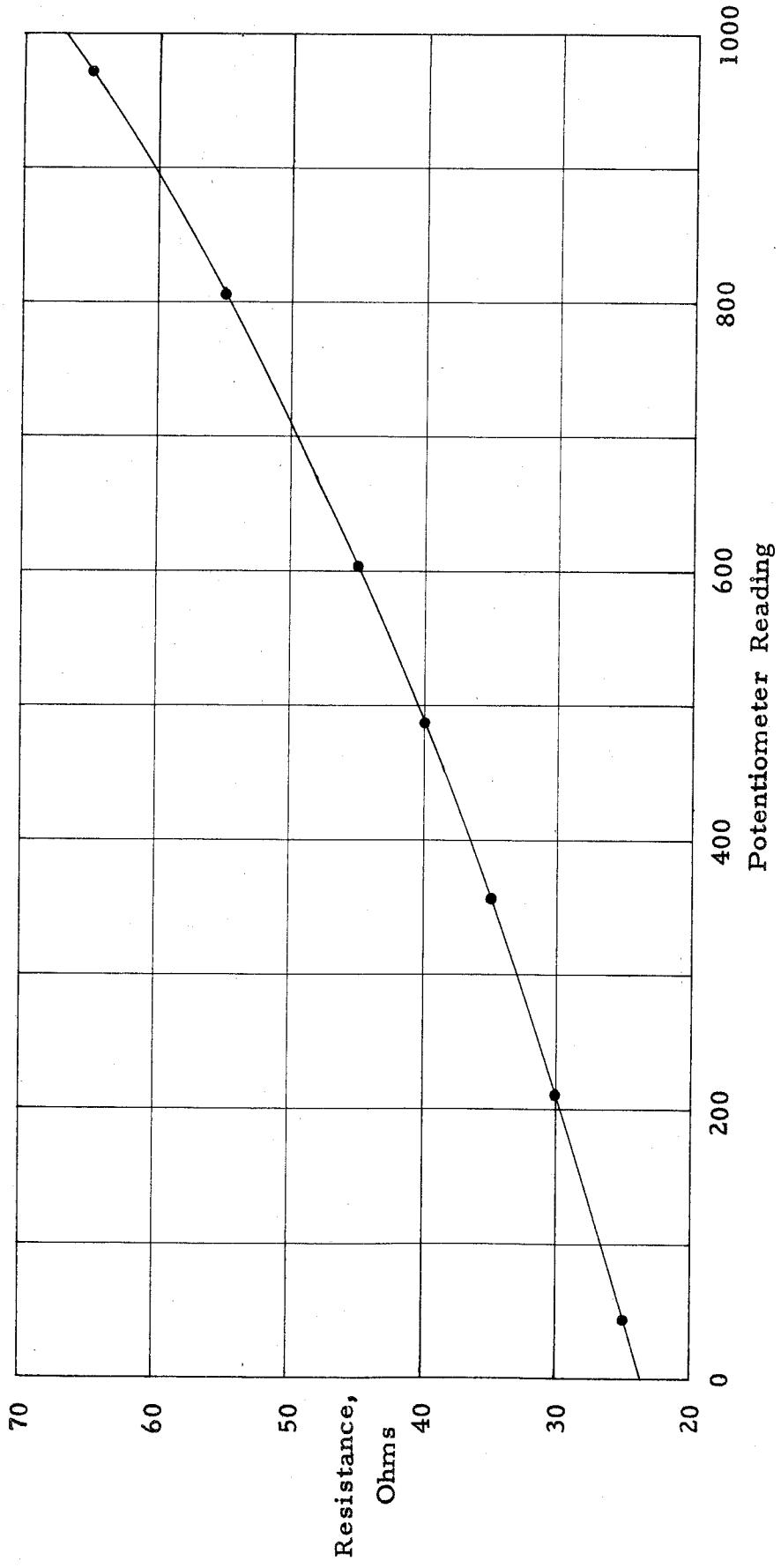

Fig. 9 - Bridge calibration

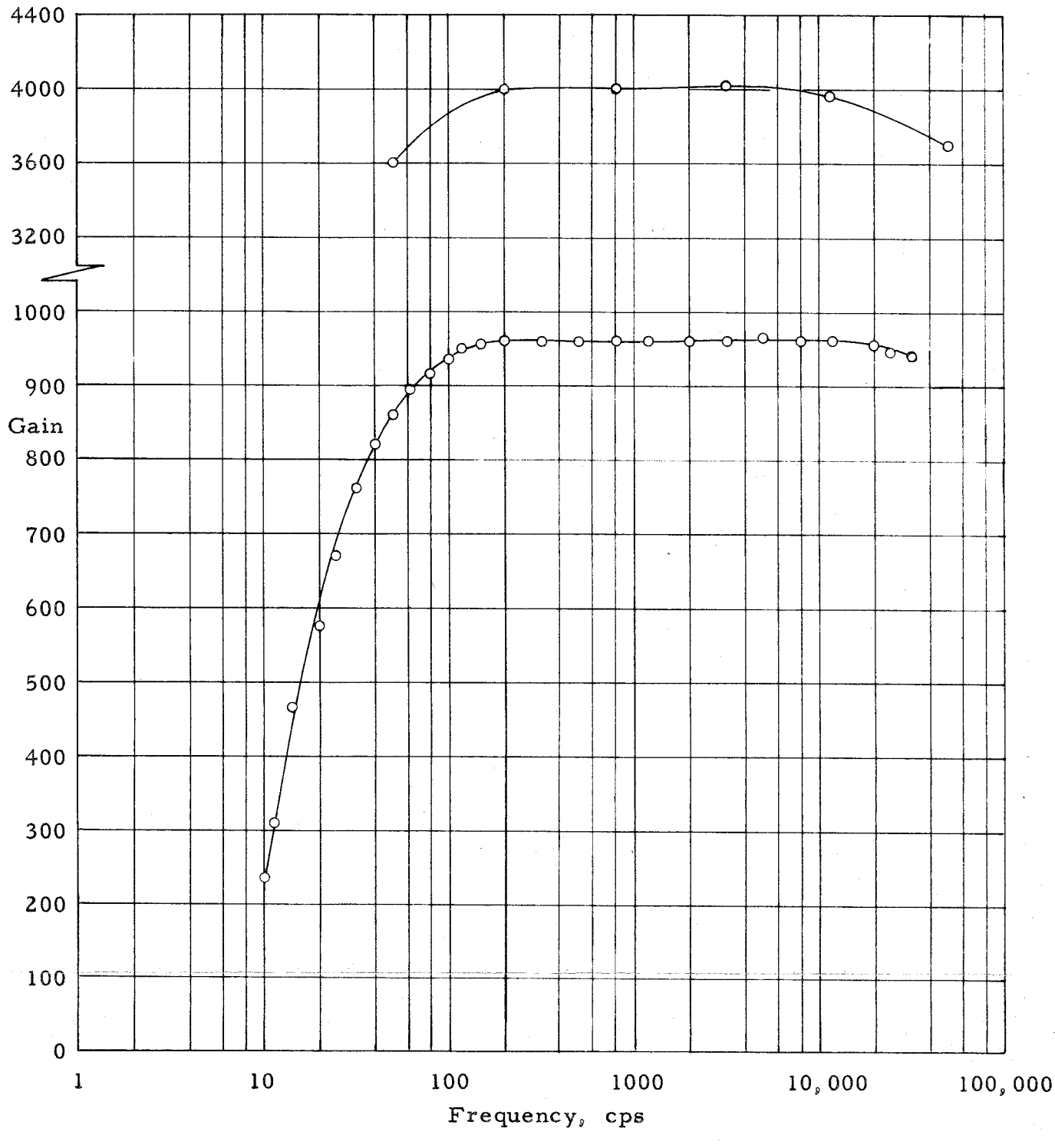

Fig. 10 - Amplifier calibration

(a) Special amplifier, (3) of fig. 7

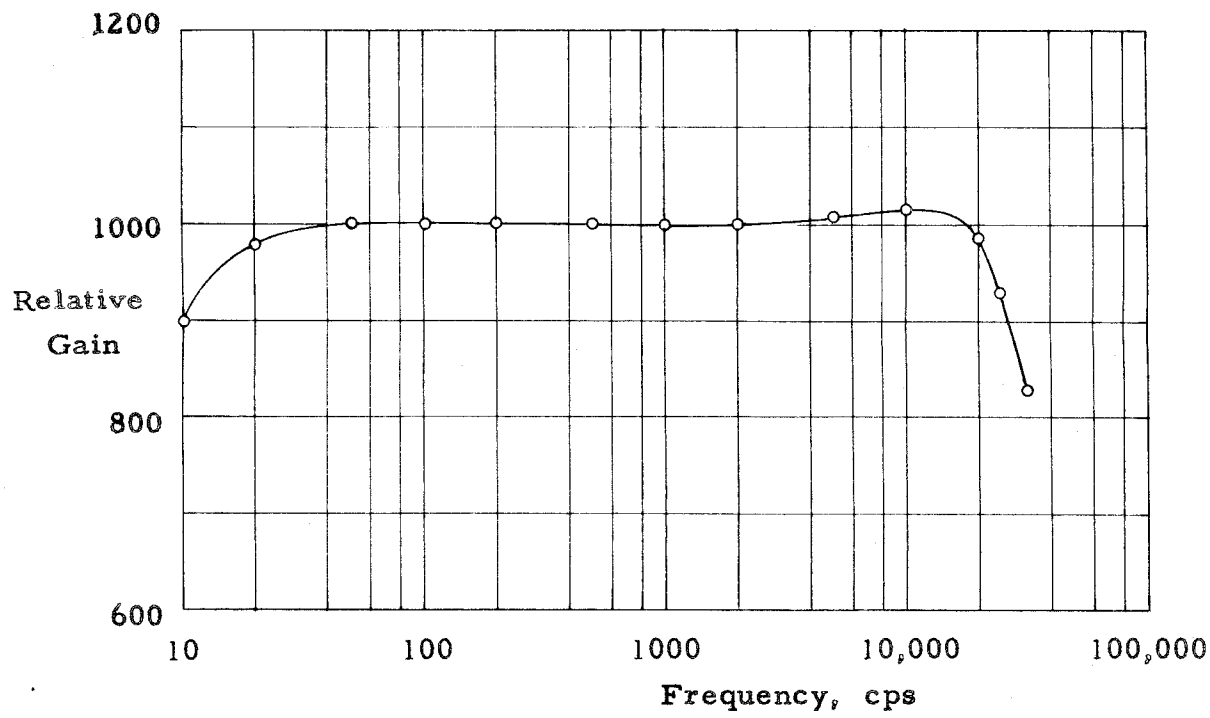

Fig. 10 (continued) - Amplifier calibration

(b) Amplifier of TP 627 Analyzer, (4) of fig. 7

for the special 3-channel amplifier [(3) in Fig. 7] and for the amplifier part of the Harmonic Analyzer [(4) in Fig. 7].

Installation of low-noise amplifier and bridge close to wind tunnel working section is shown in figure 11.

Harmonic analysis of gauge and amplifier output is provided by the TP-625 Analyzer System - a heterodyne type analyzer, with linear frequency scale, balanced modulator and demodulator circuits, and a selection of several constant bandwidth crystal network filters.

Discrete frequency peaks were identified by beating analyzer output against an oscillator on an oscilloscope screen and identifying frequencies on a crystal controlled electronic counter.

Power spectral density plots of the output signal were obtained by automatically sweeping the spectrum at a constant rate (18.5 cps/sec in most cases) and plotting output voltage squared (and time-integrated) versus frequency. Accuracy of the true-root-mean-square voltmeter used as a squaring device was found to be quite adequate over a range of 20:1 in voltage. Plots were monitored and attenuator ranges switched as required to keep within these limits.

The complete electronic system was checked for noise, spectral composition of noise and harmonic distortion under the most unfavorable environmental and load conditions; equivalent noise level at input terminals was $< 3\ \mu V$ (rms); with a full load sine wave input of frequency n, voltage level of harmonic 2n was always $< 0.1\ ^{o}/o$ of fundamental, and 3n harmonic level completely negligible.

Appendix 3 discusses the reduction of power spectra obtained with this equipment.

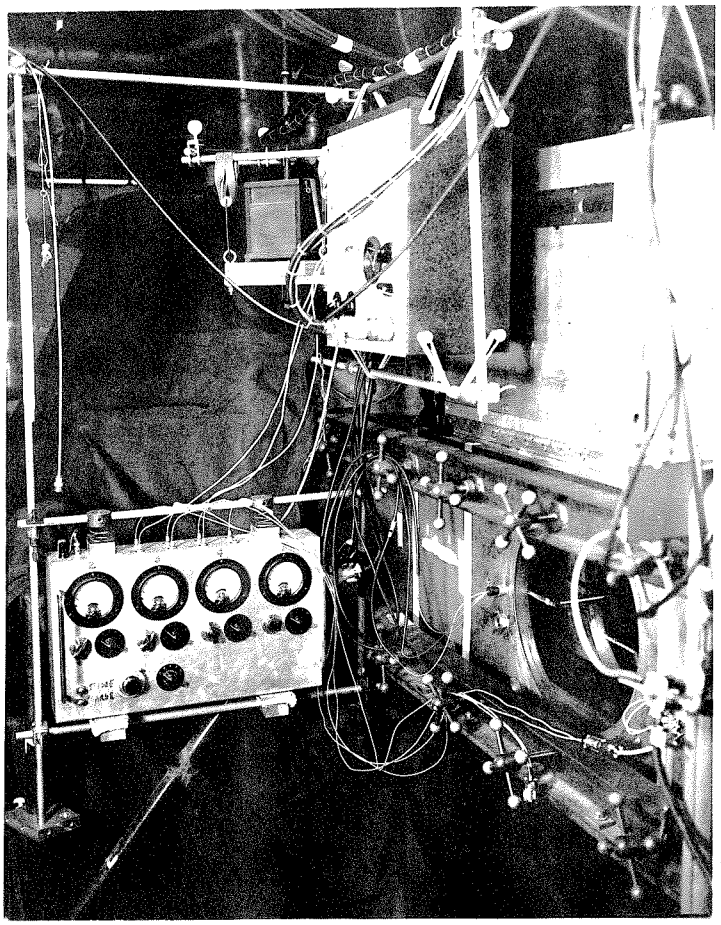

Fig. 11 - Bridge and amplifier

6. Static and dynamic characteristics of Pt film gauges

Heating currents ranging from 6 mA to 40 mA were used for the Pt film gauges; the lower values for static calibrations and temperature fluctuation work, the higher ones only for time-average heat transfer measurements.

Static calibrations of Pt films were performed initially in an adjustable temperature silicone oil bath (range 5° C to 55° C). Check points were obtained between runs by using a mercury thermometer embedded in an aluminum block 2.0 x 2.0 x 2.5 in. assembled around the model; equilibrium temperature in ambient air was then read off after a sufficiently long time.

Typical calibration curves obtained with the two methods are shown in figure 12(a) and (b), respectively.

A temperature coefficient of resistivity α, defined by

$$\frac{R_T}{R_{25}} = 1 + \alpha\,(T - 25^{\circ}C) \qquad (3)$$

was calculated from these data for each of the gauges. Its value ranged between 0.00195 $(^{\circ}C)^{-1}$ and 0.00235 $(^{\circ}C)^{-1}$ for the different gauges, and remained stationary within $\pm$ 0.00005$(^{\circ}C)^{-1}$ for any given gauge over a period of several months.

Note that for Pt in bulk the value is $\alpha \doteq 0.004\ (^{\circ}C)^{-1}$. The difference can be attributed to the thinness of the film and to its bonding to the pyrex glass base. The Wiedemann-Franz law is however believed to apply to such a film - so that the ratio of electrical and heat conductivities will remain equal to that of bulk

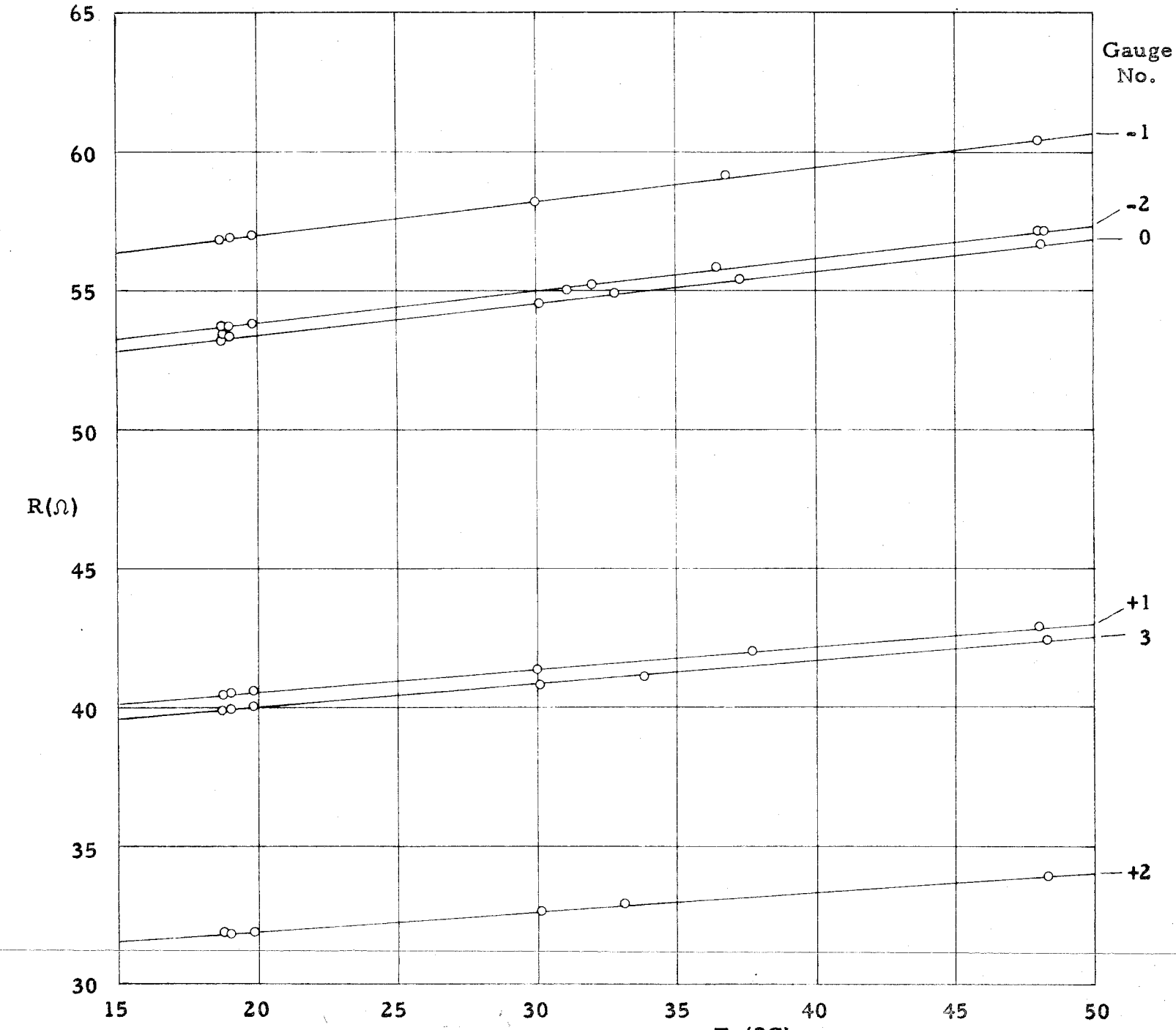

Fig. 12 - Typical platinum film calibrations

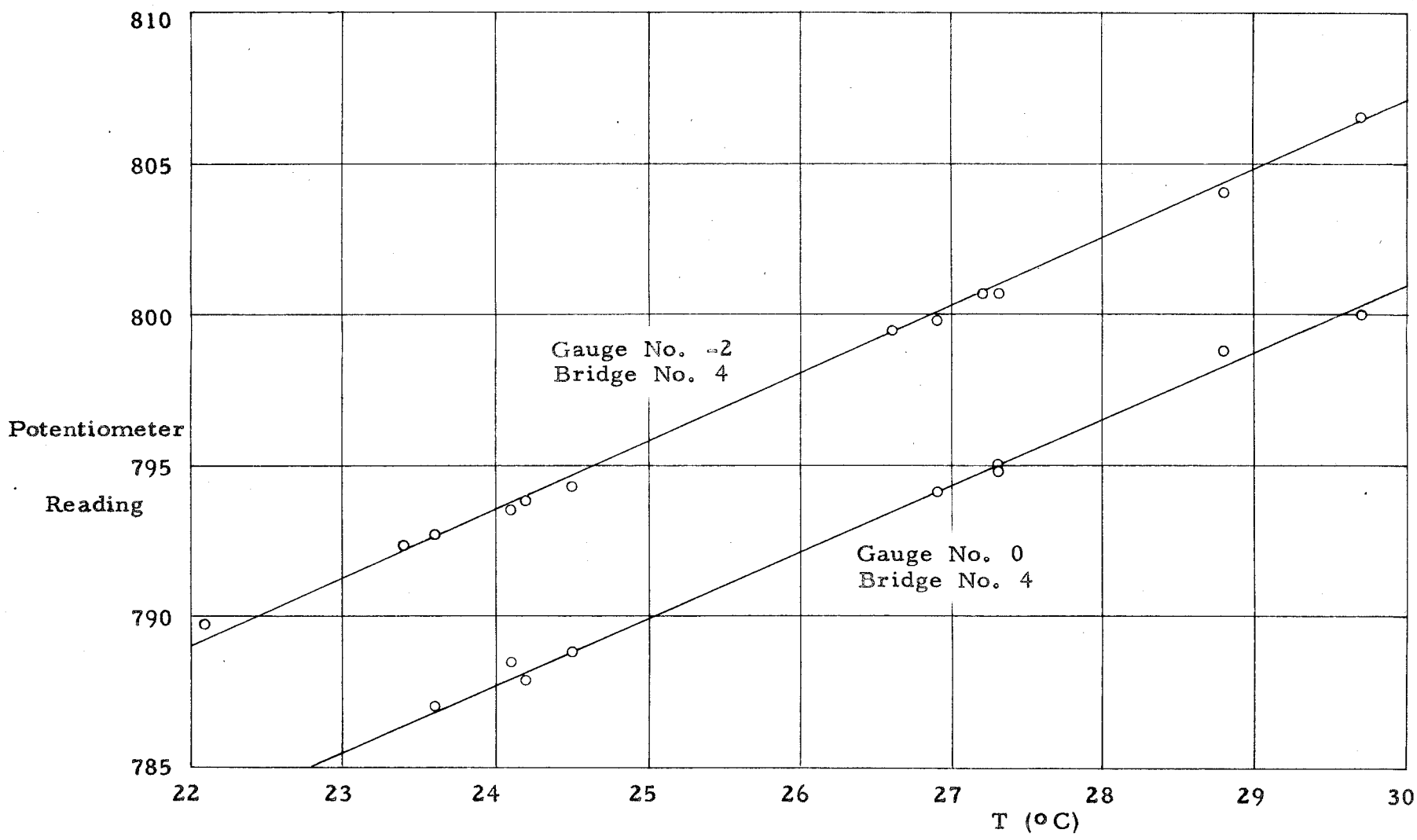

Fig. 12 (continued) - Typical platinum film calibrations

platinum.

The experimentally determined values of temperature coefficient of resistivity α were used as a basis for the reduction of both time-average temperatures and of temperature fluctuation measurements - see appendices 2 and 3.

Interpretation of measurements made with Pt film gauges in a wind tunnel depends largely on their dynamic characteristics.

The basic time constants involved in the problem of frequency response are:

(a) time τ_f necessary for the bulk of a heat pulse to penetrate film thickness t_f ; this is

$$\tau_f = \frac{t_f^2}{(k/\rho c_p)_f} \quad ; \tag{4}$$

numerical values are $t_f = 0.2\,\mu$

$= 2 \times 10^{-5}$ cm

and for platinum $k/\rho c_p = 0.24$ cm^2/sec.

Hence $\tau_f = 1.6 \times 10^{-9}$ sec; this is absolutely negligible.

(b) time necessary for temperature readjustment of model in neighborhood of gauge. This is analogous to the classical time constant of hot-wires. When a gauge is heated, so is the model in its neighborhood, and a large percentage of the power input to a gauge is transferred to the airflow by way of the adjoining model surface. A time constant τ_m is then defined as ratio of model heat content in neighborhood of

gauge to heat flow (i.e. steady state power input).

Measurements of gauge temperature rise above equilibrium vs. power input gave, in the steady state case, with our experimental conditions over a range of M_1, values of order

$$2.5 \times 10^{-2} \text{ to } 4.0 \times 10^{-2} \text{ W}(^{\circ}\text{C})^{-1};$$

"effective" heated volume in gauge neighborhood is $2 b_1 c_1 t$. Numerical values are

$$\left.\begin{aligned} c_p &= 0.20 \text{ cal/g}^{\circ}\text{C} \\ \rho &= 2.23 \text{ g/cm}^3 \end{aligned}\right\} \text{ for pyrex}$$

$$\left.\begin{aligned} b_1 &= 1.58 \text{ cm} \\ c_1 &= 0.102 \text{ cm} \\ t &= 0.132 \text{ cm} \end{aligned}\right\} \text{ see Sec. II-4}$$

$$1 \text{ cal} = 4.186 \text{ W sec}$$

Hence $\tau_m = 1.0$ to 1.6 sec with our experimental conditions.

One expects a wide range of frequencies ω such that

$$\tau_f \ll 1/\omega \ll \tau_m \tag{5}$$

over which gauge response will be independent of frequency; while for frequencies such that

$$1/\omega = O(\tau_m) \tag{6}$$

response will be frequency dependent (very much like that of a hot-wire).

Next question to consider is how are temperature fluctuations in the free stream related to temperature fluctuations at the gauge, i.e. at the interface between air and model wall.

If the wall were a perfect conductor maintained at constant temperature, heat conduction to the wall would damp out temperature fluctuations in a distance $\delta_{T'}$ which we might call a "temperature-fluctuation-thickness". Its order of magnitude is

$$(\delta_{T'})_a \doteq \sqrt{\frac{\kappa_a}{\omega}} \tag{7}$$

where $\kappa_a = (k/\rho c_p)_a$ = temperature diffusivity for air, and ω = circular frequency of fluctuations. Since the wall is neither a perfect conductor nor a perfect heat sink, temperature fluctuations penetrate into the wall to a depth of order

$$(\delta_{T'})_b \doteq \sqrt{\frac{\kappa_b}{\omega}} \tag{8}$$

where κ_b = temperature diffusivity of wall material. Note that normally $(\delta_{T'})_b \ll (\delta_{T'})_a$ and penetration of fluctuations into the wall does not affect thickness $(\delta_{T'})_a$.

At the interface $\vec{q}_a = \vec{q}_b$,

$$(k \ \text{grad} \ T)_a = (k \ \text{grad} \ T)_b \tag{9}$$

and in terms of fluctuation amplitudes

$$|T'| \left(\frac{k}{\delta}\right)_a = |T_w'| \left(\frac{k}{\delta}\right)_b \tag{10}$$

Amplitude of fluctuation at interface $|T'_w|$ is then related to amplitude of fluctuation in free stream $|T'|$

$$\frac{|T'_w|}{|T'|} = \frac{\dfrac{k_a}{\sqrt{k_a/\rho_a c_{p_a}}}}{\dfrac{k_b}{\sqrt{k_b/\rho_b c_{p_b}}}} = \frac{\sqrt{k_a \rho_a c_{p_a}}}{\sqrt{k_b \rho_b c_{p_b}}} = \frac{\beta_a}{\beta_b} \qquad (11)$$

Temperature penetration factors β are: for air, at $0^\circ C$, atmospheric pressure

$$\beta_a = 1.34 \times 10^{-4} \text{ cal/cm}^2 \text{ °C s}^{1/2}$$

for pyrex glass $\beta_b = 3.5 \times 10^{-2}$ cal /cm^2 °C s$^{1/2}$

Hence for air at NPT and pyrex glass

$$\beta_a / \beta_b \doteq 3.9 \times 10^{-3}$$

With our experimental conditions

$$T_t \doteq 30\,°C \qquad p_t = 0.975 \text{ atm}$$

the above value holds approximately at a stagnation point or a point with local $M = 0$; with the pressure and temperature conditions at a point of local $M = 1$,

$$\rho^*/\rho_t = 0.634$$

$$T^*/T_t = 0.833$$

$$\frac{k^*}{k_t} = \left[\frac{T^*}{T_t}\right]^{0.75} = 0.874$$

$$\frac{\beta_a}{\beta_b} \doteq 2.9 \times 10^{-3}$$

Intermediate values will apply to conditions between stagnation and sonic points.

The above analysis holds under the assumptions:

(a) temperature field due to fluctuations can be superimposed on steady state field;

(b) heat flow due to fluctuations is one-dimensional at interface.

Assumption (a) means that the characteristic time scale $\frac{1}{\omega}$ of fluctuations is such that

$$\frac{1}{\omega} << \tau_m . \tag{12}$$

Assumption (b) means that the characteristic dimension c_1 of gauge is large compared with $(\delta_{T'})_a$, and also that the characteristic length $\lambda_{T'}$ of temperature fluctuations is large compared with c_1,

$$(\delta_{T'})_a << c_1 \tag{13}$$

$$c_1 << \lambda_{T'} \tag{14}$$

Since κ_a (at NPT) is of order $0.2\ cm^2/sec$, equation (13) is equivalent to another low frequency limit

$$\omega \gg \frac{\kappa_a}{c_1^2} \doteq 20\ rad/sec \tag{15}$$

Equation (14) can be considered as a limit of geometrical resolution for temperature fluctuations due to temperature spottiness convected by the airstream, or for fluctuations in heat transfer caused by fluctuations in mass-flow rate past transducer. In the case of fluctuations propagated with a definite phase velocity, e.g. temperature fluctuations in sound waves, equation (14) is equivalent to another high frequency limit

$$\omega \ll \frac{a}{c_1} \doteq 3.3 \times 10^5\ rad/sec \tag{16}$$

All the experimental results reported in Part III fall into a frequency range such that

$$\tau_f < \frac{c_1}{a} \ll \frac{1}{\omega} \ll \frac{c_1^2}{\kappa_1} < \tau_m \tag{17}$$

so that reduction formula [equation (11)] can be applied.

III. EXPERIMENTAL RESULTS

Most of the tests reported in this Part were made with the $\frac{d}{H} = 0.0666$ model; corresponding Mach and Reynolds' numbers are:

M_1	Re_1
0.35	117,000
0.40	132,000
0.45	146,000
0.50	159,000
0.55	172,000
0.60	183,000
0.65	193,000
0.70	201,000

No attempt is made to correct results for tunnel blockage; i.e. all results refer to "tunnel Mach numbers" rather than "free-stream-in-absence-of-walls Mach numbers". Blockage corrections are estimated, however, in appendix 1.

1. Preliminary surveys

Before attempting temperature-fluctuation and temperature recovery experiments, some preliminary surveys were decided upon, using conventional wind tunnel techniques. These included rather complete pressure distribution tests (with slow reading mercury manometers) and a large series of schlieren surveys (both flash and time exposures) of the flow field around the model and especially its wake. A hot wire placed outside the edge of the wake was used

in these tests to identify the dominating wake frequencies.

A check was also made of the two-dimensionality of the flow pattern in the area not accessible to schlieren observation. Oil spray was introduced into the air flow and the pattern of oil streaks observed. Droplets accumulated in the separation line regions appeared as perfectly straight lines (except at the model ends, within the tunnel wall boundary layers), proving perfect two-dimensionality of the flow pattern in time-average sense.

The preliminary survey disclosed also some peculiar resonance phenomena between wake and tunnel. Their mechanism was investigated in more detail.

With a $\frac{d}{H} = 0.0666$ model resonance effects above $M_1 = 0.35$ became first apparent as a strong whistling sound around $M_1 = 0.50$; with further increase of Mach number the whistling subsided at first, and then reappeared as a roaring sound around $M_1 = 0.64$. The roar extended up to the choking limit ($M_1 = 0.73$ with this $\frac{d}{H}$ ratio). At the choking limit noise level dropped quite suddenly.

With a smaller model ($\frac{d}{H} = 0.0400$) the discrete resonance point was displaced towards $M_1 = 0.55$; the range of roaring sound extended from $M_1 = 0.64$ up to choking (around $M_1 = 0.79$).

Results of (time-average) pressure distribution measurements on the 0.624 in. diameter model ($\frac{d}{H} = 0.0666$) spanning the tunnel ($\frac{b}{d} = 6.41$) are summarized in figure 13.

Sonic conditions are indicated as C_{ps} on the graphs. They first appear locally around $M_1 = 0.60$, and quite extensively around $M_1 = 0.65$.

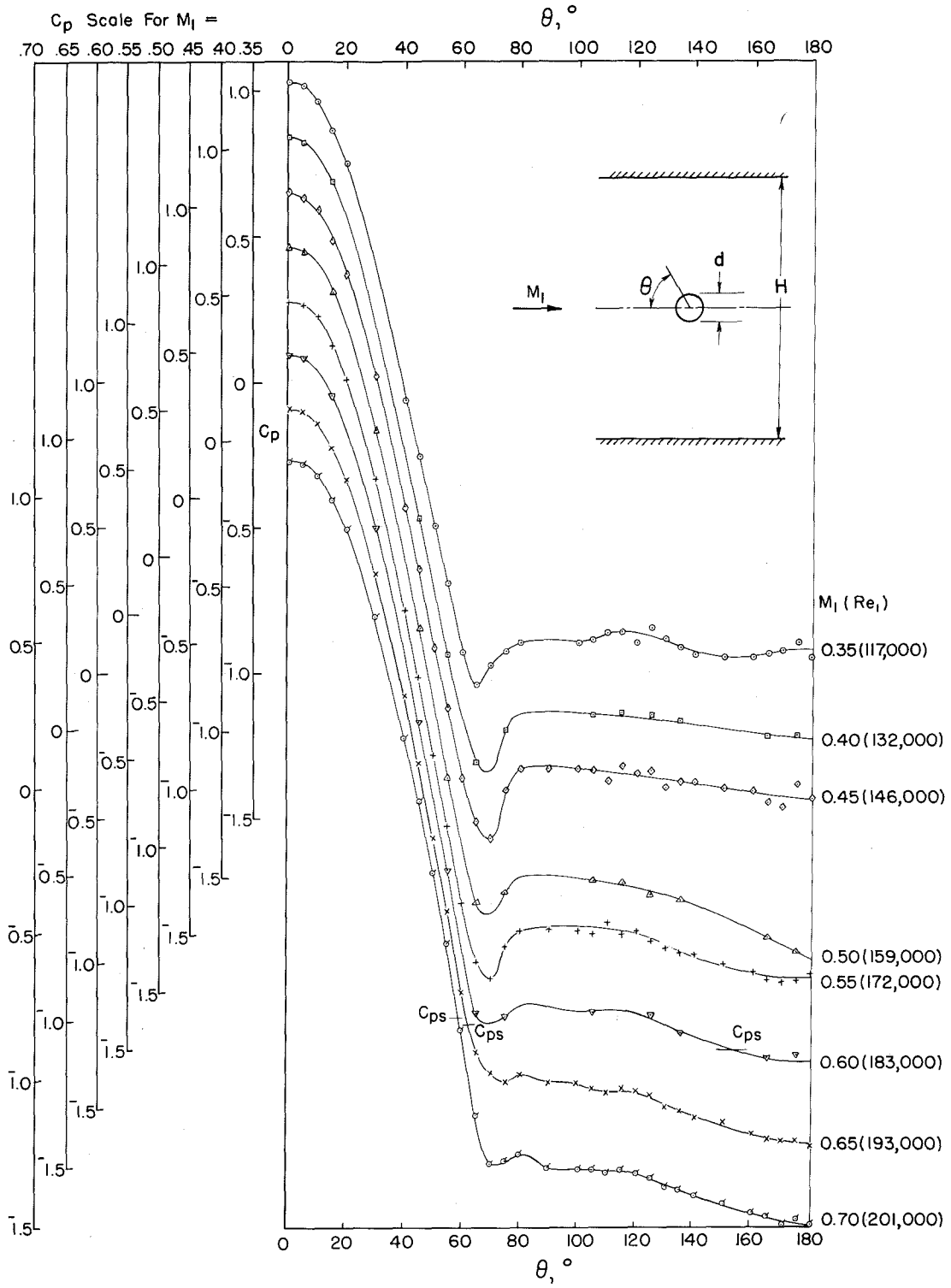

Fig. 13 - Pressure distribution (time - average)

Figure 14 shows plots of $C_p \cos\theta$. Integrated values (pressure drag coefficients)

$$C_{D_p} = \frac{1}{2\pi} \int_0^{\pi} C_p \cos\theta \, d\theta \qquad (18)$$

are shown in figure 15.

Since these pressure distributions were obtained by slow reading instruments, and since appreciable pressure fluctuations may introduce an error in time-average pressure readings - an estimate of possible error is included in appendix 4.

The reduced wake frequency (Strouhal number) $St_1 = \frac{nd}{U_1}$ was measured with a hot wire normal to flow and to cylinder axis, installed in tunnel plane of symmetry at $\frac{x}{d} = 2.0$, $\frac{y}{d} = 2.0$, i.e. well outside wake edge. (Wire holder can be seen in figures 25 to 32.) Hot wires were 0.0005 in. diameter x 0.120 in. long, and their orientation was chosen to provide least lift interaction between wire holder and vortex street. Natural frequency of the strut supporting the wire holder was very small compared with wake frequency.

Typical spectra of (uncompensated) wire output are shown in figures 16 and 17. The dominating wake frequency or frequencies recorded in such spectra were checked against an oscillator and counter arrangement. They are plotted in reduced form in figure 18 (for the $\frac{d}{H} = 0.0666$ model), and in figure 19 (for the $\frac{d}{H} = 0.0400$ model).

As a check on the mechanism of resonance, a series of hot-wire traverses in plane $\frac{x}{d} = 1.0$ (see figures 20 to 23) was made in which total signal from an uncompensated hot wire was recorded,

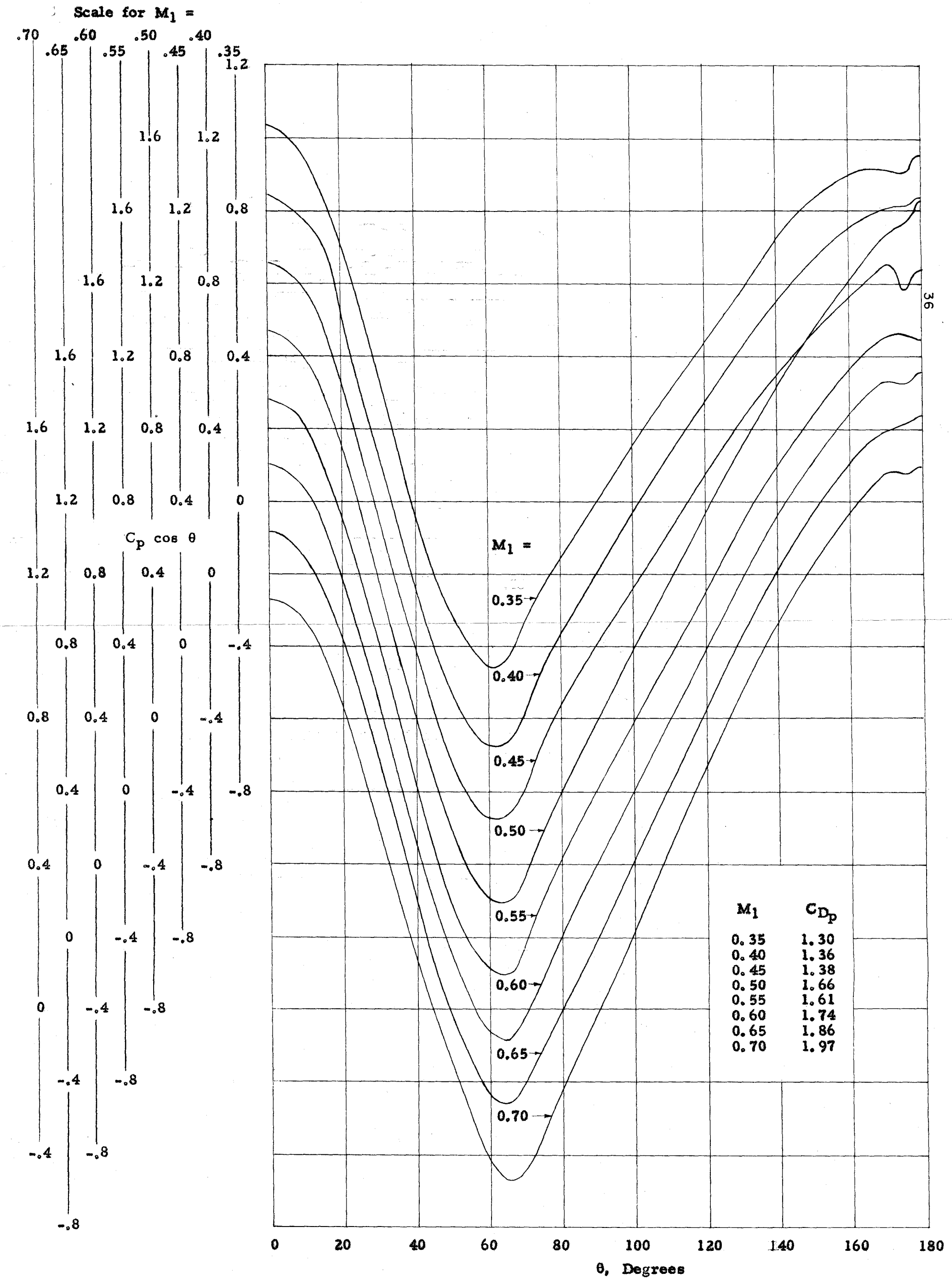

Fig. 14 - Time-average $C_p \cos \theta$

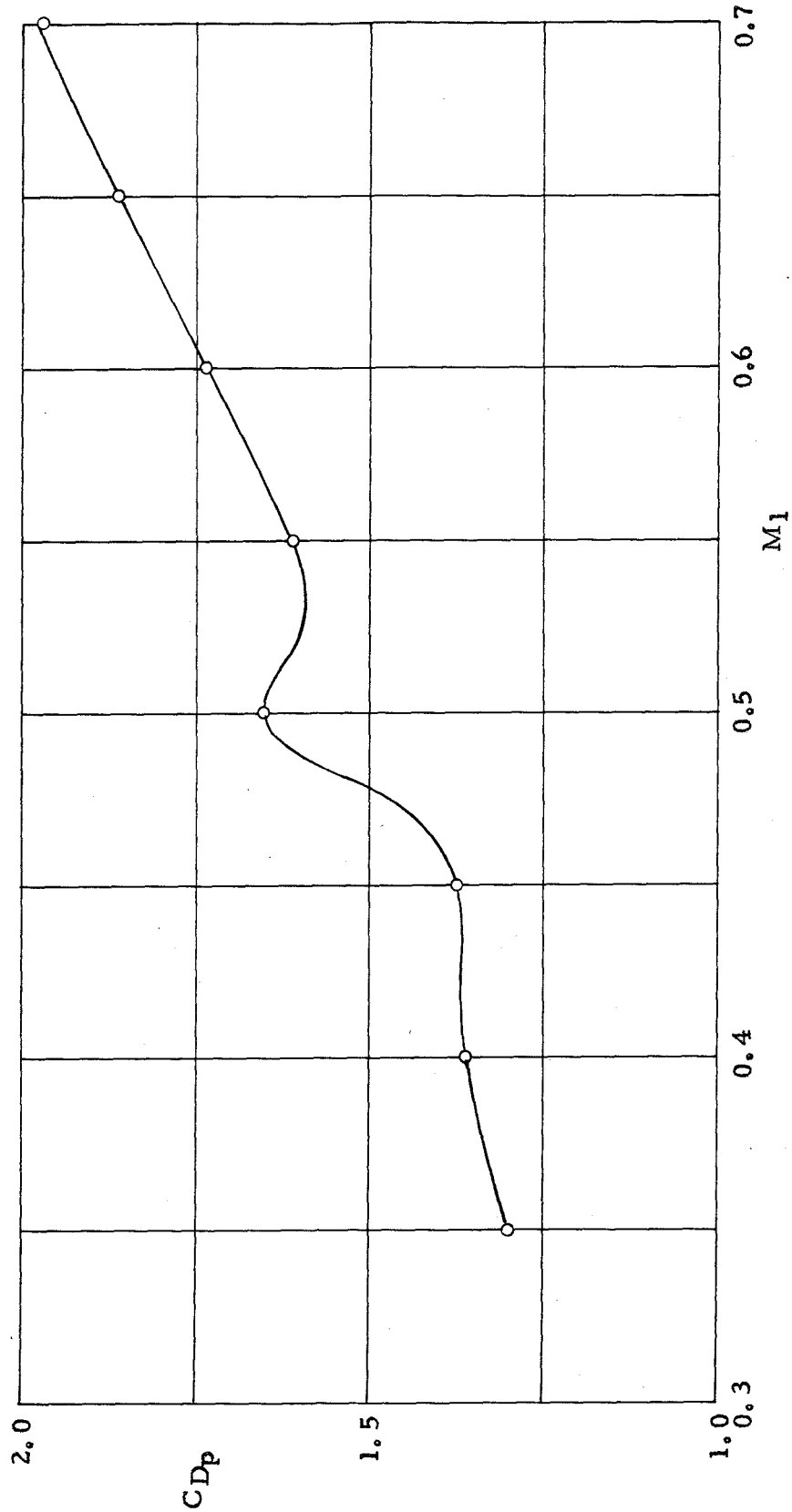

Fig. 15 - Pressure drag coefficient (time - average)

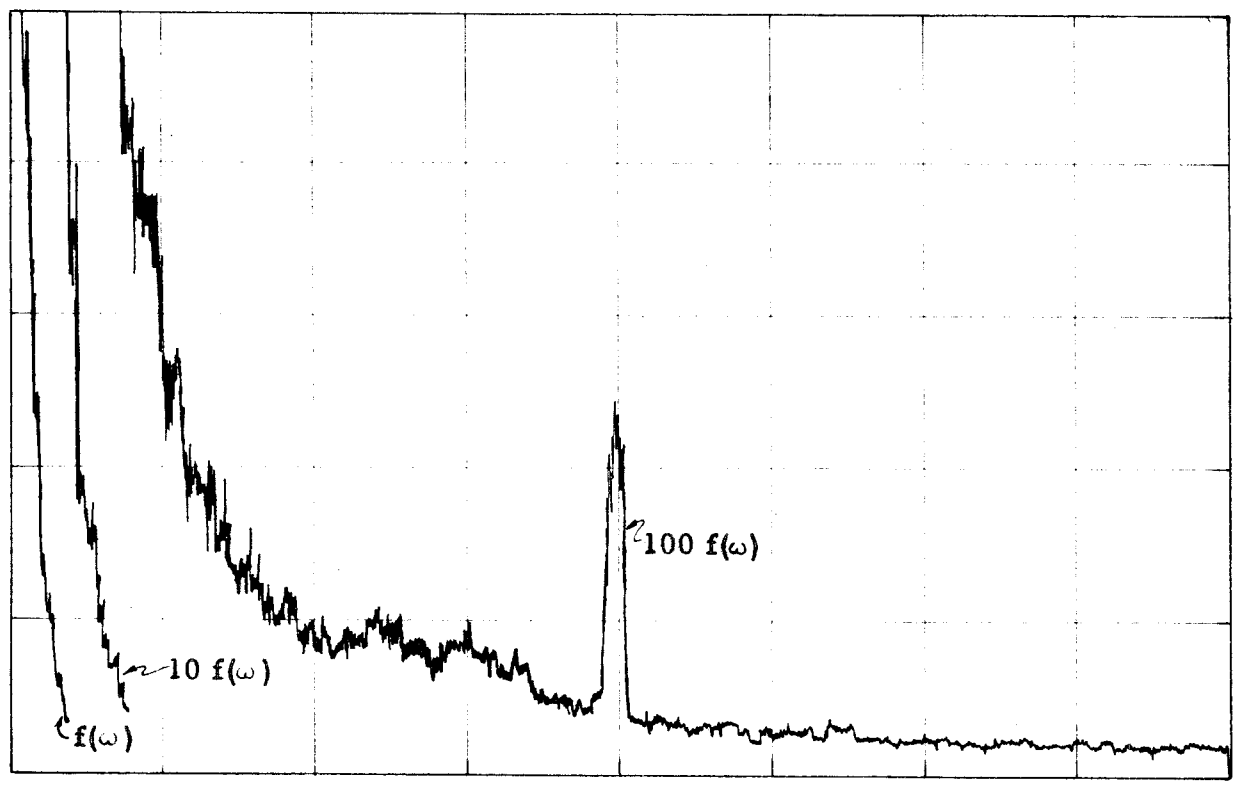

Fig. 16 - (M_1 = 0.45)

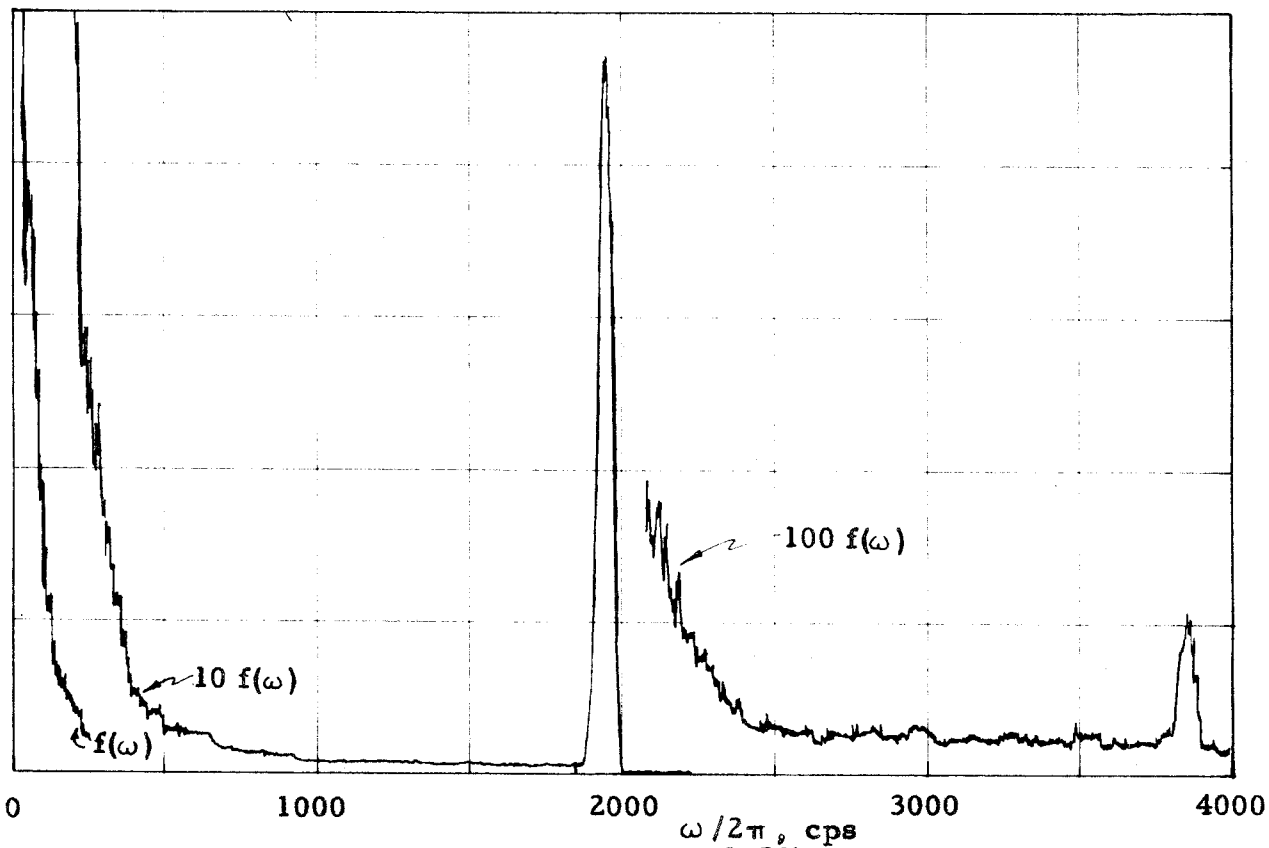

Fig. 17 - (M_1 = 0.50)

Figs. 16 and 17 - Typical hot-wire spectra at edge of wake

Uncompensated hot-wire at x/d = 2.0, y/d = 2.0

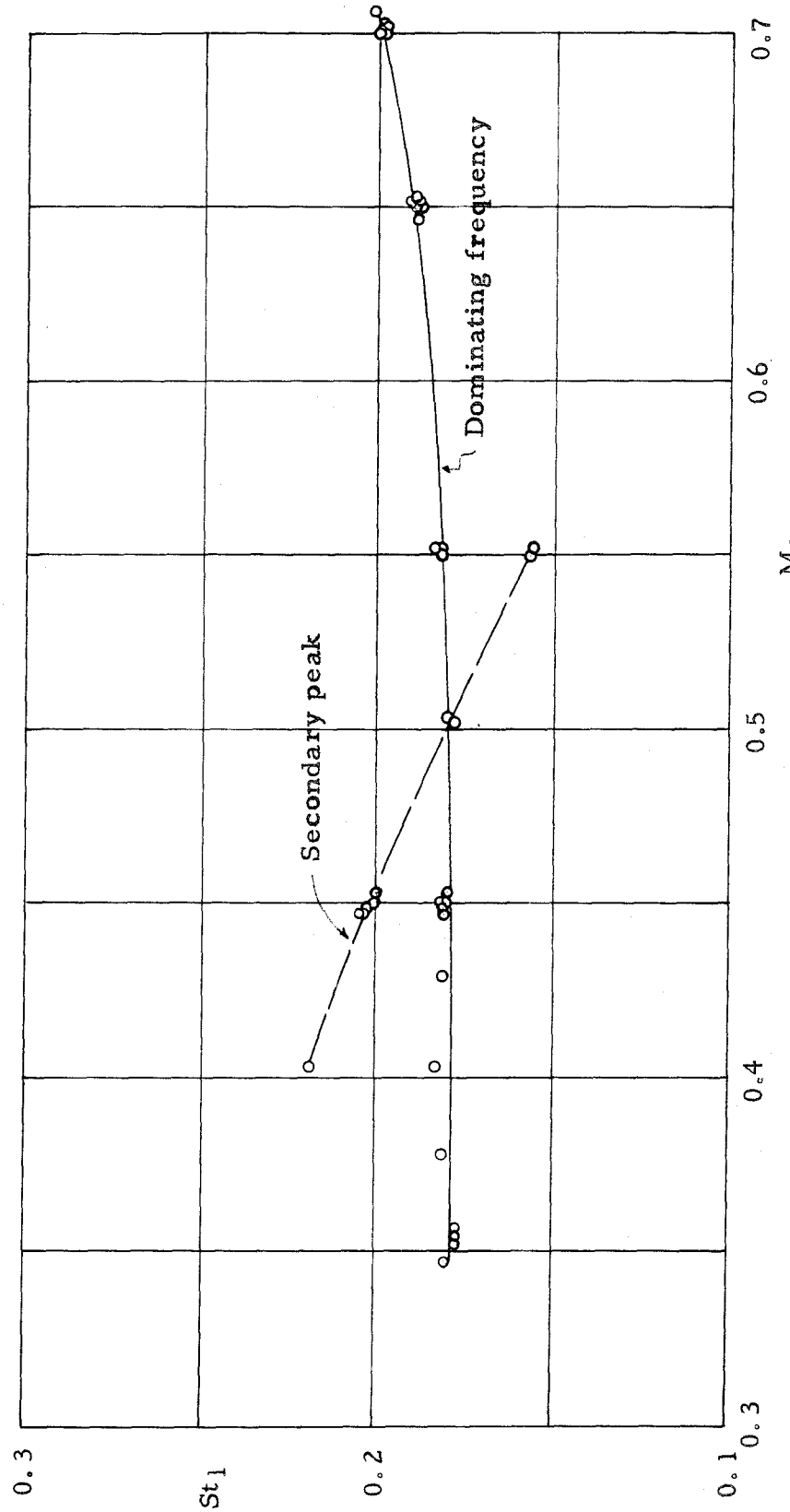

Fig. 18 - Reduced wake frequency (d/H = 0.0666)

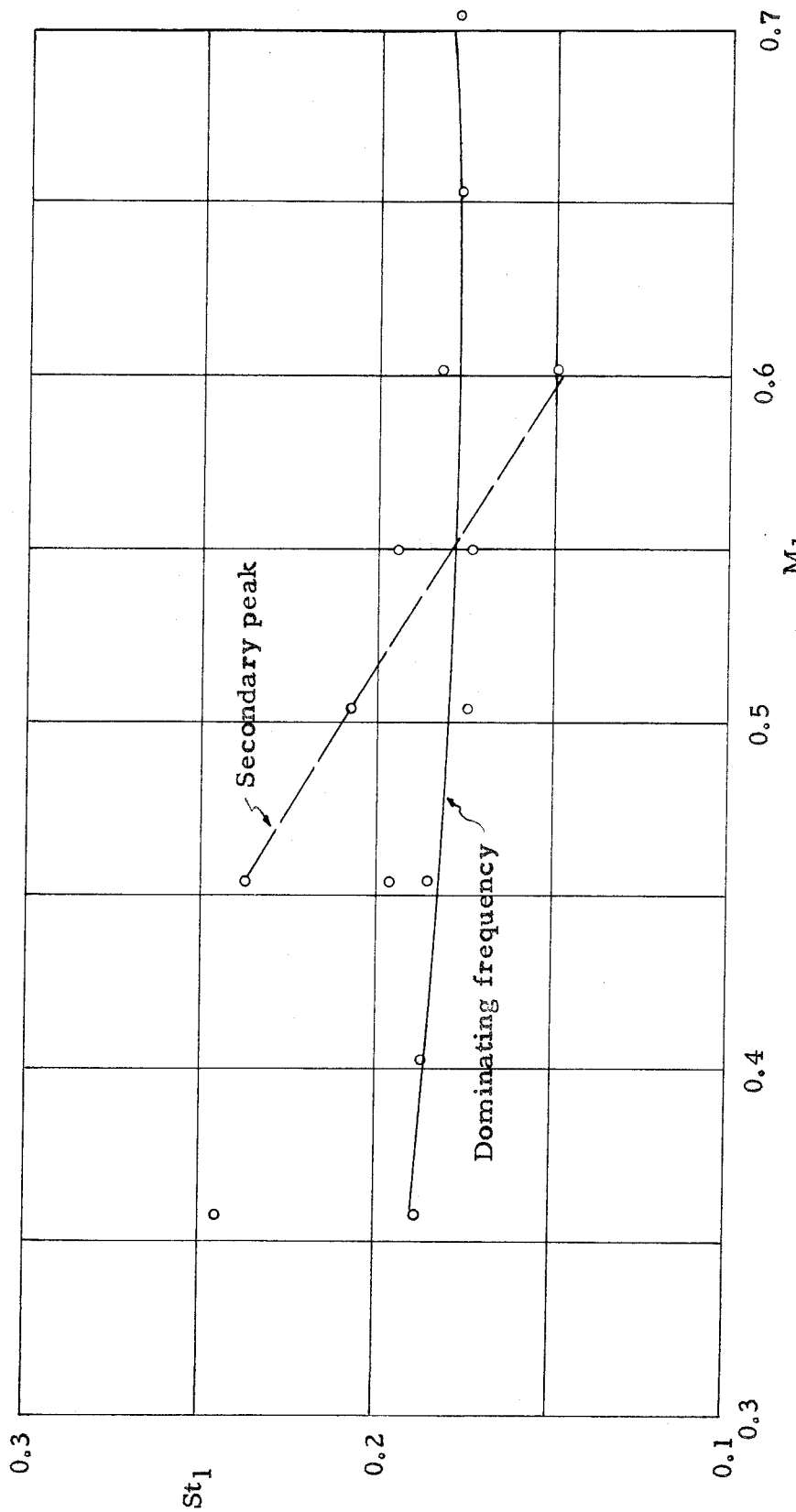

Fig. 19 - Reduced wake frequency (d/H = 0.0400)

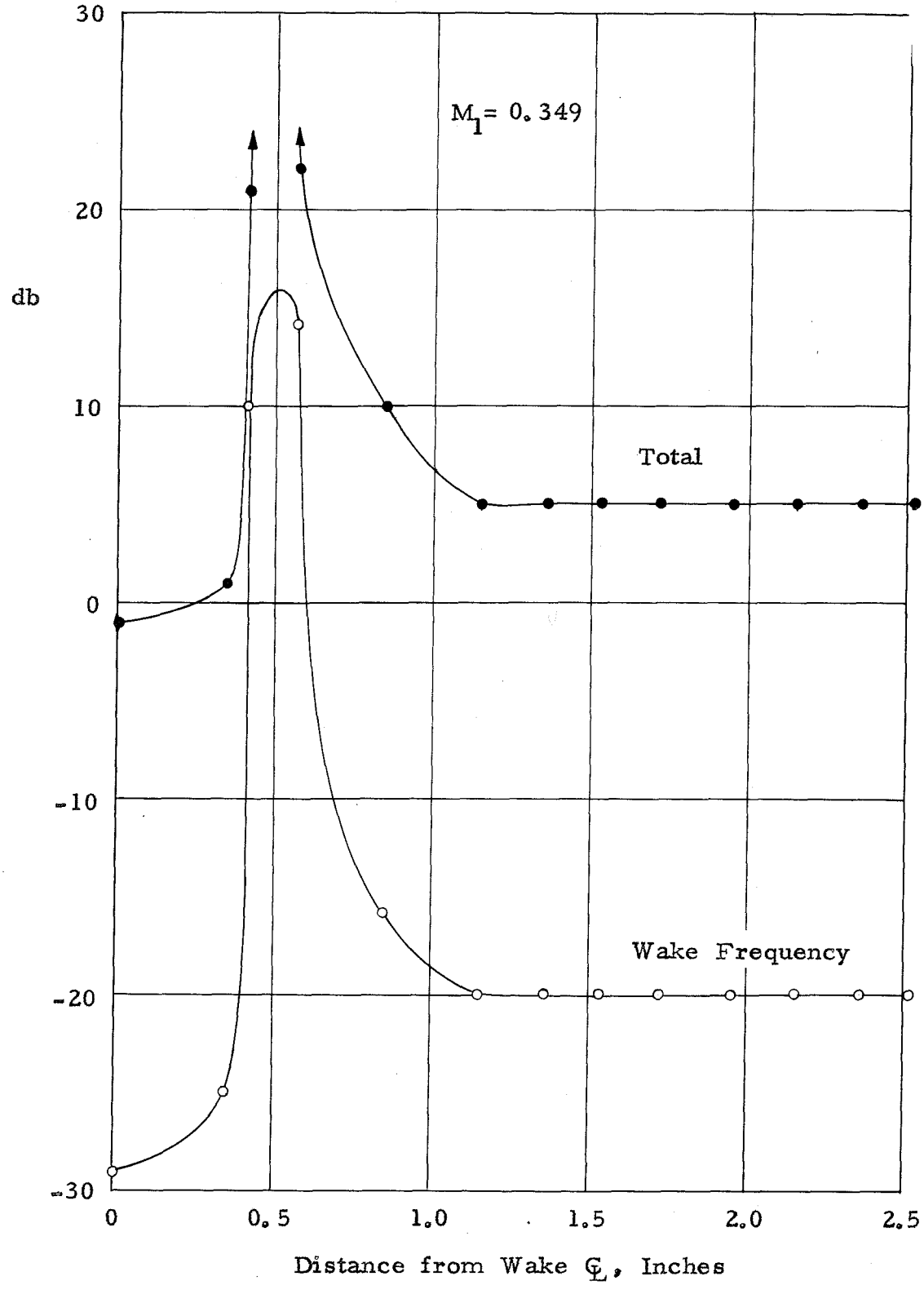

Fig. 20 - Hot-wire traverse in plane x/d = 1.0
(M_1 = 0.349)

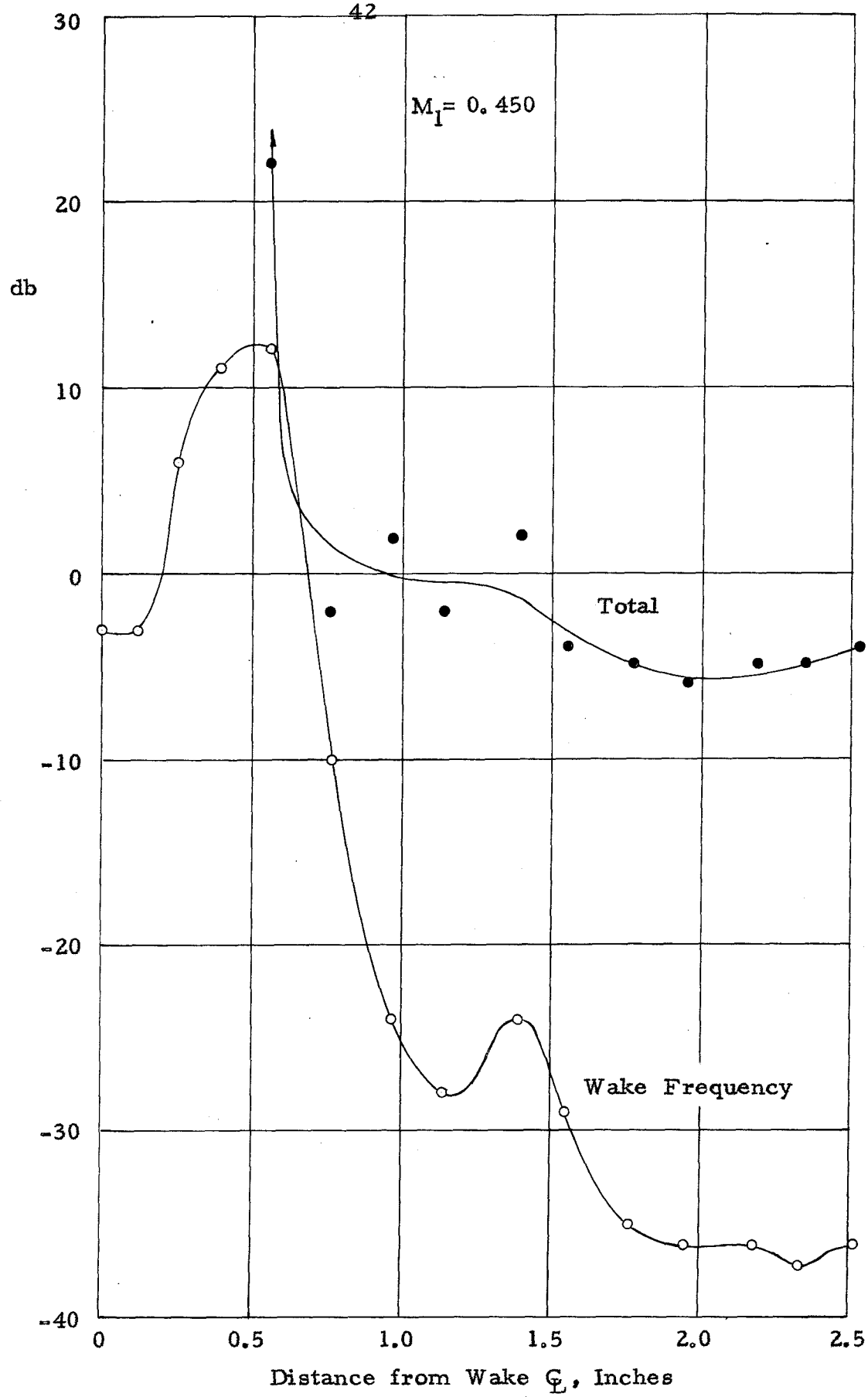

Fig. 21 - Hot-wire traverse in plane x/d = 1.0 (M_1 = 0.450)

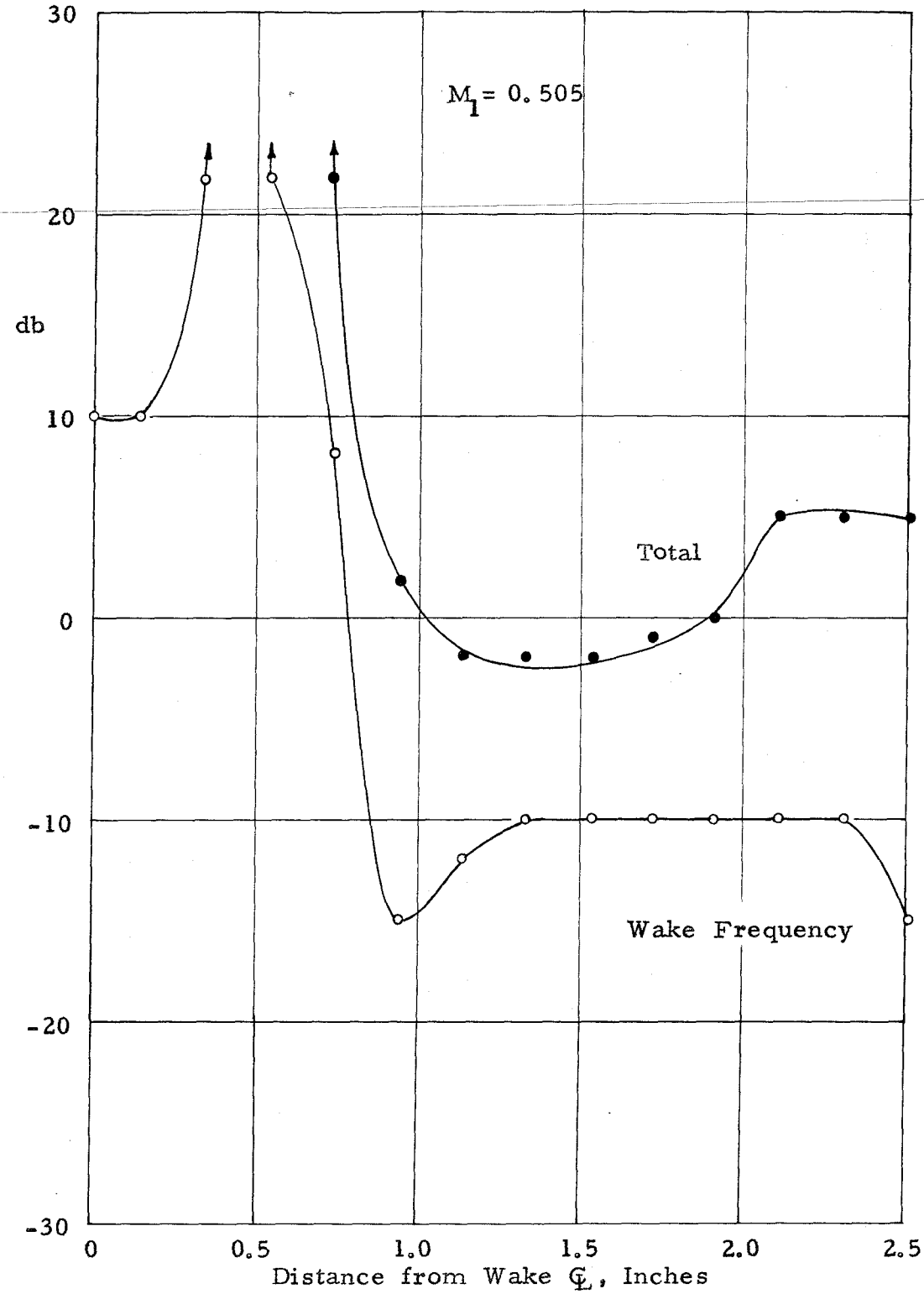

Fig. 22 - Hot-wire traverse in plane x/d = 1.0

(M_1 = 0.505)

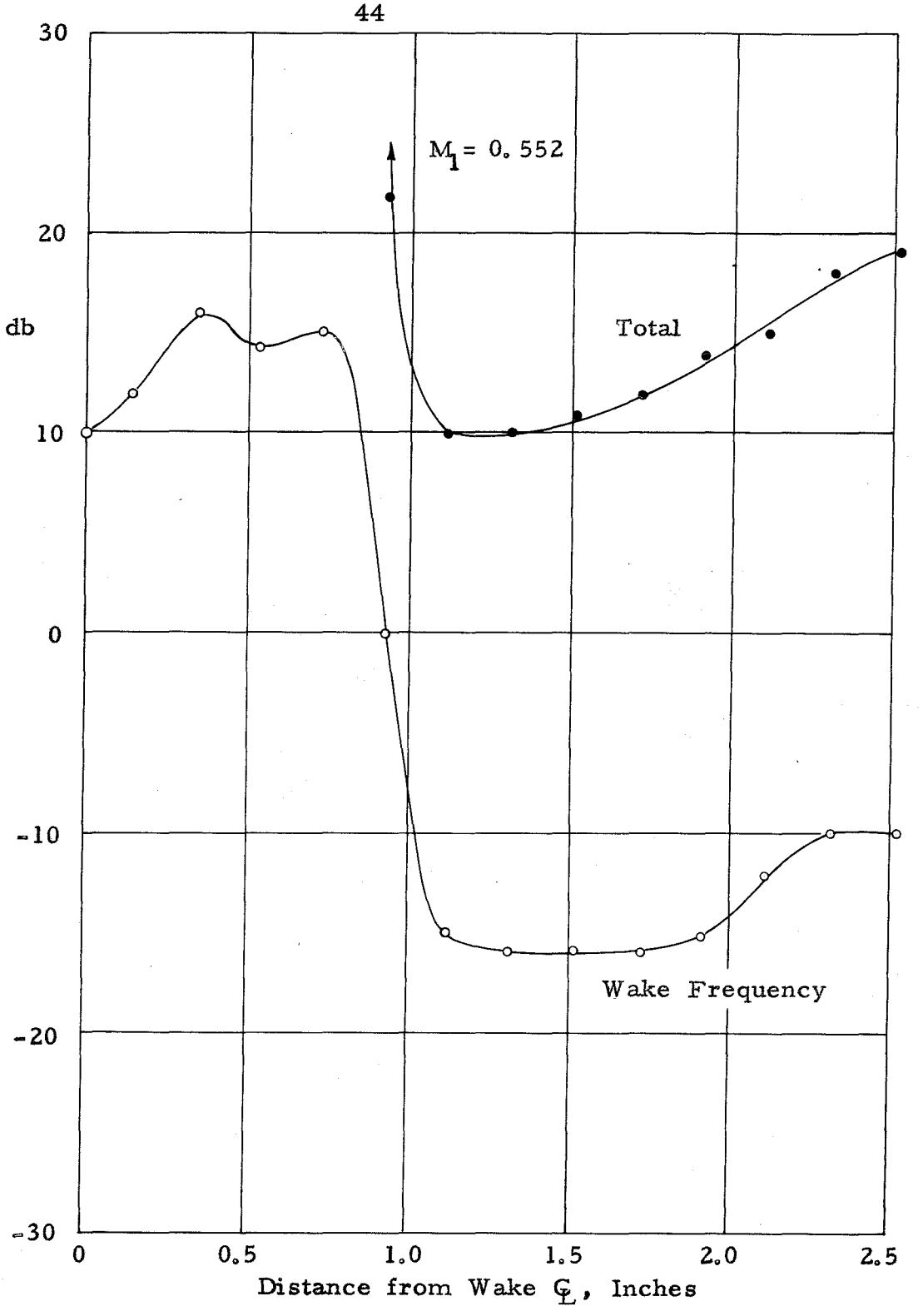

Fig. 23 - Hot-wire traverse in plane x/d = 1.0

(M_1 = 0.552)

and also the signal within a 50 cps band centered around the dominant wake frequency. Both disclosed some standing wave patterns with maxima occurring at some distance from the shear layer whenever strong whistling occurred. This in spite of the fact that the flow was definitely subsonic in these areas.

A summary of the schlieren survey is shown in figure 24; this includes both flash (3 - 4 μ sec) and time exposures ($\frac{1}{25}$ sec), with horizontal and vertical knife edge, and also many check pictures (without flow) between runs.

A sequence of typical schlieren flash photographs of wake, at Mach number from M_1 = 0.35 to 0.70 is shown in figures 25 to 32. Both pressure distribution tests and schlieren surveys show that

(1) at M_1 = 0.60 the edge of the separated shear layer becomes sonic, and so does (intermittently and locally) some of the flow outside the attached boundary layer upstream of the separation point.

(2) at M_1 = 0.65 there is a definite supersonic region extending from upstream of separation point and well into the exterior of the wake area.

A closer scrutiny of figures 25 to 32 reveals also a definite pitching oscillation pattern of the separated flow area, from separation point up to $\frac{x}{d} \doteq 1$ downstream. It was not possible to ascertain from the schlieren photographs whether this oscillation extends to the attached flow field on the front part of the cylinder.

The time exposure photograph sequences figures 33, 34 and 35 show how the evolution of the recirculation zone parallels that

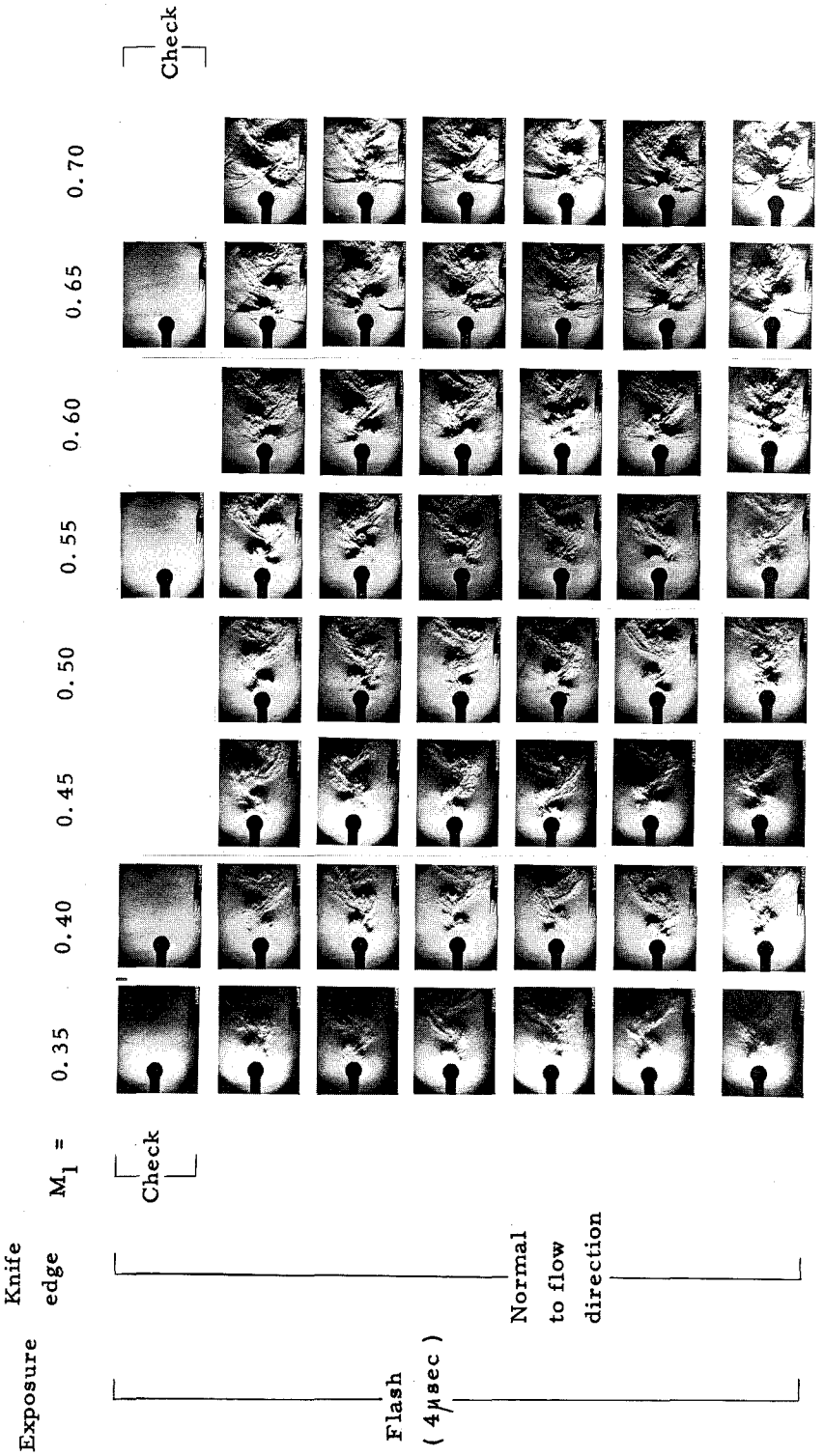

Fig. 24 - Summary of Schlieren survey

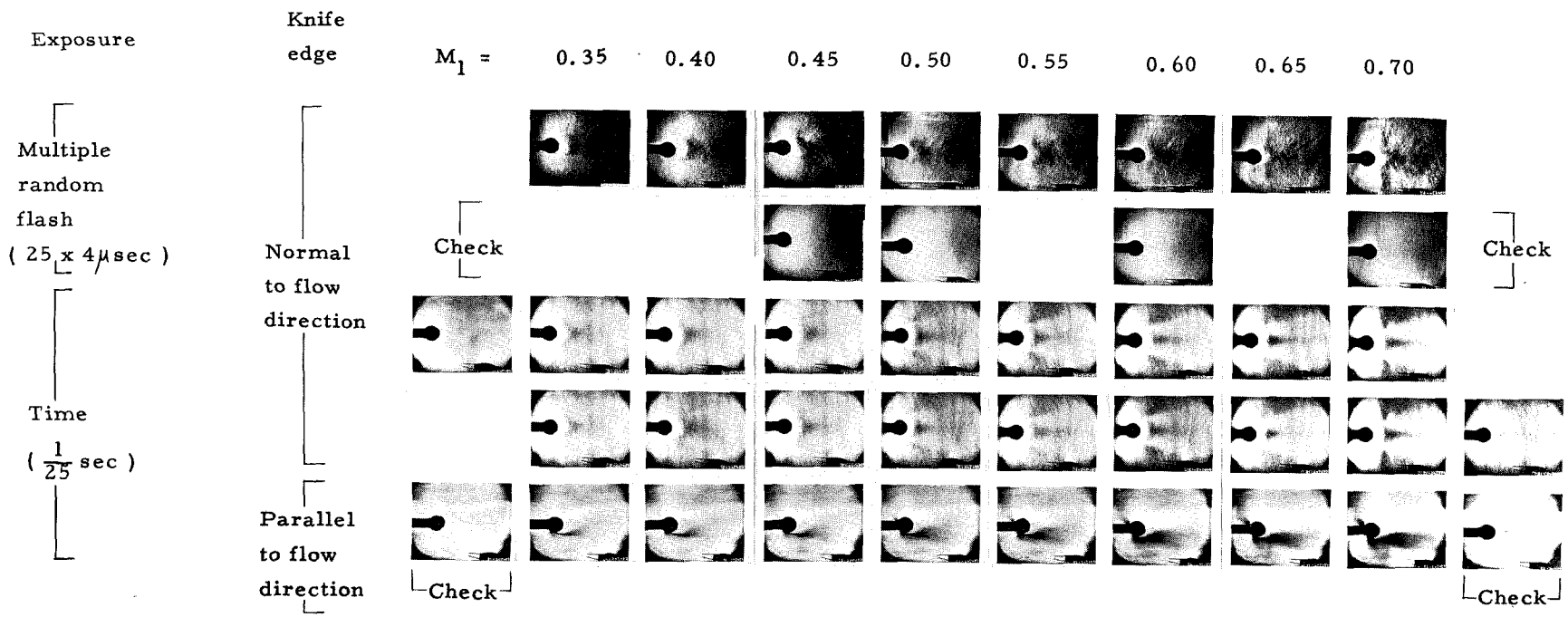

Fig. 24 (continued) - Summary of Schlieren survey

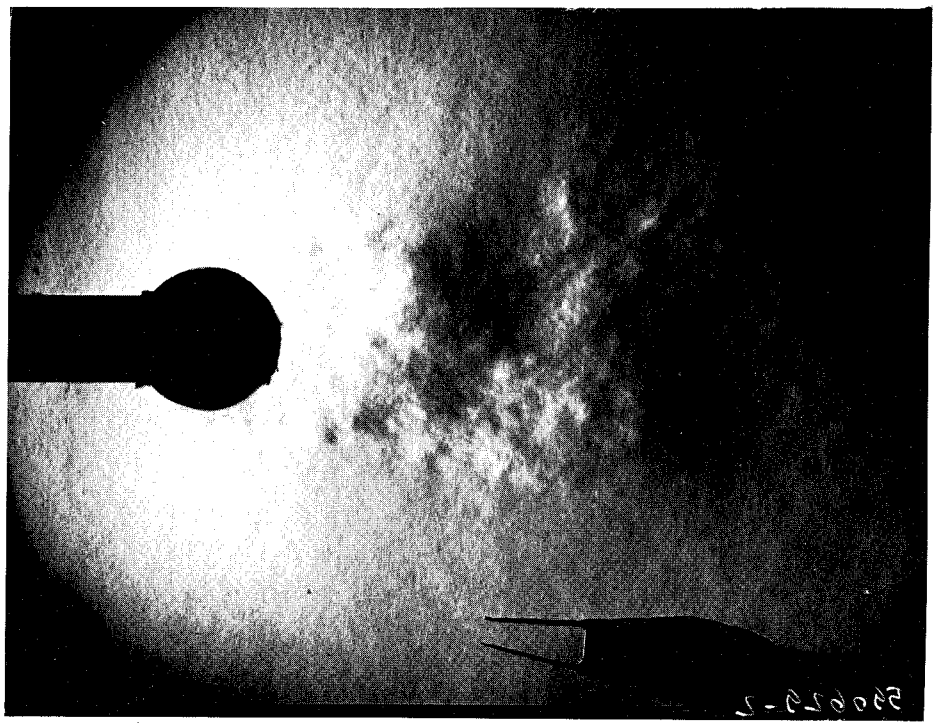

Fig. 25 - Typical Schlieren flash (4μsec) photographs of wake ; M_1 = 0.35

Fig. 26 - Typical Schlieren flash (4μsec) photographs of wake ; $M_1 = 0.40$

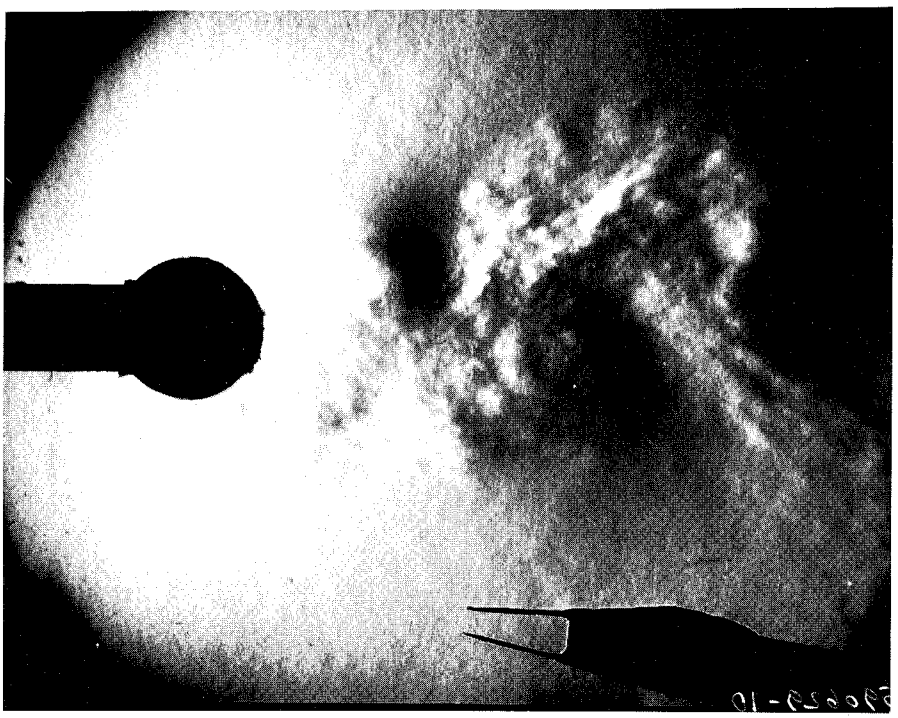

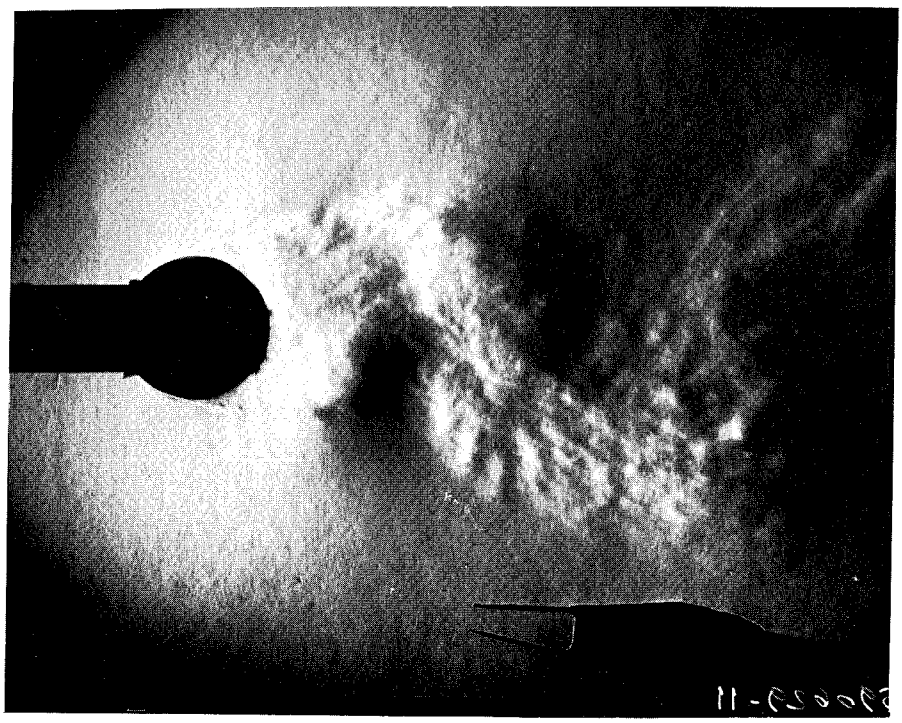

Fig. 27 - Typical Schlieren flash (4μsec) photographs of wake ; $M_1 = 0.45$

Fig. 28 - Typical Schlieren flash (4μsec) photographs of wake ; M_1 = 0.50

Fig. 29 - Typical Schlieren flash (4μsec) photographs of wake ; $M_1 = 0.55$

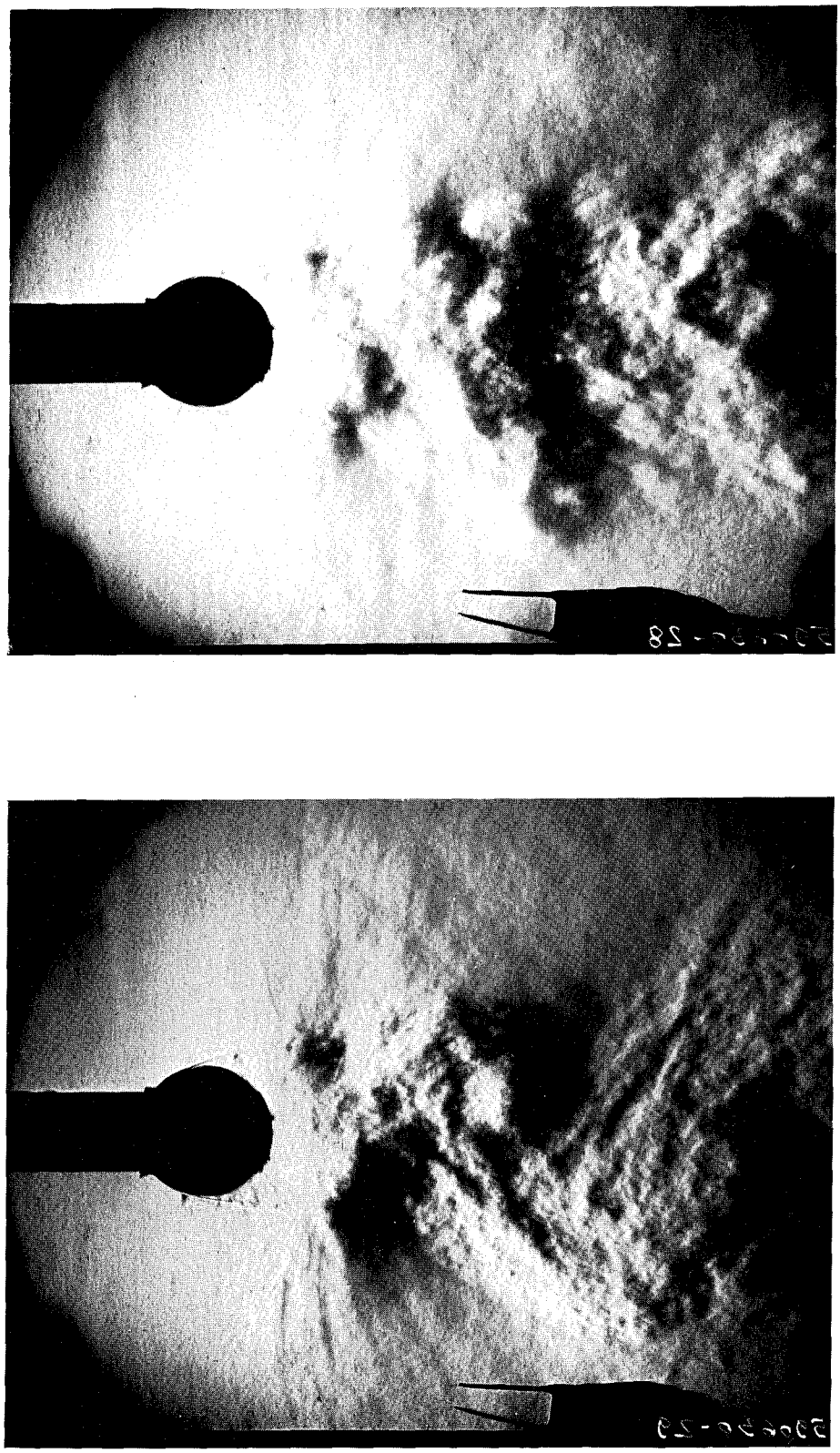

Fig. 30 - Typical Schlieren flash (4μsec) photographs of wake ; $M_1 = 0.60$

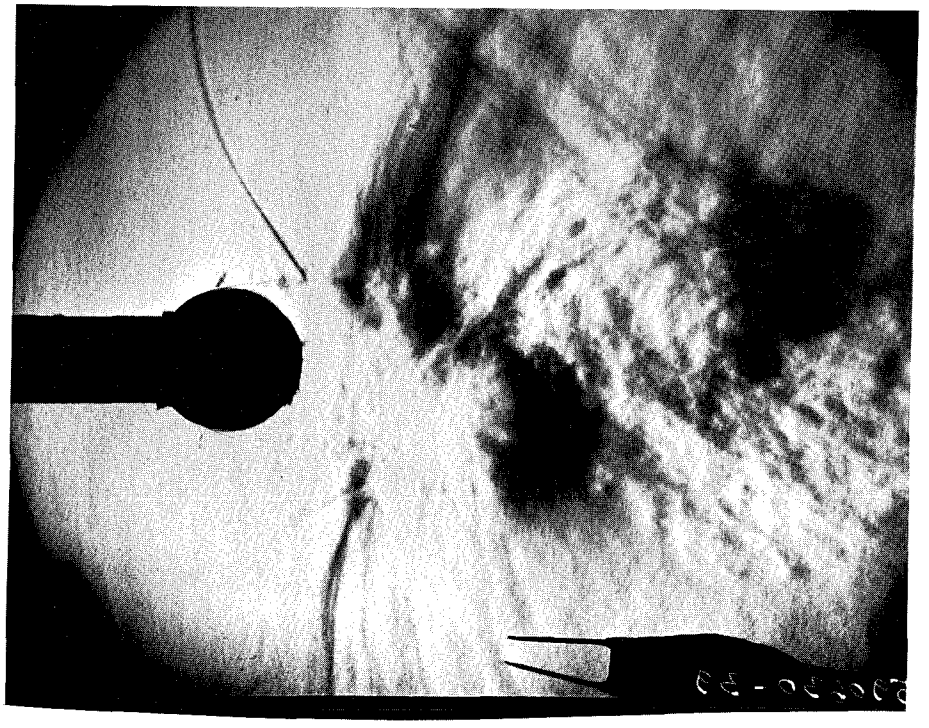

Fig. 31 - Typical Schlieren flash (4μsec) photogr
of wake ; $M_1 = 0.65$

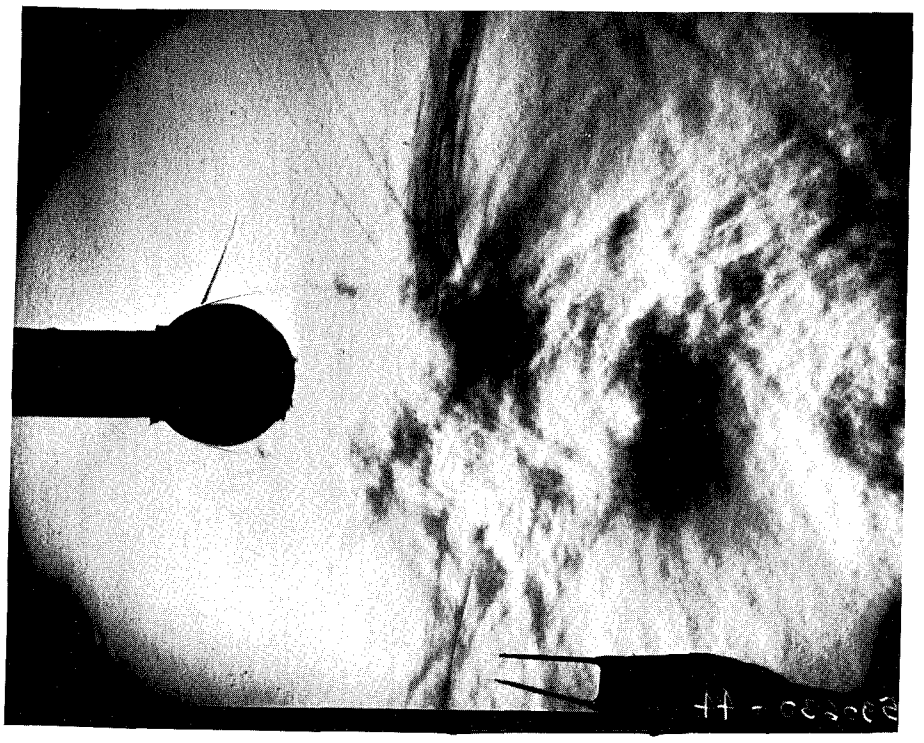

Fig. 32 - Typical Schlieren flash (4μ sec) photographs of wake ; $M_1 = 0.70$

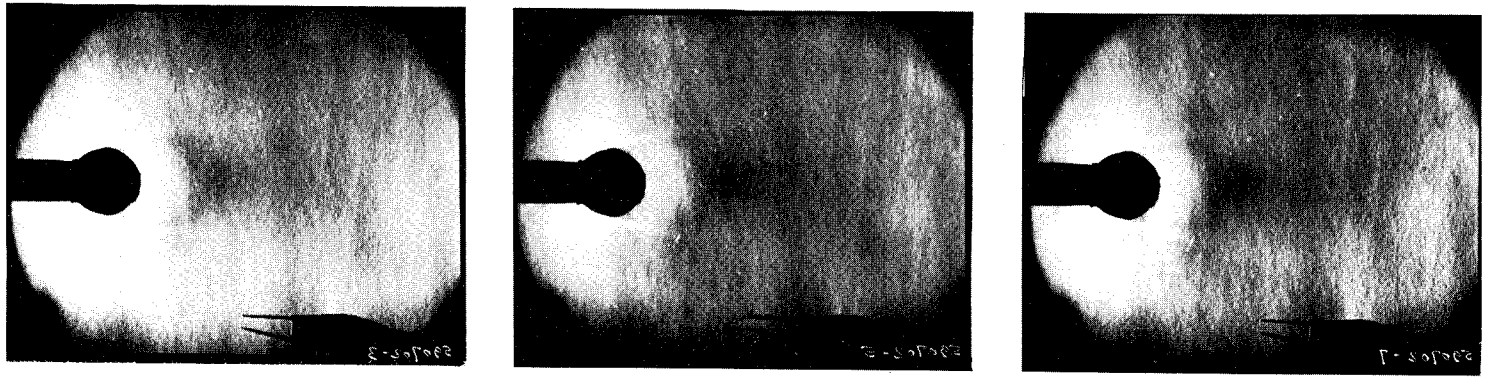

(a) knife edge normal to flow direction

$M_1 = 0.35$ $M_1 = 0.40$ $M_1 = 0.45$

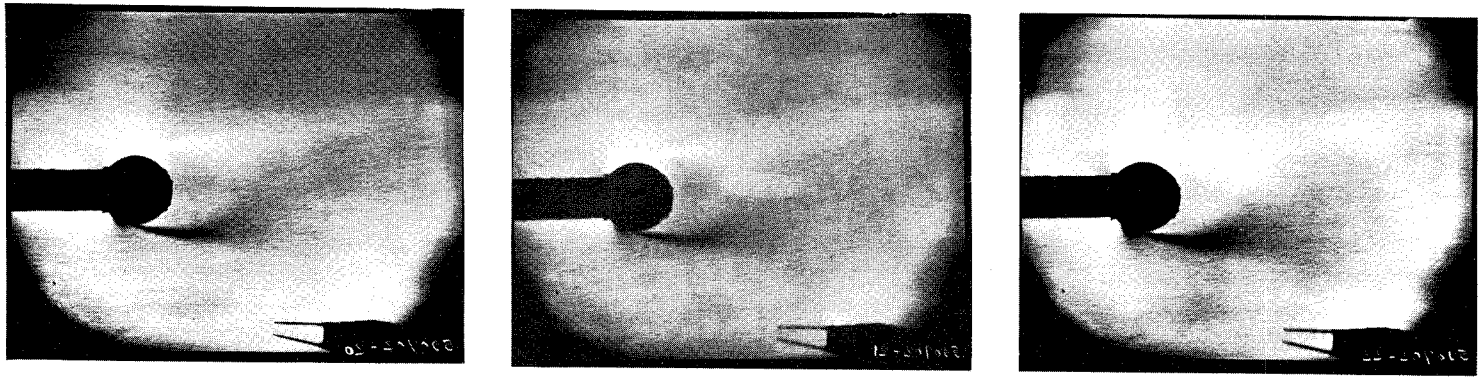

(b) knife edge parallel to flow direction

Fig. 33 - Typical Schlieren time exposure ($\frac{1}{25}$ sec) photographs of wake ; $M_1 = 0.35$ to 0.45

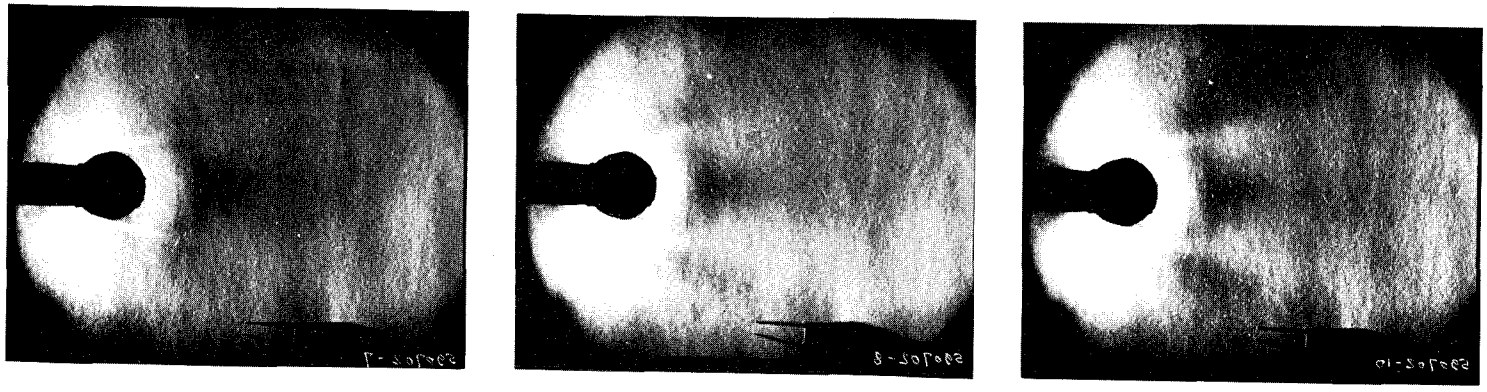

(a) knife edge normal to flow direction

$M_1 = 0.45$ $M_1 = 0.50$ $M_1 = 0.55$

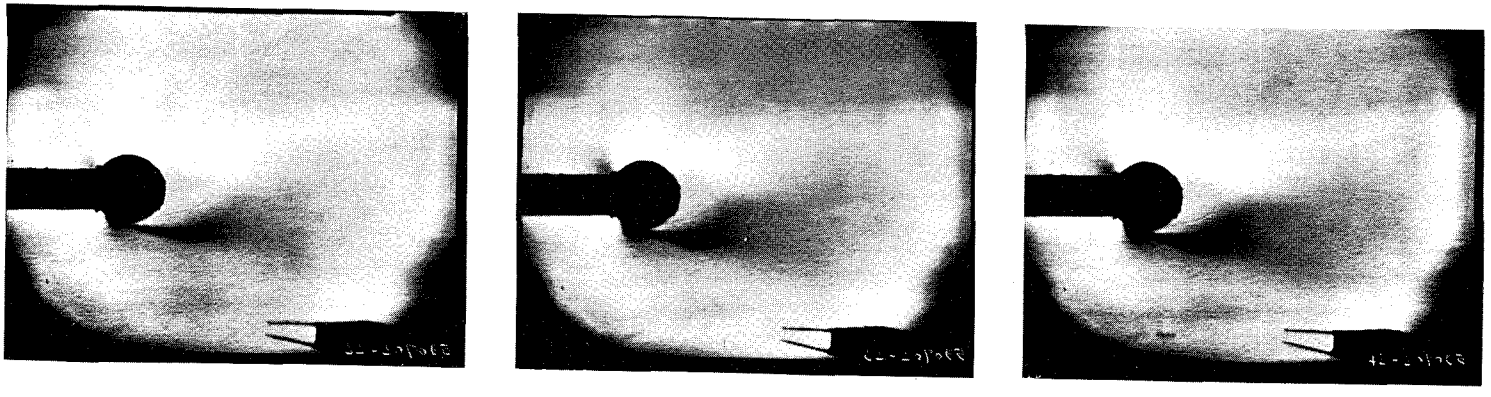

(b) knife edge parallel to flow direction

Fig. 34 - Typical Schlieren time exposure ($\frac{1}{25}$ sec) photographs of wake ; $M_1 = 0.45$ to 0.55

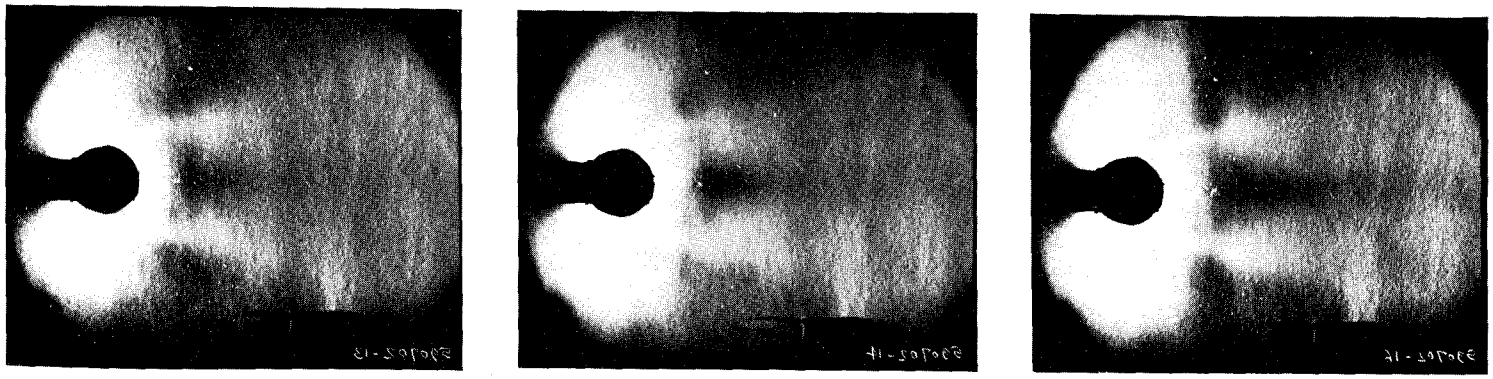

(a) knife edge normal to flow direction

$M_1 = 0.60$ $M_1 = 0.65$ $M_1 = 0.70$

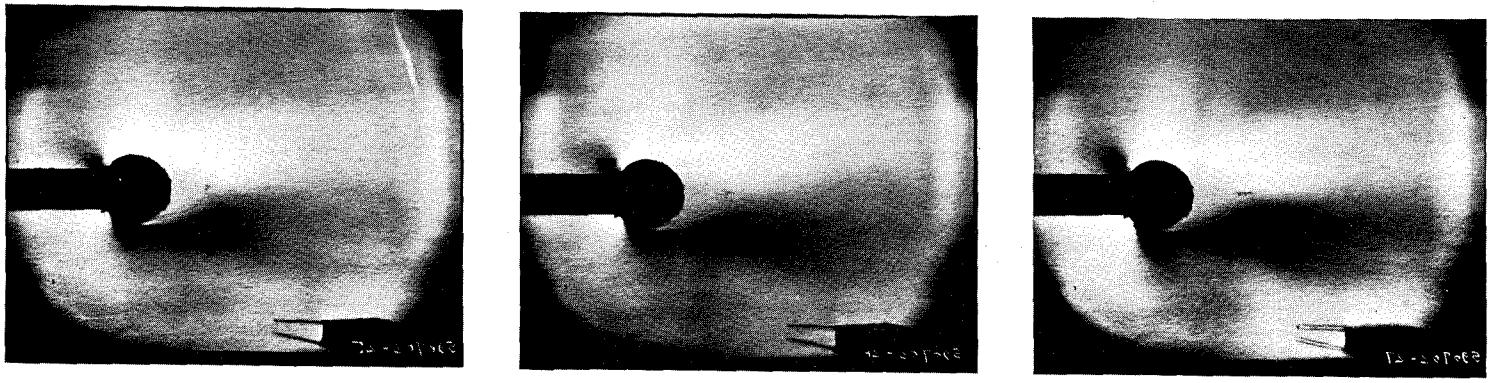

(b) knife edge parallel to flow direction

Fig. 35 - Typical Schlieren time exposure ($\frac{1}{25}$ sec) photographs of wake ; $M_1 = 0.60$ to 0.70

of pressure drag coefficient in figure 15. At $M_1 = 0.50$ the relative maximum in pressure drag coefficient corresponds not only to a relative maximum in initial wake width (at $\frac{x}{d} \doteq 1$) but also to a relative minimum in distance between body and "reattachment" point.

The lower row of pictures in figures 33, 34 and 35 shows also a transition point in the free shear layer, moving closer to the body as M_1 (and Re_1) increase. By transition point we understand here a point at which there is a definite change in the time-average rate of growth of vortex cores in the shear layer.

2. Resonance conditions

Resonance conditions between tunnel and wake, already noted in the preceding Section, had a very large effect on some of the results of temperature-fluctuation and recovery temperature tests.

Wake traverses were used to identify some of the standing wave patterns associated with resonance conditions.

In another series of tests, a splitter plate, suggested by the technique reported in reference 7, was tried as a means of influencing wake formation. The splitter plate (a thin symmetric airfoil, chord $c = 1.0$ in. $= 1.60$ d, spanning the tunnel) was placed on the wake center-line behind the model, with chord parallel to general flow direction, and moved up and down stream.

It was found that the splitter plate had a tremendous influence on wake-tunnel resonance, as evidenced by changes in whistling pattern and initial wake width. At $M = 0.50$ whistling was completely supressed when gap g between model and leading edge

of splitter plate was

$$0 < g < 0.7\,d.$$

Similarly at M = 0.65 whistling was suppressed by splitter plate at

$$0 < g < 1.4\,d.$$

In both cases the splitter plate did not seem to affect the wake structure farther downstream, at $x \geq 3$ d, say.

3. Temperature fluctuations

Temperature fluctuations at the surface of the model were measured by running a small constant current (6 to 15 mA) through a Pt film gauge and analyzing the fluctuations of voltage across it, i.e. across R_T in figure 8.

Typical spectra of voltage fluctuations, redrawn from the original records, are shown in figures 36 to 39.

Each spectrum represents [within the factor $(\alpha R_T GI)^2$, a constant for each plot] the power spectral density $f(\omega)$ of temperature fluctuations on model surface.

Note: (a) the changes of scale used within each plot to accommodate large changes in power spectral density; (b) integrating device used in the recording of spectra had a time constant of the order of 1.8 sec - this was not sufficient to smooth out large scale ($\tau >> 1.8$ sec) intermittencies; (c) spectra are distorted below 150 cps, since amplifier system gain drops off sharply in that range (see Fig. 10).

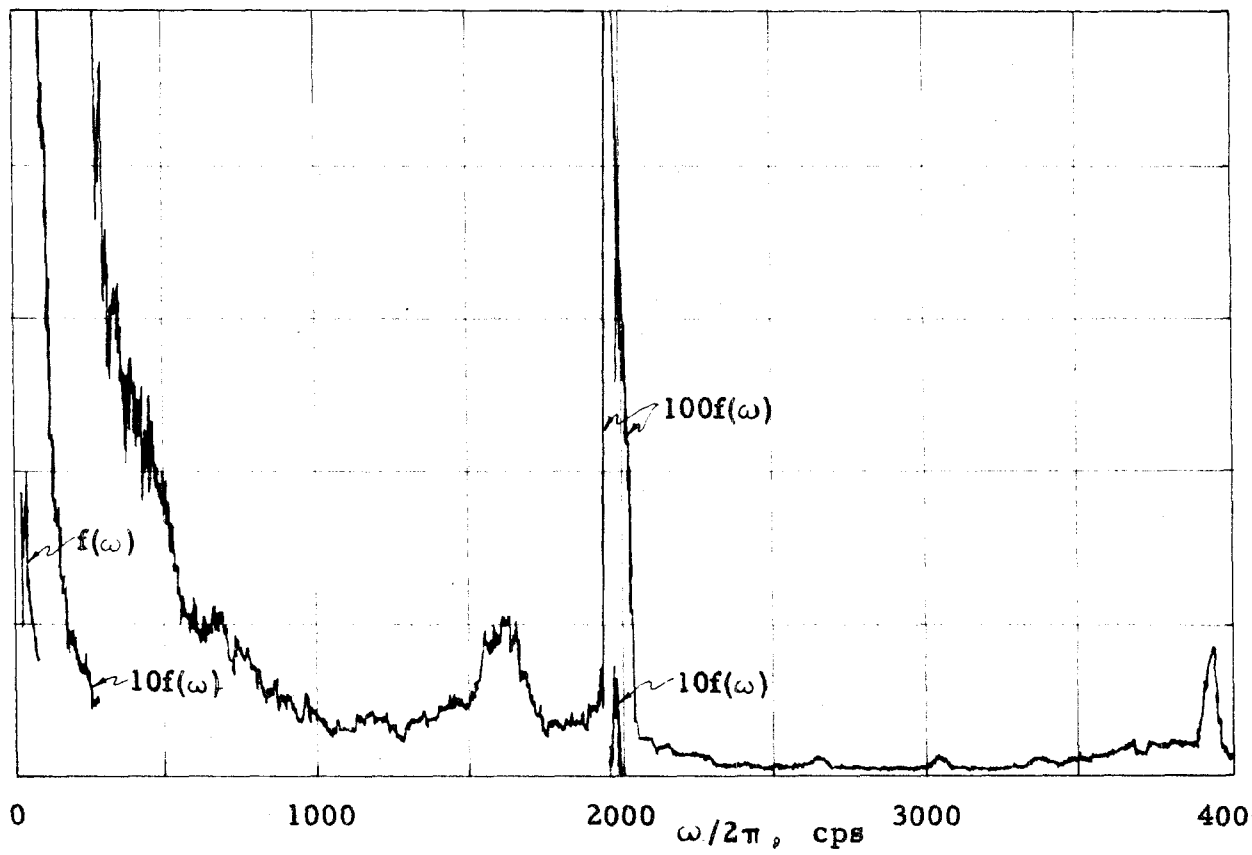

Fig. 36 (M_1 = 0.45)

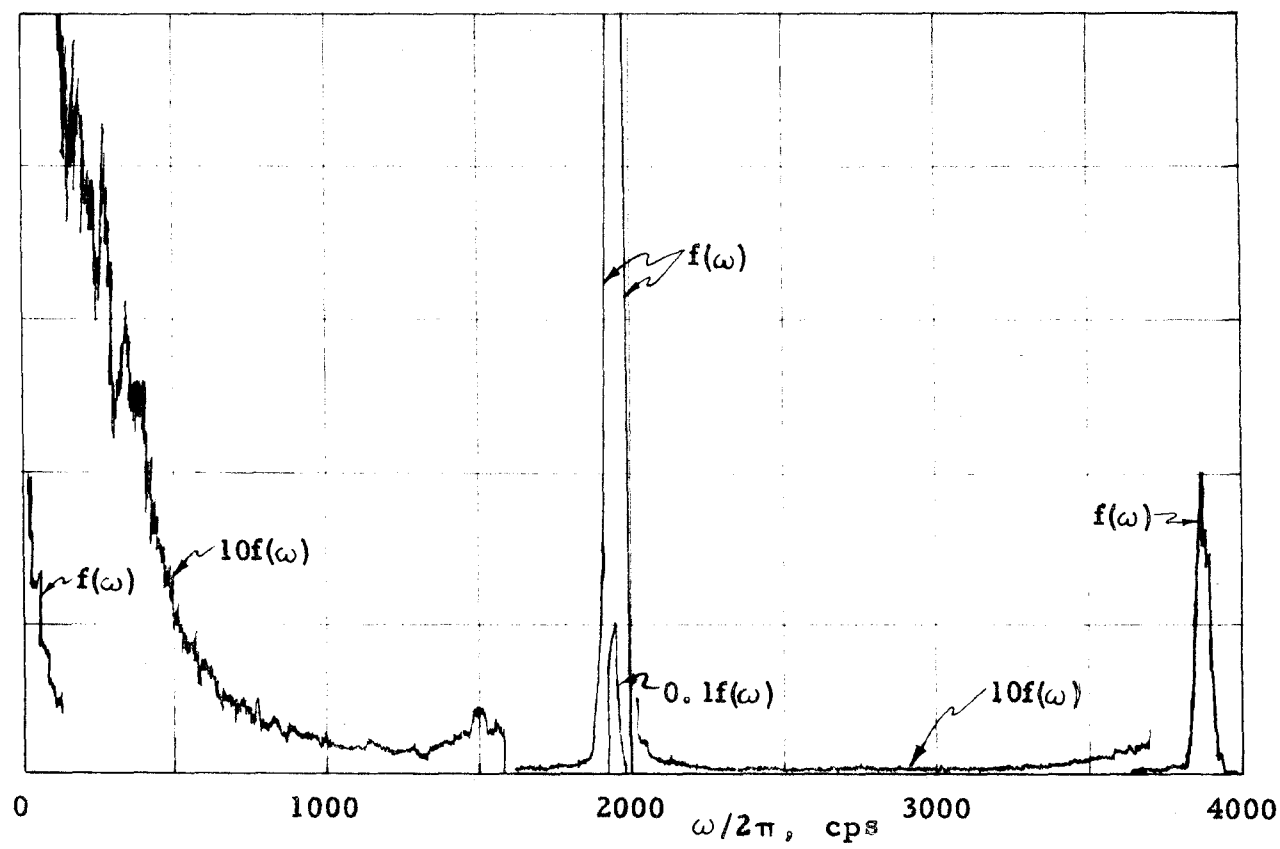

Fig. 37 (M_1 = 0.50)

Figs. 36 and 37 - Typical spectra of temperature fluctuations on cylinder surface (θ = 10°)

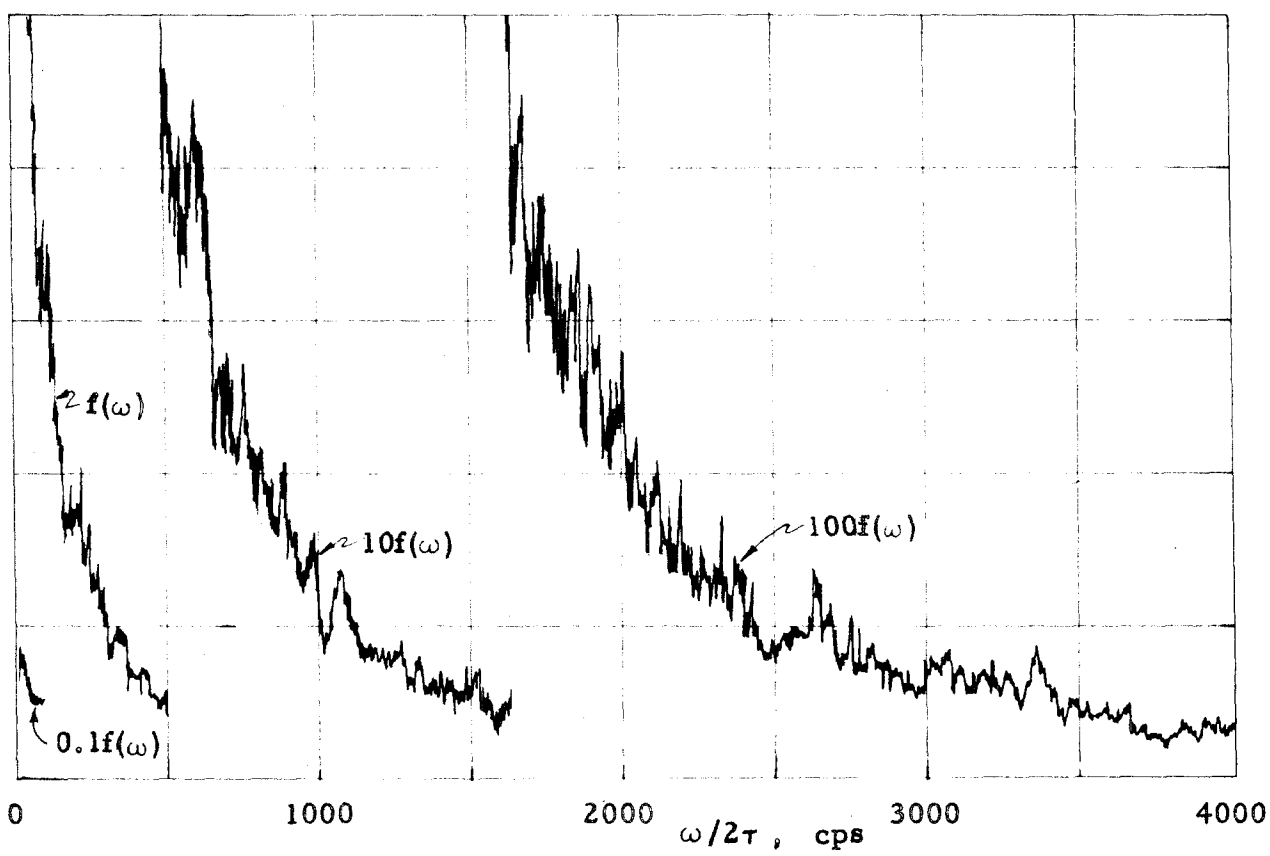

Fig. 38 (M_1 = 0.45)

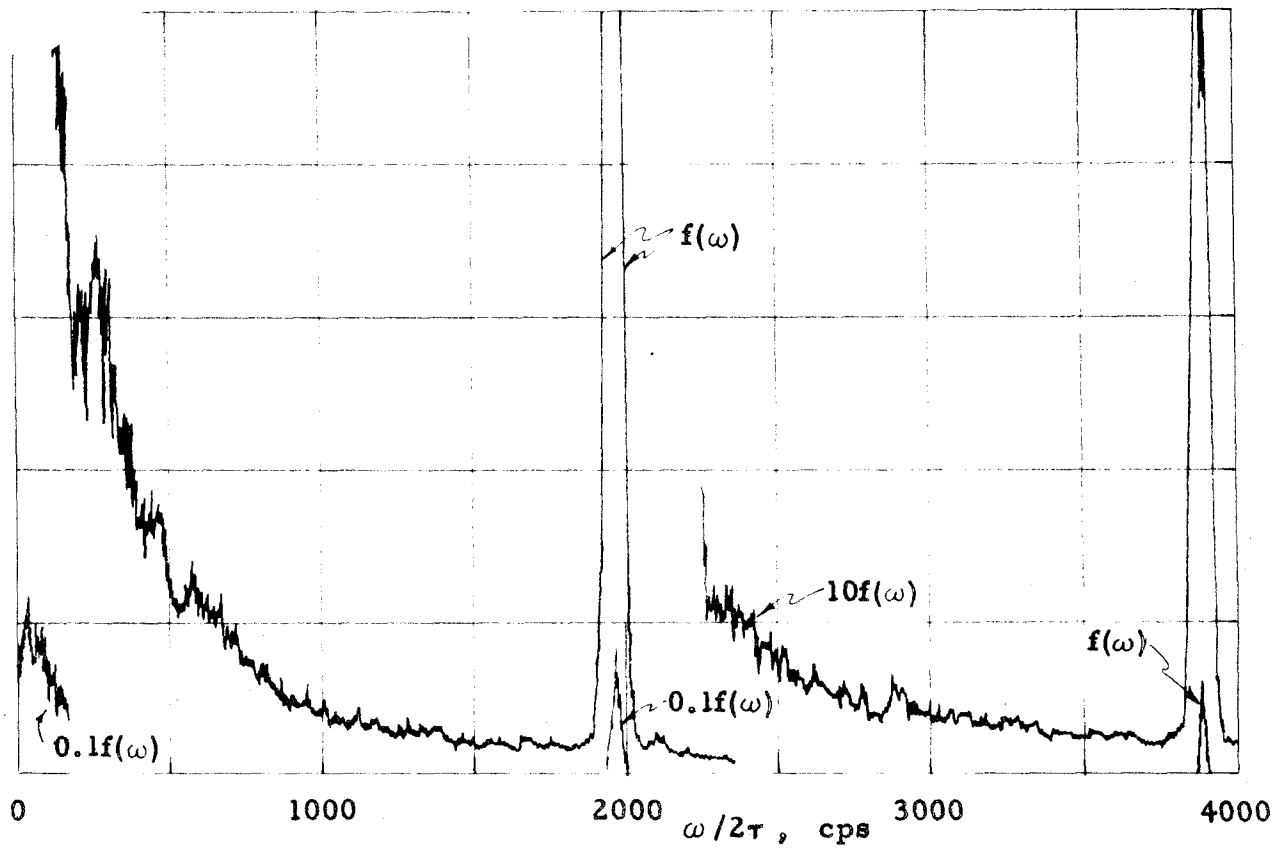

Fig. 39 (M_1 = 0.50)

Figs. 38 and 39 - Typical spectra of temperature fluctuations on cylinder surface ($\theta = -110^{\circ}$)

Reduction of temperature-fluctuation and of time-average temperature measurements is discussed in appendix 2, that of temperature fluctuation spectra in appendix 3.

Recorded spectra were generally repeatable within $\pm$ 10 $^{o}/o$ in the power spectral density of temperature fluctuations at a given tunnel condition and station on the model.

With these remarks in mind, results of power spectral density plots can be summarized as follows:

In all cases spectra consist of a continuous background, a number of discrete "sharp" peaks, and in some cases (e.g. Fig. 36) "diffuse" peaks. Analytically spectra can be represented as

$$f(\omega) = \frac{A}{1 + B\omega^2} + \sum_n C_n \, \delta(\omega - \omega_n) + \sum_m D_m e^{-\frac{(\omega - \omega_m)^2}{\beta_m^2}} \qquad (19)$$

$$n, m = 1, 2, \cdots, \quad n \neq m$$

Mean-square temperature fluctuation at the wall

$$\overline{T_w'^2} = \int_0^\infty f(\omega) d\omega \qquad (20)$$

is shown in figure 40, as a function of M_1 and with angle θ as a parameter. Note abnormal behavior at $M_1 = 0.50$ (one of the resonance points mentioned in Sec. III -2), and sharp rise at $M_1 = 0.65$.

Figures 41, 42, 43, and 44 show $\overline{T'^2}$ as a function of θ. They also include, as separate curves, the contributions of "sharp" and "diffuse" peaks

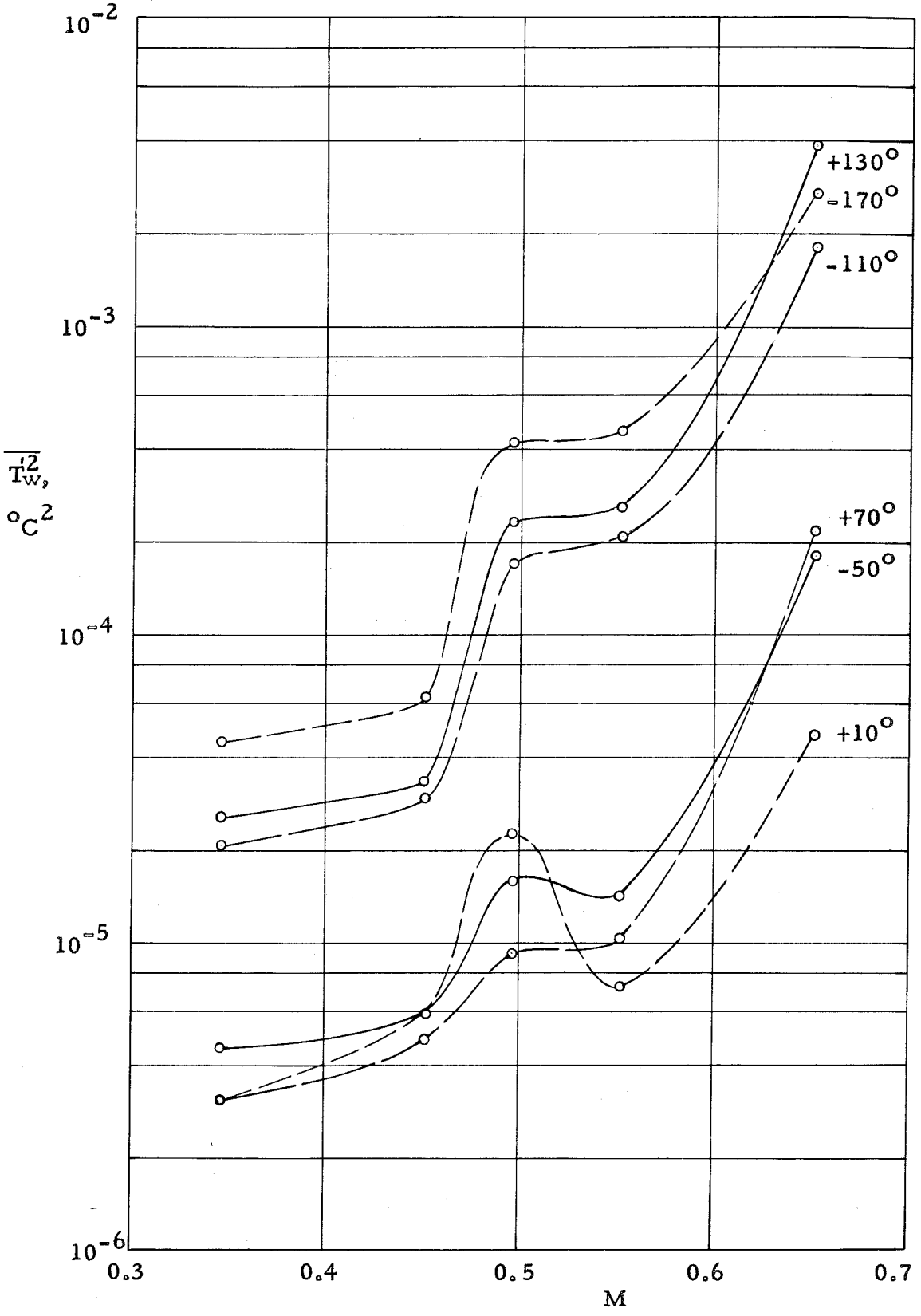

Fig. 40 - Mean-square temperature fluctuation on cylinder surface

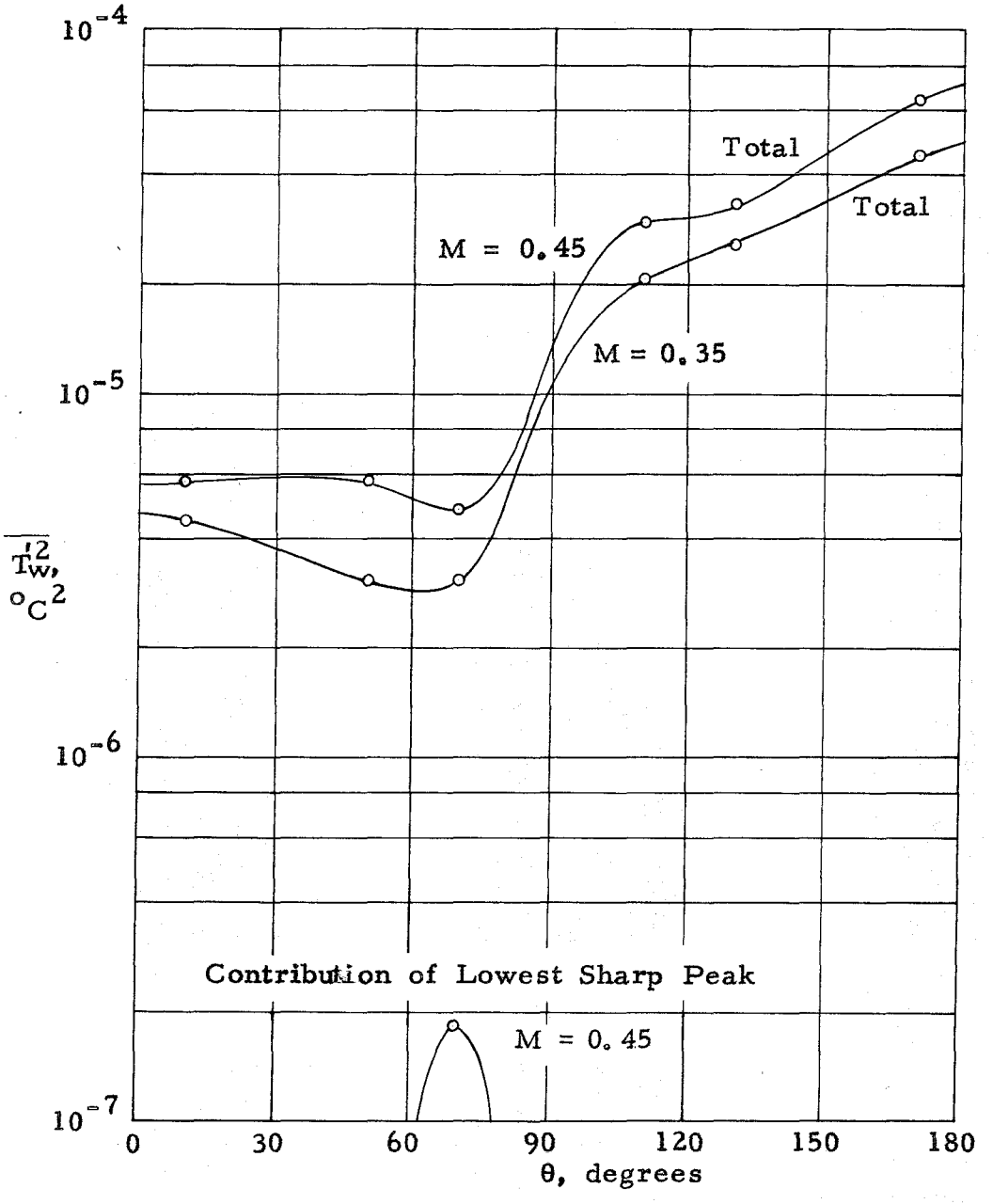

Fig. 41 - Mean-square temperature fluctuation on cylinder surface (M_1 = 0.35 and 0.45)

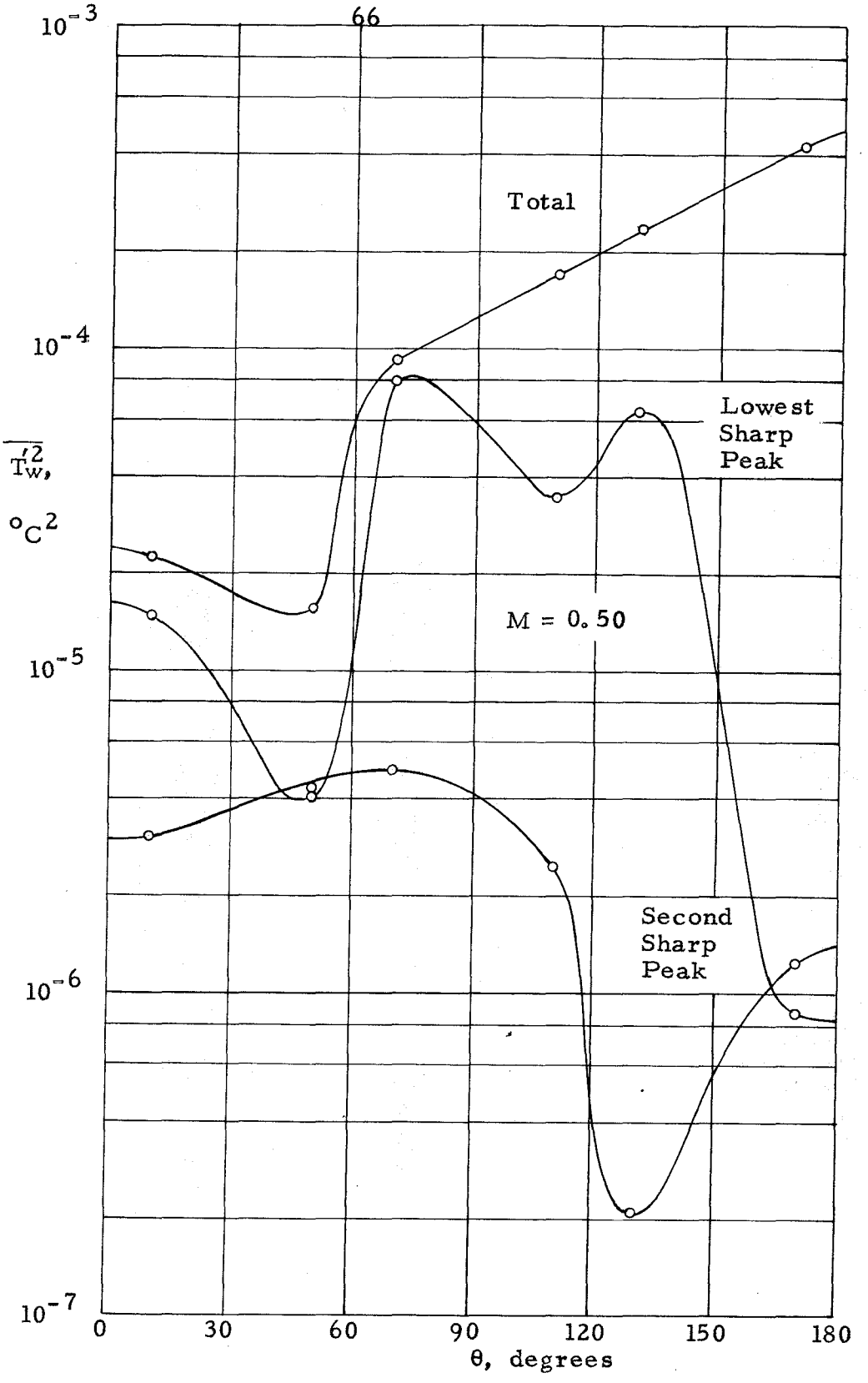

Fig. 42 - Mean-square temperature fluctuation on cylinder surface (M_1 = 0.50)

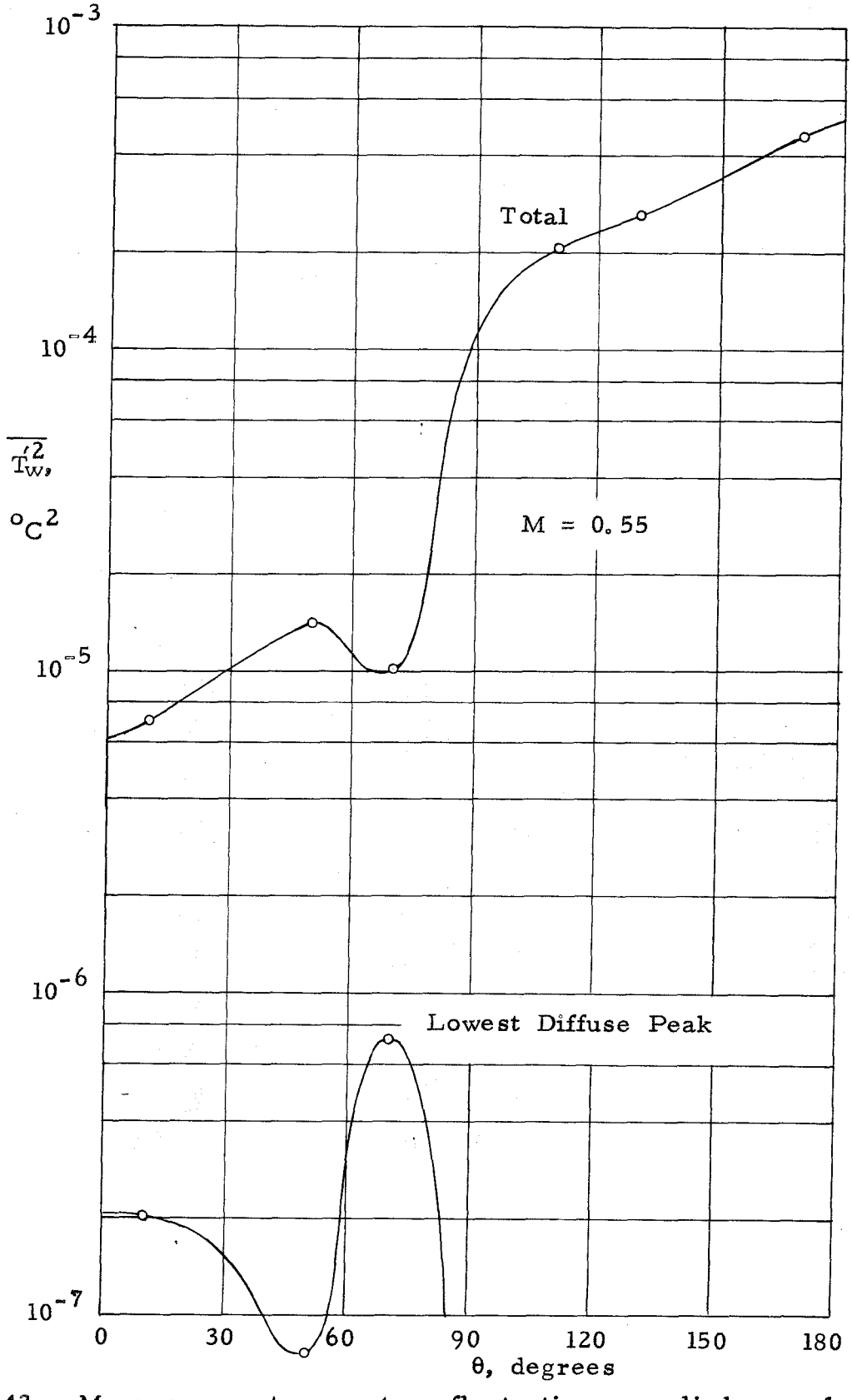

Fig. 43 - Mean-square temperature fluctuation on cylinder surface

(M_1 = 0.55)

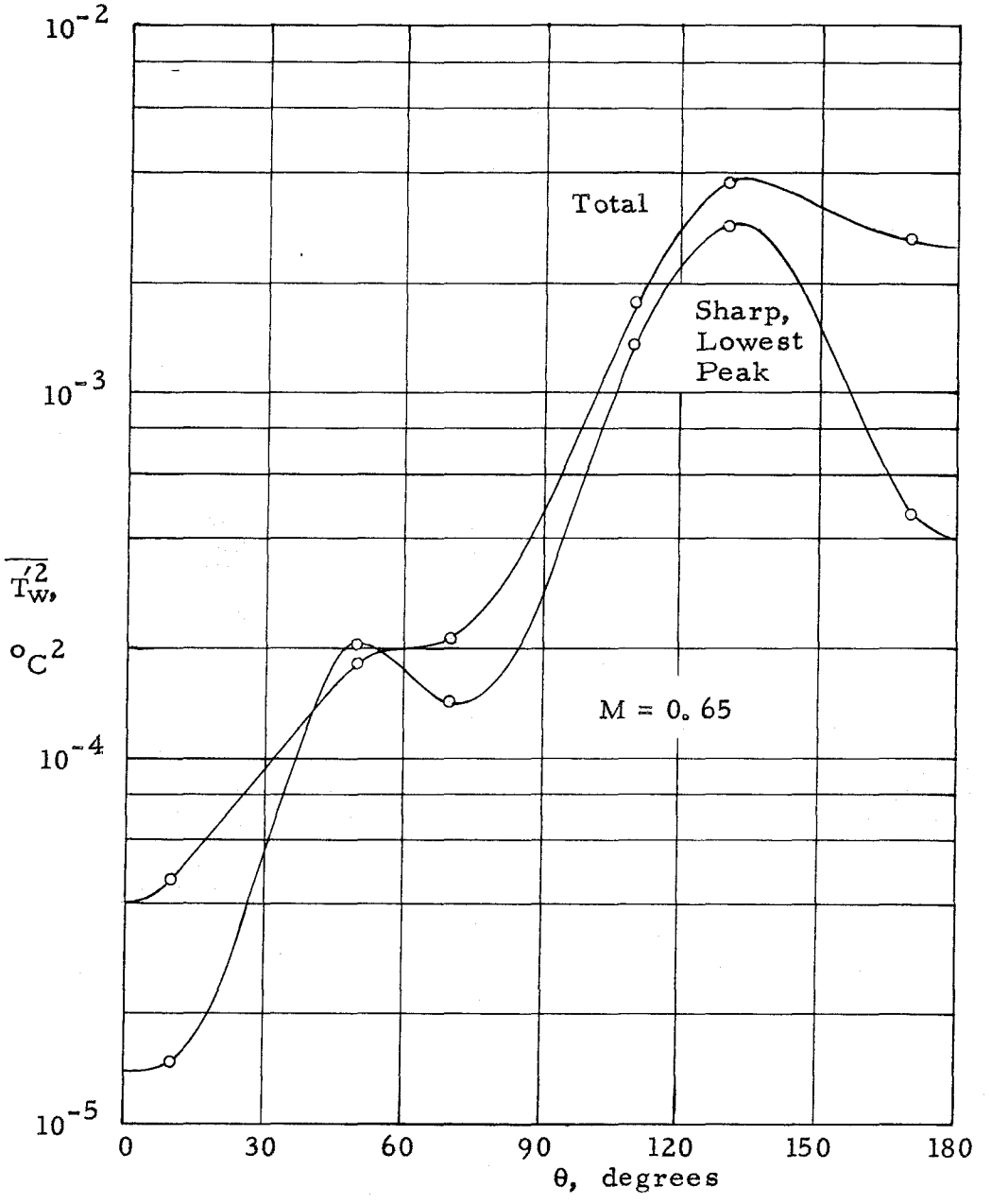

Fig. 44 - Mean-square temperature fluctuation on cylinder surface (M_1 = 0.65)

$$\int_0^\infty C_n \, \delta(\omega - \omega_n) \, d\omega = C_n \tag{21}$$

$$\int_0^\infty D_m \, e^{-(\omega-\omega_m)^2/\eta_m^2} \, d\omega = \frac{\sqrt{\pi}}{2} D_m \eta_m = \tilde{D}_m \tag{22}$$

Table 1 summarizes the recorded spectra.

Mean-square temperature fluctuations at the wall can be reduced to mean-square temperature fluctuations outside model by the methods outlined in Section II-6.

Results are shown in figure 45, for two typical points at $\theta = 10^\circ$, 170° (i.e. close to stagnation point and close to rearmost point on cylinder). Kinetic temperature

$$T_t - T_l = \frac{U_l^2}{2 c_p} \tag{23}$$

is also shown for comparison.

The continuous part of the spectrum, characteristic of random processes, dominates at conditions of no resonance; it is still present, at a relatively low level, when resonance occurs. The distribution of power spectral density provides valuable information on the type of random process involved.

Define a correlation function $\psi(\tau)$ as the Fourier (cosine)

Table 1 - Summary of recorded surface temperature fluctuation spectra

		Gauge	- 2	-1	0	+ 1	+2	3
		θ	-110°	-50°	$+10^{0}$	$+70^{\circ}$	$+130^{\circ}$	-170°
					Run 590724; $M_1 = 0.347$			
Total	$\overline{T'^2}$	$^{o}C^2$	2.08×10^{-5}	3.04×10^{-6}	4.5×10^{-6}	3.1×10^{-6}	2.58×10^{-5}	4.5×10^{-5}
Contin. f (n)	f(200)	$^{o}C^2$/cps	2.78×10^{-8}	2.62×10^{-9}	1.99×10^{-9}	2.43×10^{-9}	2.55×10^{-8}	4.2×10^{-8}
	f(800)	$^{o}C^2$/cps	2.28×10^{-9}	1.18×10^{-10}	9.1×10^{-11}	3.26×10^{-10}	3.4×10^{-9}	5.5×10^{-9}
	f(3200)	$^{o}C^2$/cps						
					Run 590727; $M_1 = 0.449$			
Total	$\overline{T'^2}$	$^{o}C^2$	2.98×10^{-5}	5.75×10^{-6}	5.75×10^{-5}	4.79×10^{-6}	3.34×10^{-5}	6.4×10^{-5}
Contin. f (n)	f(200)	$^{o}C^2$/cps	3.93×10^{-8}	4.8×10^{-9}	2.07×10^{-9}	3.55×10^{-9}	2.98×10^{-8}	4.8×10^{-8}
	f(800)	$^{o}C^2$/cps	4.7×10^{-9}	2.92×10^{-10}	1.68×10^{-10}	6.6×10^{-10}	3.8×10^{-9}	1.01×10^{-8}
	f(3200)	$^{o}C^2$/cps	1.41×10^{-10}					3.8×10^{-10}
Diffuse	n_1	cps		~1550	~1550			
	D_1	$^{o}C^2$			3.1×10^{-8}			
Sharp	n_2	cps		1940	1940	1940		
	C_2	$^{o}C^2$		9.2×10^{-9}	8.25×10^{-8}	1.83×10^{-7}		

		Gauge	- 2	- 1	0	+ 1	+ 2	3
		θ	-110°	-50°	$+10^{\circ}$	$+70^{\circ}$	$+130^{\circ}$	-170°
Run 590728; $M_1 = 496$								
Total	$\overline{T'^2}$	$^{\circ}C^2$	1.7×10^{-4}	1.57×10^{-5}	2.26×10^{-5}	9.1×10^{-5}	2.34×10^{-4}	4.22×10^{-4}
Contin. f(n)	f(200)	$^{\circ}C^2$/cps	1.55×10^{-7}	1.14×10^{-8}	1.02×10^{-8}	1.82×10^{-8}	2.43×10^{-7}	6.35×10^{-7}
	f(800)	$^{\circ}C^2$/cps	3.28×10^{-8}	6.65×10^{-10}	9.1×10^{-10}	2.16×10^{-9}	4.5×10^{-8}	7.2×10^{-8}
	f(3200)	$^{\circ}C^2$/cps	1.55×10^{-9}	2.92×10^{-10}	1.28×10^{-10}	6.1×10^{-10}	1.44×10^{-9}	6.25×10^{-9}
Sharp	n_1	cps	1910	1910	1910	1910	1910	1910
	C_1	$^{\circ}C^2$	3.44×10^{-5}	4.03×10^{-6}	1.49×10^{-6}	7.9×10^{-5}	6.35×10^{-5}	8.60×10^{-7}
Sharp	n_2	cps	3820	3820	3820	3820	3820	3820
	C_2	$^{\circ}C^2$	2.46×10^{-6}	4.35×10^{-6}	3.1×10^{-6}	4.9×10^{-6}	2.08×10^{-7}	1.22×10^{-6}
Run 590729; $M_1 = 0.552$								
Total	$\overline{T'^2}$	$^{\circ}C^2$	2.06×10^{-4}	1.4×10^{-5}	7.0×10^{-6}	1.01×10^{-5}	2.6×10^{-4}	4.63×10^{-4}
Contin. f(n)	f(200)	$^{\circ}C^2$/cps	1.01×10^{-7}	9.8×10^{-9}	2.82×10^{-9}	3.68×10^{-9}	9.5×10^{-8}	2.42×10^{-7}
	f(800)	$^{\circ}C^2$/cps	1.36×10^{-8}	6.1×10^{-10}	3.95×10^{-10}	8.56×10^{-10}	1.73×10^{-8}	2.84×10^{-8}
	f(3200)	$^{\circ}C^2$/cps	6.5×10^{-10}	1.2×10^{-10}		3.68×10^{-10}	7.1×10^{-10}	1.15×10^{-9}
Diffuse	n_1	cps		~ 1880	~ 1880	~ 1900		
	$\tilde{D}_1$	$^{\circ}C^2$		7.3×10^{-8}	2.03×10^{-7}	7.2×10^{-7}		

			Gauge	- 2	- 1	0	+ 1	+2	3
			θ	-110°	-50°	$+10^{\circ}$	$+70^{\circ}$	$+130^{\circ}$	-170°
			Run 590730, $M_1 = 0.652$						
Total	$\overline{T'^2}$	$^{o}C^2$		1.78×10^{-3}	1.80×10^{-4}	4.65×10^{-5}	2.11×10^{-4}	3.75×10^{-3}	2.64×10^{-3}
Contin. f (n)	f(200)	$^{o}C^2$/cps		1.21×10^{-6}	1.19×10^{-8}	2.31×10^{-8}	2.64×10^{-8}	1.31×10^{-6}	2.25×10^{-6}
	f(800)	$^{o}C^2$/cps		2.74×10^{-7}	5.36×10^{-9}	1.41×10^{-8}	1.19×10^{-8}	3.84×10^{-7}	4.5×10^{-7}
	f(3200)	$^{o}C^2$/cps		7.1×10^{-8}	3.6×10^{-9}	7.0×10^{-9}	9.0×10^{-9}	9.6×10^{-8}	7.0×10^{-8}
Diffuse	n_1	cps			1525	1525			
	$\tilde{D}_1$	$^{o}C^2$			2.46×10^{-6}	5.65×10^{-6}			
Sharp	n_2	cps		2680	2680	2680	2680	2680	2680
	C_2	$^{o}C^2$		1.38×10^{-3}	2.07×10^{-4}	1.47×10^{-5}	1.41×10^{-4}	2.86×10^{-3}	4.67×10^{-4}

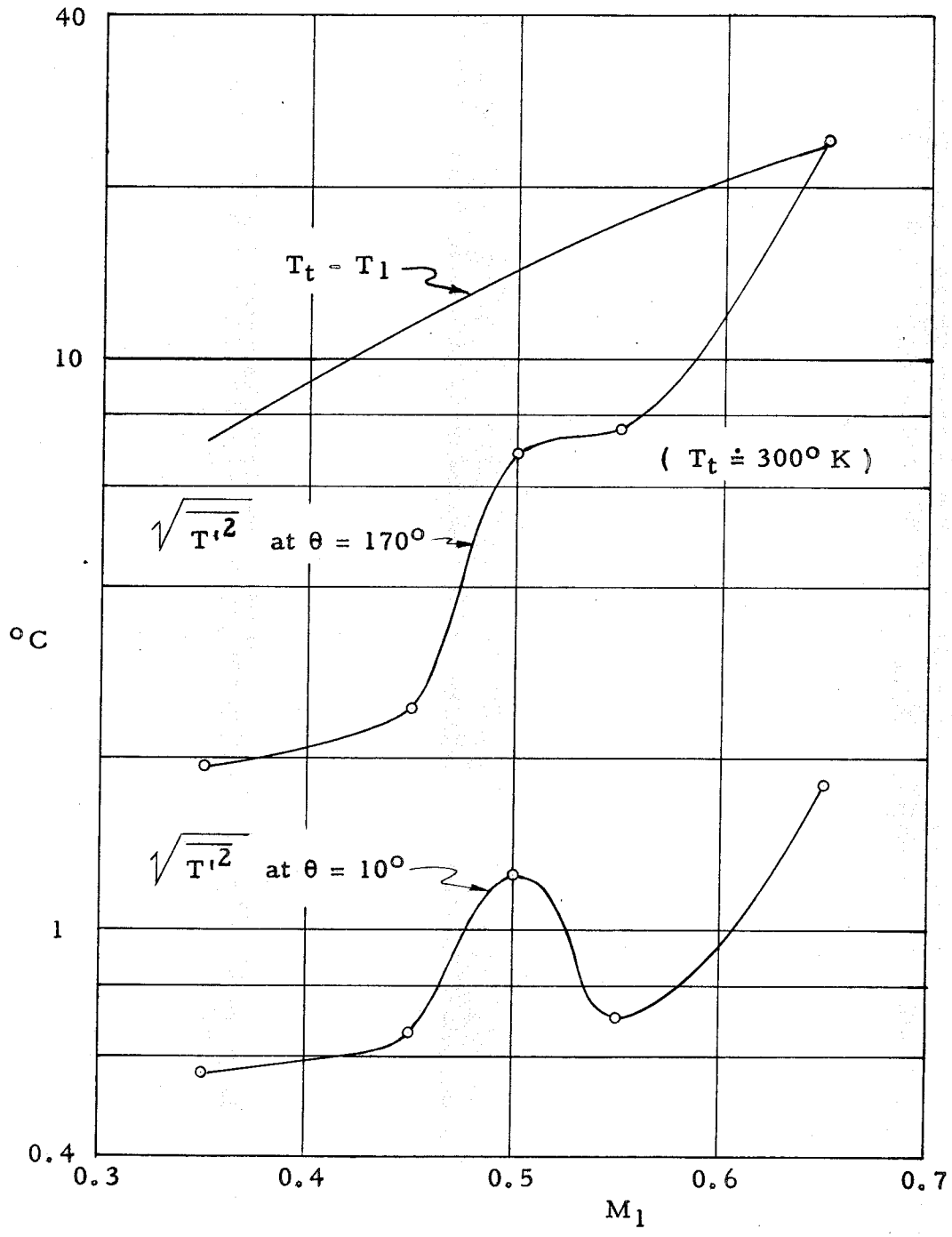

Fig. 45 - Mean-square temperature fluctuation outside cylinder

transform of the power spectrum

$$\psi(\tau) = \frac{2}{\pi}\int_0^\infty f(\omega)\ \cos\ \omega\tau\ d\omega \tag{24}$$

Then

$$\psi(0) = \frac{2}{\pi}\int_0^\infty f(\omega)d\omega = \frac{2}{\pi}\overline{T'^2} \tag{25}$$

A characteristic correlation time τ_c can be obtained as

$$\tau_c = \frac{\int_0^\infty \psi(\tau)\, d\tau}{\psi(0)} \tag{26}$$

and reduced to a non-dimensional form with the characteristic velocity U_1 and linear dimension d; $\frac{\tau_c U_1}{d}$ obtained in this way from the continuous part of the spectrum is plotted in figure 46 (for conditions at the model surface).

Near the front stagnation point reduced correlation time decreases continuously with Mach number. Two different regimes seem to occur for the correlation time near the rearmost point on the model. Least correlation times are always obtained in the range $\theta = 70^\circ \ldots 130^\circ$, near the "crest"line of the model.

4. Recovery temperature

Time-average temperatures at model wall ("recovery" temperatures) were measured at very low current (6 mA) using

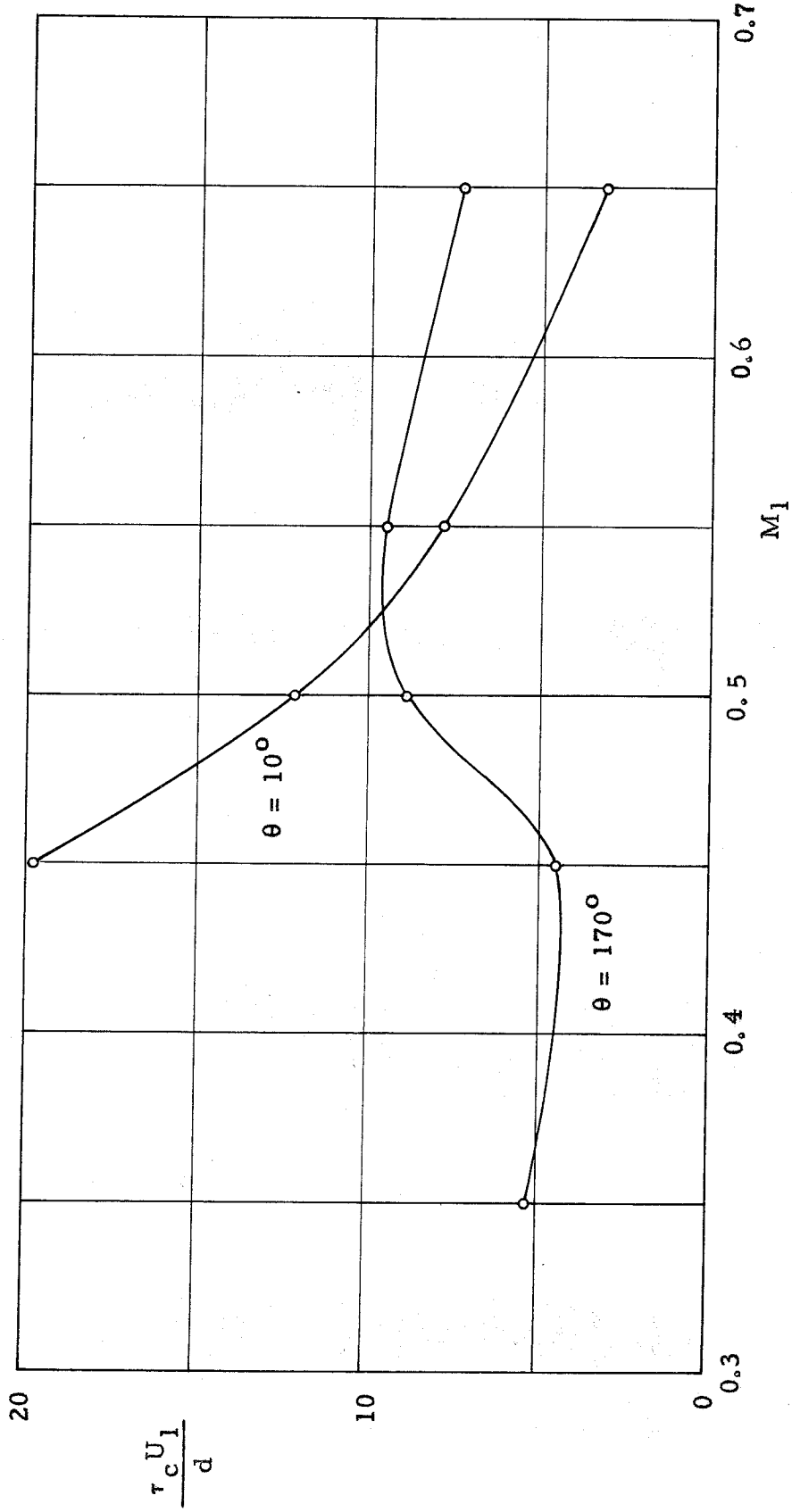

Fig. 46 - Reduced correlation time of temperature fluctuations on cylinder surface

standard balanced bridge technique.

Results are shown in figures 47 and 48, in terms of "recovery factor"

$$r = \frac{T_t - \overline{T_w}}{T_t - T_l} \tag{27}$$

A comparison with figure 40 shows that sudden drops in recovery factor parallel increases in mean-square temperature fluctuation at wall whenever wake-tunnel resonance occurs.

Note also that under conditions of no resonance the recovery factor on rear surface of model ($r = 0.6$) measured in the low turbulence GALCIT Transonic Wind Tunnel is much higher than value ($r = 0$ to -0.25) reported in references 13 and 14. At resonance conditions the agreement is quite good, however. This suggests that free stream turbulence is one of the factors which may trigger the abnormal cooling mechanism.

A qualitative check was made with artificially induced turbulence (from the wake of a cruciform configuration of 0.125 x 0.500 in. strut spanning the tunnel height, and a 0.125 in. dia. round rod spanning the tunnel width, at station $x = -24.5$ in). It showed a decrease of recovery factor, due to additional vorticity in the free stream, to a level comparable to that of references 13 and 14.

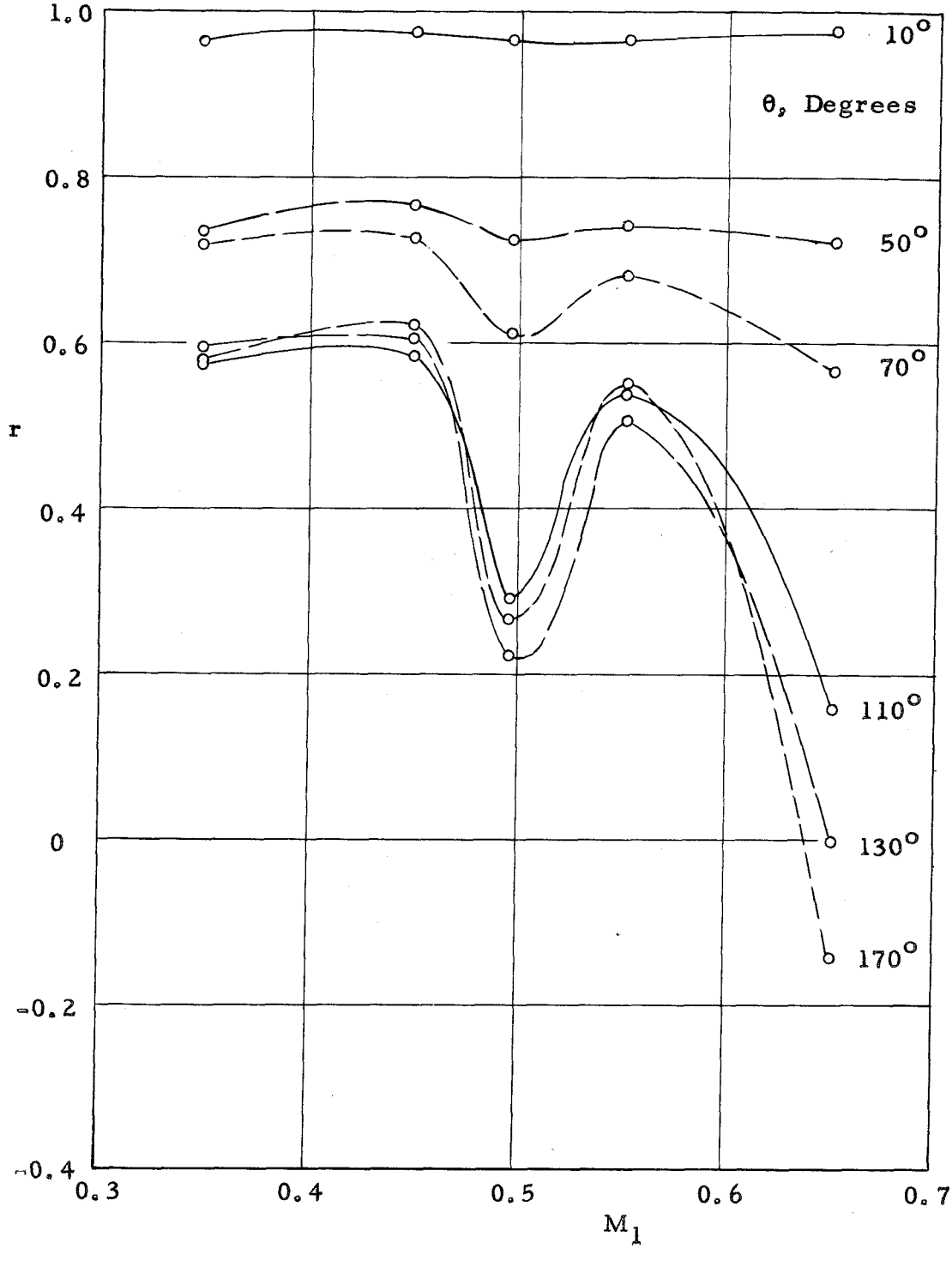

Fig. 47 - Temperature recovery factor

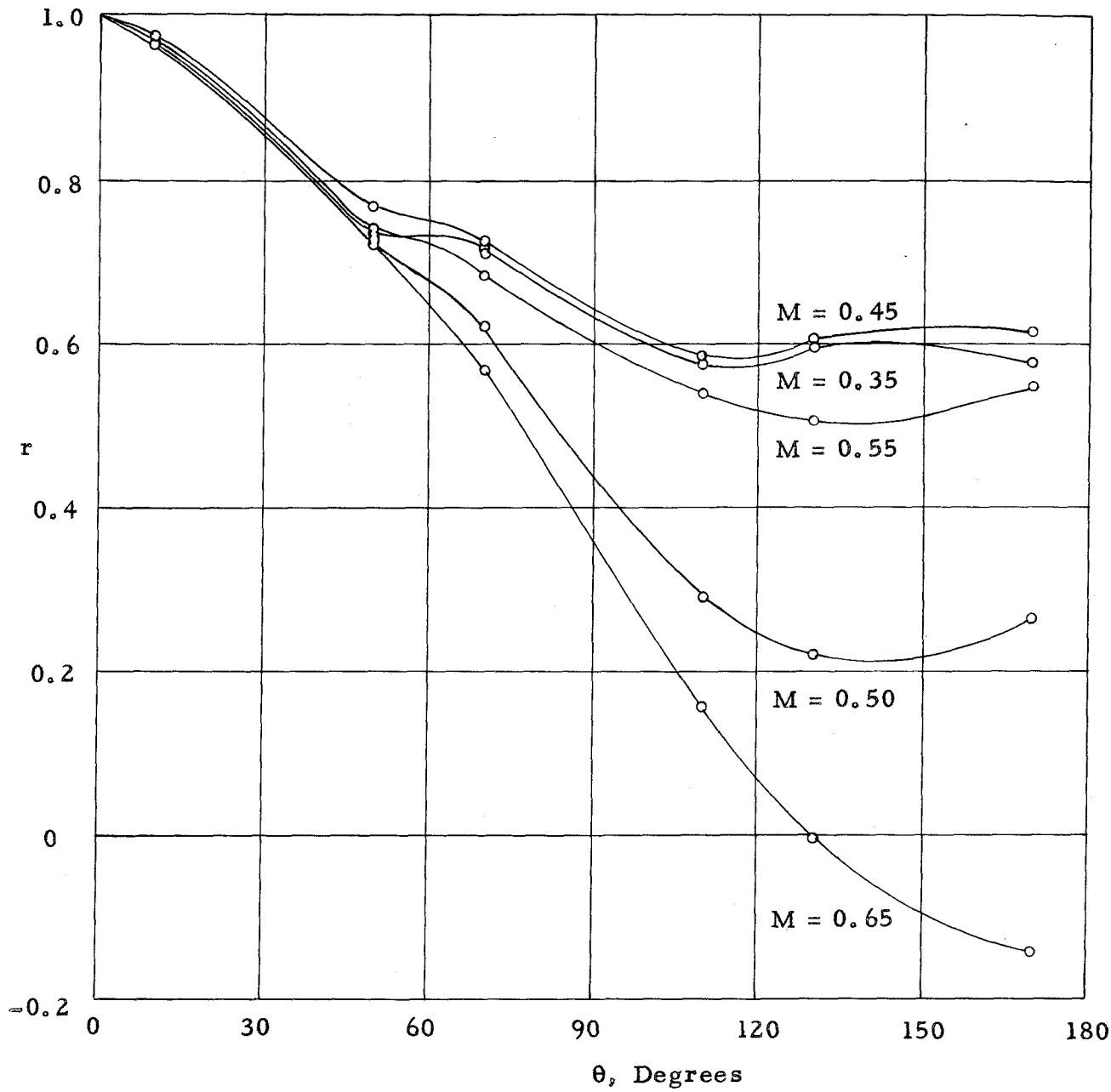

Fig. 48 - Temperature recovery factor

IV. DISCUSSION

The experimental results summarized in Part III (within their somewhat restricted range $M_1 = 0.35 \ldots 0.70$, $Re_1 = 117,000 \ldots 201,000$) display many features of interest both in the problem of abnormal cooling and in that of constructing more satisfactory simplified models of the flow about bluff bodies.

These features are:

(a) Under normal conditions (no resonance effects) disturbances at the surface of the body are very much dominated by random processes, with periodic effects hardly noticeable. Spectra on the body surface are essentially of the type

$$f(\omega) = \frac{A}{1 + B\omega^2} \tag{28}$$

i.e. those of a generalized shot process. Only farther downstream ($x/d \geq 2$) does the periodic character of hot-wire spectra taken at edge of wake become very strong, although random background is still present and some large scale intermittencies occur.

This suggests that the initial formation of discrete vortex cores from the free shear layers is a random process, of the generalized shot effect type. Observation of very many schlieren pictures confirms the basic lack of correlation between the initially formed vortex cores and those organized in a vortex street farther downstream. This feature seems to be quite characteristic of conditions at the higher Reynolds' numbers. Observations at much lower Reynolds' numbers, reported in reference 7 and particularly reference 8 (down to Re = 56) show a very high degree of periodicity

even in the region of vortex core formation (a few diameters downstream of the body in that case).

(b) When strong whistling occurs at a definite tunnel condition ("resonance") standing wave patterns can be detected with maxima away from the disturbance centers in what is otherwise a subsonic (elliptic type) field. Spectrum of disturbances on body surface and at edge of wake becomes predominantly periodic. Some of the periodicity extends into the attached flow area on the front of the body. It is also quite remarkable that the total intensity of disturbances at a given station on the body is not significantly changed between a non-resonance condition and a neighboring resonance condition - power is simply shifted from the random components to discrete periodic components.

This suggests that formation of vortex cores from the free shear layer is accompanied by an impulsive type of disturbance. Total intensity of disturbances available per unit time is limited in a given shear layer, and highly dependent on Mach number. Wind tunnel resonance is presumably only one of several possible initial instability triggering mechanisms, while vortex core formation is the final stage of the instability, limited by nonlinear effects.

(c) Inspection of figure 46, the reduced autocorrelation time of the continuous part of the spectrum, shows that $\tau_c U_1/d$ is of the same order of magnitude as $1/(St)_1$, on the rear part of the body. This points to a definite time scale or time delay between the initial triggering pulse and completion of the triggered disturbance. The two different regimes apparent in figure 46 for conditions on the rear

part of the body appear to be due to transition in the free shear layer.

Near the stagnation point autocorrelation time decreases continuously with M. Minimum of autocorrelation times occurs always in the neighborhood of $\theta = \pm 90^{\circ}$. This may suggest that random fluctuations on the front part of the body are independent of fluctuations on the rear part of the body. Additional cross-correlation measurements would be required to clarify this point.

(d) Interaction between the two shear layers is particularly important in the region of vortex core formation, as evidenced by experiments with splitter plates. Main effect of splitter plates is to hinder propagation of disturbances between the two shear layers and thus reduce triggering effects from one layer to another.

(e) Resonance conditions occur whenever disturbances emitted by a shear layer and reflected from tunnel walls arrive at the opposite shear layer with a time delay

$$\frac{2j+1}{2n}, \qquad j = 0, 1, 2, \cdots$$

where n is the basic vortex street frequency.

These additional triggering pulses will not only enhance periodic processes in the region of vortex core formation, but also displace this region closer to the body.

A simplified theoretical model for this process can be assumed (see sketch), with a uniform velocity U across the test section, except in the wake area (zero velocity). Propagation of disturbances takes place with a constant speed of sound a.

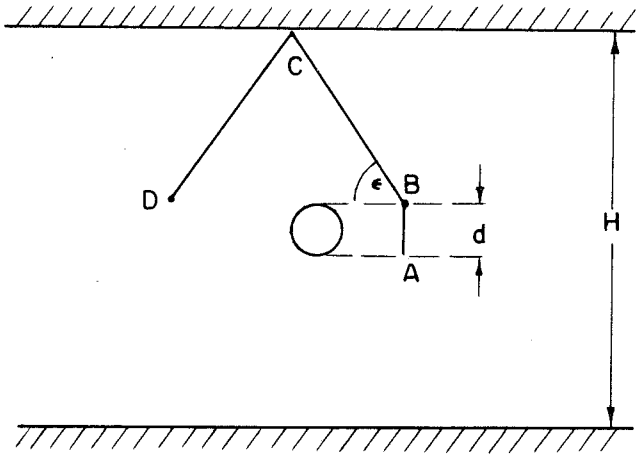

A ray, emitted at A will need time $\frac{d}{a} + \frac{H-d}{a \sin \epsilon}$ to reach point D (in system moving with fluid), while fluid has transported pt. D into B.

Hence

$$t = \frac{d}{a} + \frac{H-d}{a \sin \epsilon} = \frac{d}{a} + \frac{H-d}{U \tan \epsilon} = \frac{2j+1}{2n} \qquad (29)$$

This is equivalent to conditions

$$U/a = \cos \epsilon \qquad (30)$$

and

$$1 + \frac{\frac{H}{d} - 1}{\sin \epsilon} = \frac{2j+1}{2(St)\frac{U}{a}} = \frac{2j+1}{2(St)\cos \epsilon}, \qquad j = 0, 1, 2, \cdots \qquad (31)$$

Solution of equation (31) gives the resonance conditions, with resonant points spaced more and more closely, in terms of M, as $M \to 1$. See appendix 5. Agreement between observed and calculated resonance points is quite good.

(f) Measurements of temperature recovery on the body surface in the separated flow area indicate that either wake-tunnel resonance or high free stream turbulence level cause a large reduction in temperature recovery factor. In subsonic flow about cylinders r may drop from 0.6 to 0 or even -0.25 under these conditions. Effective Prandtl number $Pr = \left(\frac{\nu}{\kappa}\right)_{eff.} = \left(\frac{\mu c_p}{k}\right)_{eff.}$ of recirculation zone flow is thus reduced by a large factor.

The main non-stationary effect responsible for abnormal cooling appears to be due to impulsive formation of vortex cores rather than their simple streaming by. Resonance effects or free-stream turbulence provide two additional triggering effects for this impulsive process, bring it closer to body and thus increase non-stationary effects at the body surface.

It appears that Ackeret's theory of abnormal cooling will provide results consistent with the spectral measurements if the non-stationary term in equation 1 is assumed to be due to the impulsive process. Ackeret's theory in its original form may be applied, however, to cooling effects in a fully developed vortex street, at $x/d \geq 2$, in region where vortices are already formed.

V. CONCLUSIONS

Spectral analysis of fluctuations on the surface of a bluff body in two-dimensional, subsonic, compressible flow, in the range between $M = 0.35$, $Re = 117,000$ and $M = 0.70$, $Re = 201,000$, and analysis of fluctuations around the wake, indicate that formation of discrete vortex cores from the separated shear layers involves initially impulsive disturbances, random in phase, which can be described as a "generalized shot process". Schlieren observations support this view, and show also that farther downstream the wake has periodic structure, but the turbulent background becomes quite strong at the higher values of M and Re investigated. Sound waves are an essential feature of wake structure at the higher Mach numbers.

Intensity of the disturbances involved in the initial stage of wake formation is highly dependent on Mach number. The impulsive process can be visualized as an "explosive" - or rather "implosive" - formation of vortex cores.

The process of impulsive formation of vortex cores appears to be triggered either by disturbances due to formation of other vortices, or by free-stream turbulence. The triggering process may be enhanced, at certain discrete Mach numbers, by wake-tunnel resonance. A simple model of this resonance effect, presented in Part IV (e), gives numerical results which compare satisfactorily with experience.

Fairly detailed measurements of recovery factor and of temperature fluctuations on surface of body, discussed in Part III, show correlation of abnormal cooling with the additional triggering effect of wake-tunnel resonance. A modification of the Ackeret theory of

abnormal cooling is suggested in Part IV (f).

While the measurements of conditions on the surface of a body, summarized in Part III, are quite detailed, discussion of the formation of vortex cores in Part IV is strictly qualitative. A quantitative study of the problem of vortex core formation from a shear layer, under controlled conditions, is suggested as a topic for future research, both theoretical and experimental. A theoretical study of the final stage of vortex core formation, limited by nonlinear effects, would seem especially useful, since application of linearized small-perturbation methods is extremely restricted in the case of a free shear layer. An experimental study, with independent variation of Mach and Reynolds' number, and possibility of either forcing a shear layer with large disturbances or of isolating it from disturbances (e.g. by splitter plates on both sides), also seem very interesting.

Note: During the final stage of preparation of this thesis reference 29 was brought to the author's attention. It extends recovery temperature measurements and interesting schlieren observation of wakes through the transonic range (in a tunnel with slotted walls) and up to M = 3. It shows that wake is no longer periodic at Mach numbers above 0.95 or 1.0, when a nearly stationary wake shock appears. Information on conditions below this Mach number is however somewhat fragmentary, since only one Mach number was investigated in detail (M = 0.556).

APPENDICES

Appendix 1. Blockage corrections

Results reported in Part III were reduced in terms of "tunnel Mach number" M_1 based on static pressure at station $x = -7.50$ in. This station is sufficiently far upstream from the model, so that perturbation pressure gradient is negligible.

A complete estimate of blockage corrections in two-dimensional flow would require some knowledge of the pressure distribution on tunnel upper and lower walls, far upstream and far downstream from model, besides drag or wake measurements. In the present test series pressure distribution was measured on tunnel upper wall at stations $x = -7.50$ in. up to $x = +1.50$ in., and (pressure) drag obtained from pressure distribution tests (Fig. 13 and 15).

Station $x = +1.50$ in. is considered representative of conditions opposite the model and the recirculation zone adjacent to it.

Figure 49 shows the pressure difference on tunnel upper wall

$$\Delta p_w = p_{+1.50} - p_{-7.50}$$

in terms of total pressure p_t.

Velocity perturbation on tunnel wall is due to doublet and source terms from model and wake respectively.

The doublet term (and its images) produce a peak velocity increment at the walls equal to 3 times the tunnel center-line velocity increment u_d (due to the images alone). This is independent of Mach number in linearized subsonic flow.

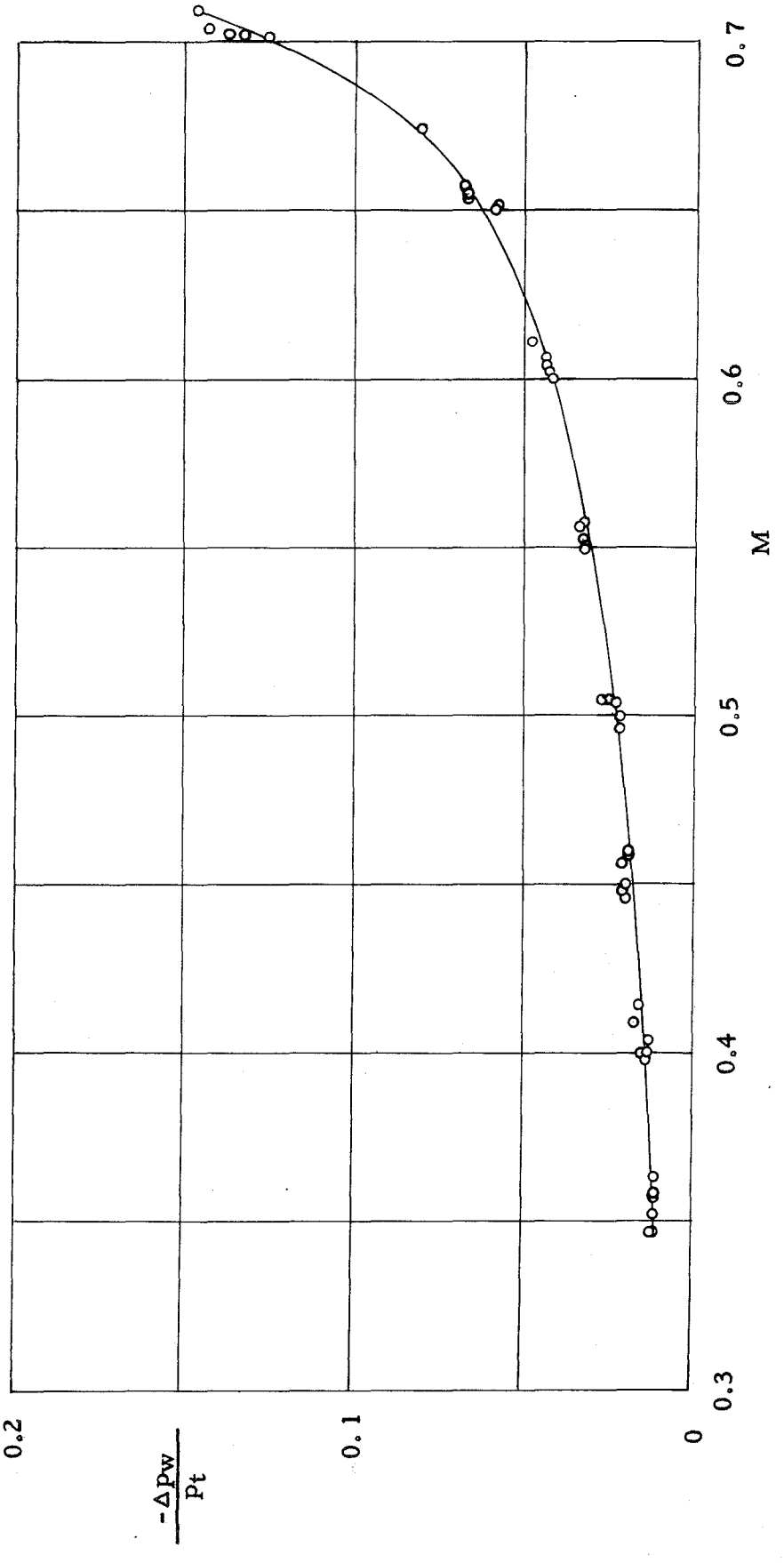

Fig. 49 - Data for blockage corrections

The source term, according to Allen and Vincenti (Ref. 27) should be represented by a source Q

$$Q = \frac{(\rho U C_D)_1 \, d}{2} \left[1 + (\gamma - 1) M_1^2 \right] . \tag{32}$$

Velocity increment due to this source, uniform across tunnel height sufficiently far from it, is .

$$u_s = \frac{Q}{2\rho H (1 - M_1^2)} = \frac{1 + (\gamma - 1) M_1^2}{1 - M_1^2} \frac{C_{D1}}{4} \left(\frac{d}{H}\right) U_1 \tag{33}$$

Hence velocity increment at wall

$$\Delta u_w = 3 u_d + u_s \tag{34}$$

can be related to velocity increment Δu on tunnel center-line

$$\Delta u = u_d + u_s = \frac{\Delta u_w}{3} + \frac{2}{3} u_s \tag{35}$$

Both terms in this expression are obtained from measurements - of tunnel wall pressure distribution or of drag.

Blockage corrections are then (Ref. 28)

$$\frac{U - U_1}{U_1} = \frac{\Delta u}{U_1} \tag{36}$$

$$\frac{\Delta M}{M_I} = \frac{M - M_I}{M_I} = \left[1 + \frac{1}{2}(\gamma - 1) M_I^2\right] \frac{\Delta u}{U_I} \tag{37}$$

$$\frac{\Delta C_D}{C_{D_I}} = \frac{C_D - C_{D_I}}{C_{D_I}} = -(2 - M_I^2) \frac{\Delta u}{U_I} \tag{38}$$

Table 2 summarizes the blockage corrections for the $\frac{d}{H} = 0.0666$ models.

These blockage corrections are believed to be quite accurate under steady state conditions; their validity may be somewhat restricted under conditions of wake-tunnel resonance with the large non-stationary effects.

Table 2 - Blockage corrections

($\frac{d}{H}$ = 0.0666 models)

1	M_1	0.35	0.45	0.50	0.60	0.70
2	$\Delta p_w/p_t$	- 0.011	- 0.019	-0.024	- 0.042	-0.125
3	C_{D_1}	1.30	1.38	1.66	1.74	1.97
4	$\frac{1}{2}\rho_1 U_1^2/p_t$	0.0788	0.1234	0.1475	0.1976	0.2473
5	$-\frac{1}{2}$(2) / (4)	0.070	0.077	0.081	0.106	0.253
6	$1 + 0.4M_1^2$	1.049	1.081	1.100	1.144	1.196
7	$1 - M_1^2$	0.8775	0.7975	0.7500	0.6400	0.5100
8	(6) / (7)	1.195	1.358	1.468	1.79	2.34
9	0.01666 x(3)x(8)= $\frac{u_s}{U_1}$	0.026	0.031	0.041	0.052	0.077
10	$\frac{(5)}{3} + \frac{2}{3}$(9) = $\frac{\Delta u}{U_1}$	0.041	0.048	0.054	0.070	0.136
11	$1 + 0.2M_1^2$	1.0245	1.0405	1.050	1.072	1.098
12	$\Delta M/M_1$	0.042	0.050	0.057	0.075	0.149
13	M	0.365	0.472	0.528	0.645	0.804
14	$2 - M_1^2$	1.8775	1.7975	1.750	1.640	1.510
15	$\Delta C_D/C_{D_1}$	- 0.077	- 0.086	- 0.094	- 0.115	- 0.205
16	C_D	1.20	1.26	1.50	1.54	1.57

Appendix 2. Reduction of time-average temperature and of temperature-fluctuation measurements

Resistance of platinum film gauges was calibrated vs. temperature and temperature coefficients of resistivity α obtained, as described in Section II-6. Some calibration points were also checked before and after each run, to insure that no changes in contact resistance occurred.

Time-average temperature measurements were made by balancing bridge (Fig. 8) after tunnel and gauges had reached equilibrium temperature. Difference between gauge temperature and reservoir temperature was then obtained from calibration curves, within $\pm$ 0.1°C. Note that temperature fluctuations as measured by Pt gauges on model surface were so small $\left(\sqrt{T'^2} \leq 10^{-2}\,^{\circ}C\right)$ that squaring effect of bridge could be neglected in time-average temperature measurements.

Kinetic temperature $T_t - T_l$ used in the definition of recovery factor was computed by standard isentropic formula, with $\gamma = 1.40$.

In temperature-fluctuation work the balanced bridge technique was used to obtain R_T and the bridge supply current was recorded in each case. Hence value of gauge current I could be computed.

Amplifier gain G was known; note that resistive and capacitive loading across R_T, due to bridge and connecting cables, was included in amplifier gain calibration.

Amplifier output voltage and gauge temperature were therefore related as $(\alpha R_T G I)$, and mean-square or power spectral density values as $(\alpha R_T G I)^2$.

Mean-square values measured directly by a true-root-mean-

square-voltmeter agreed within 15 ^{o}/o with those obtained from integration of power spectral density plots, within the frequency band defined by amplifier response (see Fig. 10; half-power points for complete system are 25 cps and 32 kcps).

Appendix 3. Reduction of power spectra

Reduction of power spectra of temperature fluctuations is based on same principles as that of mean-square values (App. 2), taking into account characteristics of filters, integrating circuit and recording device.

Filters were calibrated; effective width of filter used for most measurements was found to be $\Delta n = 50.7$ cps either from a static calibration of gain vs. off-center frequency or from a dynamic calibration of complete system with a white noise generator; this value was used for the reduction of the continuous or slowly varying part of the power spectrum.

Since rise-time of recorder was approximately 1/3 of time constant of integrating device, a non-negligible value, response of system to discrete frequency peaks was obtained in a separate dynamic calibration; this is reproduced in part in figure 50. Results for sharp peaks, including this effect of recorder transfer function, can be represented then by another effective filter width, $\Delta n = 40.9$ cps.

So that finally power spectral density of temperature fluctuations f(n) can be obtained from the plot of voltage squared, $\overline{E^2}(n)$ as

$$f(n) = \frac{\overline{E^2}(n)}{(\alpha R_T G I)^2 \Delta n} \tag{39}$$

with $\Delta n = 50.7$ cps for constant or slowly varying signals

$\Delta n = 40.9$ cps for sharp peaks

Since power spectral density plots are distorted below 150 cps due to amplifier gain drop (see Fig. 10), correlation times were

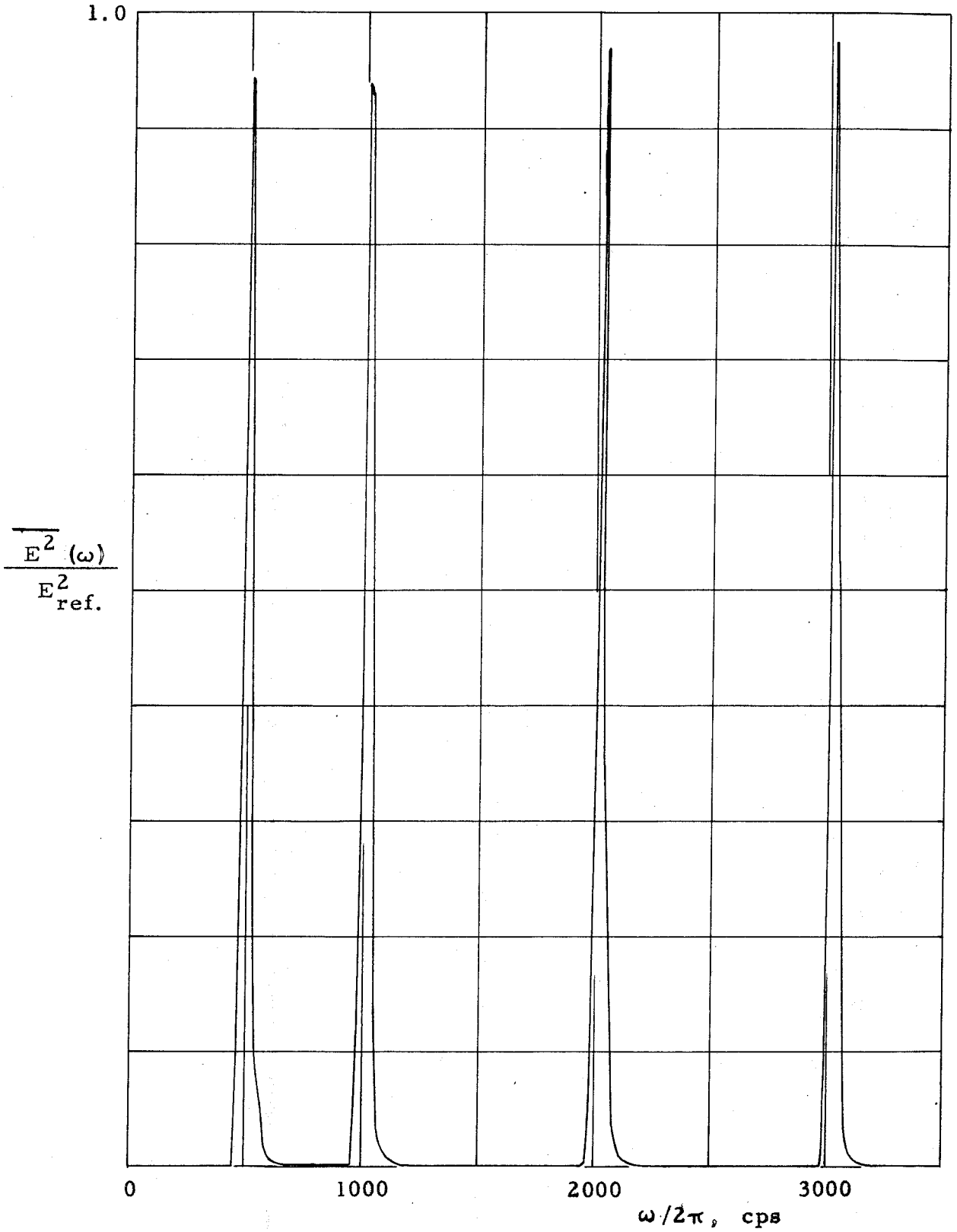

Fig. 50 - Calibration of harmonic analyzer system

obtained from ratio of power spectral density at $n = 200$ cps and $n = 800$ cps, or $n = 800$ cps and $n = 3200$ cps, recorded in Table 1.

If spectrum has form $f(\omega) = \frac{A}{1 + B\omega^2}$, correlation time is $\tau_c = \sqrt{B}$. Now, if

$$y = \frac{f(\omega_0)}{f(4\omega_0)} = \frac{1 + 16 B\omega_0^2}{1 + B\omega_0^2} = \frac{1 + 16x}{1 + x} \tag{40}$$

$$B\omega_0^2 = x = \frac{y-1}{16-y} \tag{41}$$

The relation used to compute correlation times is then

$$\tau_c = \frac{1}{\omega_0} \sqrt{\frac{y-1}{16-y}} \tag{42}$$

Appendix 4. Error in time-average pressures readings due to pressure fluctuations

When fluctuating pressures are applied to a pressure tap connected by a small tube to a large reservoir - manometer tube and leads - the pressure indicated by the manometer will not give the time-weighted average of the applied pressure. The principal nonlinearities in such a system stem from the fact that the compressible laminar mass-flow rate in the entrance tube is a non-linear function of the applied pressure, and so is the pressure drop due to a sudden contraction.

The corrections, with periodic fluctuations and assuming the validity of the quasi-stationary approach, have been computed in reference 30 and 31. Some experimental checks with periodic pressure fluctuations are also reported in reference 31.

In our tests the entrance tube had dimensions: I. D. = 0.020 in., length L = 2.0 in. and was connected to the manometer by an 0.125 in. I. D. tube, approximately 20 ft. long. Time constant of manometer connection was $\tau_0 = 0.2$ sec, and $L/a = 1.6 \times 10^{-4}$ sec. Methods of reference 31 can be applied to fluctuations of period T

$$2\pi\tau_0 \gg T \gg L/a \tag{43}$$

This is very nearly the case, since low frequency components dominate in the continuous part of the spectrum, while periodic components have frequencies n = 2700 cps or less.

Mean-square fluctuations on model surface at $\theta = 170^\circ$ or 180° (assuming that local temperature and pressure fluctuations

are related adiabatically) are estimated as

M_1	$\sqrt{\overline{p'^2}}/p$
0.35	0.10
0.65	0.80

Routine computation following reference 31 gives correction C to be subtracted from indicated value of pressure:

M_1	$C(^o/o)$
0.35	0.23
0.65	8.8

These corrections are fairly small, considering that they apply to points of extreme pressure fluctuations at any given Mach number. In the case M = 0.65 possible error in pressure drag coefficient would amount to less than 5 $^o/o$.

Appendix 5. Solutions of an equation for tunnel-wake resonance

Equation (31)

$$1 + \frac{\frac{H}{d} - 1}{\sin \epsilon} = \frac{2j + 1}{2(St)\cos \epsilon}, \qquad j = 0, 1, 2, \cdots$$

with $\cos \epsilon = U/a = M$

can be solved numerically for any given set of values $\frac{H}{d}$, (St), and j.

With our numerical value $\frac{d}{H} = 0.0666$, and experimentally observed (St) = 0.18, it becomes

$$\underbrace{1 + \frac{14.0}{\sin \epsilon}}_{\text{LHS}} = \underbrace{\frac{2j + 1}{0.36 \cos \epsilon}}_{\text{RHS}}$$

Numerical solution yields:

j	ϵ, deg.	LHS	RHS	$M = \cos \epsilon$
0	80	15.22	16.0	
	79	15.28	14.28	
	79.5	15.24	15.23	0.182
1	60	17.16	16.68	
	61	17.02	17.20	
	60.7	17.06	17.04	0.489
2	45	20.8	19.62	
	46	20.5	20.0	
	47	20.1	20.4	
	46.7	20.23	20.23	0.686

The first value is outside the experimental range. The agreement of the last two values with experiment ($M_1 = 0.50$, $M_1 = 0.65$) seems quite good, considering the extremely simple theoretical model.

REFERENCES

1. Birkhoff, G., and Zarantonello, H.: "Jets, wakes and cavities." New York, Acad. Press (1957).

2. Helmholtz, H. von: "Über discontinuirliche Flüssigkeits-bewegungen." Monatsber. K. Akad. Wiss. Berlin (1868), 215-228.

3. Kirchhoff, G.: "Zur Theorie freier Flüssigkeitsstrahlen." Crelles Journal 70 (1869), 289-298.

4. Roshko, A.: "A new hodograph for free-streamline theory." NACA TN 3168 (1954).

5. Strouhal, V.: "Über eine besondere Art der Tonerregung." Wiedemann's Ann., Neue Folge, 5 (1878), 216-251.

6. Kármán, Th. von: "Über den Mechanismus des Widerstandes den ein bewegter Körper in einer Flüssigkeit erfährt." Gött. Nachr., Math.-Phys. Kl. (1911), 509-517; (1912), 547-556.

7. Roshko, A.: (a) "On the development of turbulent wakes from vortex streets." NACA TN 2913 (1953).
(b) "On the drag and shedding frequency of two-dimensional bluff bodies." NACA TN 3169 (1954).

8. Kovasznay, L. S. G.: "Hot-wire investigation of the wake behind cylinders at low Reynolds' numbers." Proc. Roy. Soc. London (A) 198 (1949), 174-190.

9. Pohlhausen, K.: "Zur näherungsweisen Integration der Differentialgleichung der laminaren Grenzschicht." ZAMM 1 (1921), 252-268.

10. Crocco, L., and Lees, L.: "A mixing theory for the interaction between dissipative flows and nearly isentropic streams." J. Aero. Sci. 19 (1952), 649-678.

11. Korst, H. H., Page, R. H., and Childs, M. E.: "Compressible two-dimensional jet mixing at constant pressure." Univ. of Ill., Engr. Exp. Sta., Mech. Engr. Dept., TN 392-1 (1954); "A theory for base pressures in transonic and supersonic flows." Univ. of Ill., Engr. Exp. Sta., Mech. Engr. Dept., TN 392-2 (1955).

12. Chapman, D. R., Kuehn, D. M., and Larson, H. K.: "Investigation of separated flows in supersonic and subsonic streams with emphasis on the effect of transition." NACA Rep. 1356 (1958).

13. Eckert, E., and Weise, W.: "Messungen der Temperaturverteilung auf der Oberfläche schnell angeströmter unbeheizter Kőrper." Forsch. Geb. Ing.-Wes. 13 (1942), 246-254.

14. Ryan, L. F.: "Experiments on aerodynamic cooling." ETH Zűrich, Inst. f. Aerodynamik, Mitt. 18 (1951), 5-52.

15. Liepmann, H. W.: "On the application of statistical concepts to the buffeting problem." J. Aero. Sci. 19 (1952), 793-801.

16. Schmidt, E., and Wenner, K.: "Wärmeabgabe über den Umfang eines angeblasenen geheizten Zylinders." Forsch. Geb. Ing.-Wes. 12 (1941), 65-73.

17. Walter, L. W., and Lange, A. H.: "Surface temperature and pressure distributions on a circular cylinder in supersonic cross-flow." NAVORD Rep. 2854 (1953).

18. Bingham, H. H., Weimer, D. K., and Griffith, W.: "The cylinder and semicylinder in subsonic flow." Princeton Univ., Dept. of Physics, Tech. Rep. II-13 (1952).

19. Vidal, R. J.: "Model instrumentation techniques for heat transfer and force measurements in a hypersonic shock tunnel." WADC TN 56-315 (1956).

20. Rabinowicz, J., Jessey, M. E., and Bartsch, C. A.: "Resistance thermometer for heat transfer measurement in a shock tube." GALCIT, Hypersonic Res. Project, Memo. No. 33 (July 1956).

21. Rabinowicz, J.: "Aerodynamic studies in the shock tube." Ph. D. Thesis, Calif. Institute of Technology, Pasadena, Calif. (1957).

22. Liepmann, H. W.: "The interaction between boundary layer and shock waves in transonic flow." J. Aero. Sci. 13 (1946), 623-637.

23. Dhawan, S., and Roshko, A.: "A flexible nozzle for a small supersonic wind tunnel." J. Aero. Sci. 18 (1951), 253-258.

24. Liepmann, H. W., and Skinner, G. T.: "Shearing stress measurements by use of a heated element." NACA TN 3268 (1954).

25. Ackeret, J.: "Űber die Temperaturverteilung hinter angestrőmten Zylindern." ETH Zurich, Inst. f. Aerodynamik, Mitt. 21 (1954), 5-17. ["On the temperature distribution behind cylinders in a flow." NASA Tech. Transl. F-2 (1959).]

26. Schultz-Grunow, F.: "Turbulenter Wärmedurchgang im Zentrifugalfeld." Forsch. Geb. Ing.-Wes. 17 (1951), 65-76.

27. Allen, H. J., and Vincenti, W. G.: "Wall interference in a two-dimensional flow wind tunnel, with consideration of the effect of compressibility." NACA Rep. 782 (1944).

28. Holder, D. W., Macphail, D. C., and Thomson, J. S.: "Experimental methods," Ch. XI of Howarth, L. (ed.) "Modern developments in fluid dynamics - high speed flow." Oxford, Clarendon (1953), vol. II, 516-532.

29. Thomann, H.: "Measurement of the recovery temperature in the wake of a cylinder and of a wedge at Mach numbers between 0.5 and 3." Sweden, FFA Rep. 84 (1959).

30. Nesbitt, M. V.: "The measurement of true mean pressures and Mach numbers in oscillatory flow." Gt. Brit., NGTE, Memo. M.180 (1953).

31. Johnson, R. C.: "Averaging of periodic pressure pulsations by a total pressure probe." NACA TN 3568 (1955).